Predicting effects of stroke lesions and recovery through whole-brain modeling and brain dynamics

Sebastian Ariel Idesis

TESI DOCTORAL UPF / YEAR: 2023

THESIS SUPERVISOR

Prof. Dr. Gustavo Deco, Center for Brain and Cognition – UPF

DEPARTMENT OF MEDICINE AND LIFE SCIENCES

Dedication

I dedicate this thesis work to my partner, Melina, whose unconditional support, and encouragement have been invaluable throughout the difficulties of graduate school and life. I am deeply grateful to have you by my side. I also extend this dedication to my parents, Hugo and Graciela, who have consistently loved me without conditions and whose admirable examples have instilled in me the value of hard work in pursuing my aspirations. Lastly, I would like to acknowledge my dog and faithful companion, Mafalda, for providing tireless companionship throughout these years.

Acknowledgements

I want to sincerely express my appreciation to Prof. Deco, my advisor, for the unwavering support he has provided throughout my PhD studies and related research. His patience, motivation, and extensive knowledge are deeply valued. His guidance has been indispensable throughout the entire research and writing journey of this thesis. I couldn't have asked for a more exceptional advisor and mentor for my PhD studies.

I also extend my heartfelt thanks to Prof. Corbetta for giving me the opportunity to join his team as an intern and granting me access to the laboratory and research facilities. Without their invaluable support, this research would not have been possible.

My gratitude extends to my fellow labmates who engaged in stimulating discussions, worked tirelessly during late nights leading up to deadlines, and shared enjoyable moments with me over the past three

years. I want to give a special acknowledgment to Daniel Diaz, my desk partner, for the numerous scientific and life discussions we shared.

Furthermore, I want to express my appreciation to my external collaborators who provided guidance throughout the process. Specifically, I am particularly grateful to Dr. Joshua Faskowitz for his academic and personal support over the years.

Last but certainly not least, I want to express my gratitude to my family, including my partner, parents, brother, and sister, for their unwavering spiritual support throughout the thesis writing process and in all aspects of my life.

Funding acknowledgements

The project developed in this thesis has received the support of a fellowship from the EU-project euSNN (MSCA-ITN-ETNH2020-860563).

Abstract

Stroke is the second leading cause of death worldwide and a major contributor to disability. However, our understanding of the consequences of stroke lesions remains limited, relying mainly on behavioral reports and descriptive correlations from neuroimaging techniques.

Functional magnetic resonance imaging (fMRI), one of the most commonly used methods, offers various possibilities that have not been extensively explored in stroke patients. In this thesis, we introduce a novel analysis approach that shifts the focus to the connections between brain regions, aiming to identify biomarkers for severity and recovery. Moreover, by employing whole-brain models, we demonstrate how the integration of structural and functional information can enhance the accuracy of existing analyses. Additionally, we present a model capable of predicting the functional information based only on the structural damage of the patients. Lastly, given the high-dimensional nature of the data, we utilize a deep learning autoencoder to uncover the embedded information and nonlinear dynamics of the brain following a stroke event. All of the findings presented in this thesis contribute to the improvement of diagnostics, classification, and prediction of recovery for this significant disorder.

Keywords: Stroke; Brain Dynamics; Functional Connectivity; Whole-brain model; Structural Disconnection mask; Dimensionality reduction; Longitudinal cohort; Recovery prediction.

Resumen

Los accidentes cerebrovasculares son la segunda causa de muerte a nivel mundial y una de las principales causas de discapacidad. Sin embargo, nuestra comprensión de las consecuencias de las lesiones por accidentes cerebrovasculares sigue siendo limitada y se basa principalmente en reportes de comportamiento y correlaciones descriptivas de técnicas de neuroimagen. La resonancia magnética funcional (fMRI), el método más utilizado, ofrece varias posibilidades que no se han explorado ampliamente en pacientes con accidente cerebrovascular. En nuestro estudio, presentamos un enfoque novedoso centrado en las conexiones entre las regiones del cerebro, con el objetivo de identificar biomarcadores de severidad y recuperación. Al emplear modelos de cerebro completo, demostramos cómo la integración de información estructural y funcional puede mejorar la precisión de los análisis existentes. Adicionalmente, presentamos un modelo capaz de predecir la información funcional basándose únicamente en el daño estructural de los pacientes. Por último, dada la naturaleza de alta dimensionalidad de los datos, utilizamos un codificador automático para investigar la información latente y la dinámica no lineal del cerebro después de un accidente cerebrovascular. Todos los hallazgos presentados en este estudio contribuyen a mejorar el diagnóstico, la clasificación y la predicción de la recuperación de este importante trastorno.

Palabras clave: Accidente cerebrovascular; dinámica cerebral; conectividad funcional; modelo de cerebro completo; máscara de desconexión estructural; reducción de dimensionalidad; cohorte longitudinal; pronóstico de recuperación.

List of publications

Publications included in the thesis

Idesis, S., Faskowitz, J., Betzel, R. F., Corbetta, M., Sporns, O., & Deco, G. (2022). Edge-centric analysis of stroke patients: An alternative approach for biomarkers of lesion recovery. *NeuroImage: Clinical*, 103055.

Idesis, S., Favaretto, C., Metcalf, N. V., Griffis, J. C., Shulman, G. L., Corbetta, M., & Deco, G. (2022). Inferring the dynamical effects of stroke lesions through whole-brain modeling. *NeuroImage: Clinical*, 103233.

Oral and poster presentations

Idesis, S. (May 2022). Edge-centric analysis of stroke patients: An alternative approach for biomarkers of lesion recovery. Barcelona Computational, Cognitive and System Neuroscience (BARCCSYN 2022), Barcelona, Spain

Idesis, S. (July 2022). Inferring the dynamical effects of stroke through whole-brain modelling, FENS conference, Paris, France

Idesis, S. (July 2022). Dimensionality reduction in stroke patients. Complexity conference, Barcelona, Spain

Idesis, S. (September 2022). Brain dynamics in stroke patients. Donders Cognition Brain and Technology summer school (DCBT), Nijmegen, The Netherlands.

Idesis, S. (March 2023). Latent representation of fMRI data. DGKN conference, Hamburg, Germany.

Contents

List of Figures

Chapter 1

1.Preface

In 1970, the World Health Organization (WHO) defined stroke as the rapid development of clinical symptoms indicating cerebral function disturbance lasting over 24 hours or leading to death, without any apparent cause other than vascular origin (Aho et al., 1980). Despite significant advances in acute care, many patients continue to experience lasting deficits that only partially recover spontaneously or through rehabilitation. The mechanisms underlying recovery and the impact of rehabilitation remain poorly understood. Gaining insight into these mechanisms is crucial for exploring innovative treatment approaches, such as neurostimulation.

Over the years, the field of human neuroscience has undergone a transformation due to advancements in recording techniques. These techniques have enabled researchers to progress from studying behavioral aspects to describing patterns of coordinated activation of brain regions. In this line, a notable development in neuroscience is the conceptualization of the brain as a dynamic system consisting of interconnected networks that process information through integration and segregation. As a result, the paradigm of neuroscientific studies has undergone a significant shift, partially thanks to the discovery of resting-state activity and the exploration of spatiotemporal patterns. This concept has led to the application of formal methods from graph theory and statistical mechanics to study the structure and dynamics of these networks (Sporns, 2013, 2014). While network-based understanding of the brain existed prior to these applications, recent advancements have been inspired by the empirical discovery of the brain's resting-state physiology using functional magnetic resonance imaging (fMRI) and the measurement of the blood-oxygenation-level-dependent (BOLD)

signal (Power et al., 2011; Yeo et al., 2011). Resting-state functional connectivity (FC) measures the inter-regional correlation of the BOLD signal, revealing the spatiotemporal structure of the brain's resting-state physiology.

Computational brain network modeling has become a potent tool for exploring the causal dynamics of the human brain. By incorporating functional and structural connectivity data obtained from empirical neuroimaging studies, this approach offers valuable insights into the intricate workings of the brain. In particular, this theoretical framework has proven successful in elucidating the organized dynamics observed during resting-state networks (RSNs), despite the paradoxical notion that the resting brain is never truly at rest (Deco et al., 2017).
Consequently, the development of accurate whole-brain models is crucial for comprehending how the brain's structural and functional organization influences its information processing abilities. Such models have the potential to predict functional and behavioral abnormalities in patients based on simple measurements like structural MRI. They can also facilitate the assessment of the therapeutic effects of brain stimulation, a subject of significant interest (Deco et al., 2019; Wagner et al., 2007).

In this thesis we apply a specific model, using the most general form of expressing both noisy asynchronous dynamics and oscillations, namely a normal form of a Hopf bifurcation (Deco et al., 2017). Extensive studies in the past have demonstrated the effectiveness, versatility, and wide applicability of this model in describing dynamics at the local node level (Deco et al., 2019; Deco et al., 2017; Jobst et al., 2017). By employing this representation, we were able to accurately fit the models to neuroimaging data, not just by aligning with the overall average FC, but also by capturing the temporal patterns of fluctuations and functional connectivity dynamics.

This dissertation aims to explore various methodological approaches and their application in understanding the brain dynamics of stroke patients. Our primary objective is to develop a computational model capable of investigating the abnormal resting brain physiology resulting from specific lesions. Throughout this document, we will provide an overview of existing techniques, introduce novel methodological approaches, delve into cutting-edge whole-brain modeling, and explore recovery prediction. Additionally, we will employ dimensionality reduction techniques to extract embedded information from the commonly studied BOLD signal. Ultimately, our findings will contribute strategies to enhance patient treatment, improve diagnostic accuracy, and enhance their overall quality of life.

1.1 Topics and outline of the thesis

The outline of the main topics covered in each chapter is as follows:

In chapter 2, we present the dataset utilized throughout the subsequent chapters. The database comprises individuals who experienced their first stroke and were examined at 1-2 weeks, 3 months, and 12 months following the onset of the stroke. Additionally, the cohort includes a group of healthy individuals matched in age, who underwent evaluation twice within a three-month interval. This approach allows for the assessment of both the differences between healthy controls and stroke patients, as well as the evolution of stroke effects on the brain over time.

In chapter 3, we explore the utility of a novel approach, known as edge-centric analysis, within a dataset of stroke patients. We employ newly developed measures that unveil information at the edge level, thereby providing fresh evidence for the potential of this approach as a promising link between structure and function. Additionally, we present a novel direction for mapping the brain in a clinical setting. This analysis yields indicators that are closely

associated with lesion severity and reveal the recovery of lesions, making our study the first to adopt an edge-centric approach with clinical applications over time. As a result, the goal of this chapter is to investigate the functional brain dynamics following stroke incidents.

In Chapter 4, we construct a causal mechanistic generative model of the entire brain to elucidate the functional and behavioral consequences of stroke lesions. Notably, the incorporation of structural disconnection masks proves to be a pivotal factor in the model's performance, enabling the classification of severity and the differentiation of asymmetries in network communication. By utilizing the whole-brain model, in combination with the anatomical disconnection information, we demonstrate the emergence of changes in network dynamics after a stroke injury.

In chapter 5 we introduce a novel predictive whole-brain computational model, specifically designed to predict functional information following a stroke-induced lesion. Significantly, our findings reveal that the predictive model achieves a comparable level of accuracy to previously reported models, despite not incorporating the patients' functional information during model optimization. This suggests that the model is able to capture relationships between structural and functional activity. The generative nature of the model facilitates its applicability to new datasets and has the potential to advance our comprehension of the disrupted brain dynamics observed in stroke patients.

In chapter 6 we focus on the dimensionality reduction of the recordings by using a special type of neural network, called autoencoder, in order to uncover non-linear components of brain dynamics in stroke patients. We determined that at the acute stage, the latent representation yielded greater diagnostic power. Additionally, we utilize the embedded information to compare the prediction of recovery after one year following the incident with other

established methods. Our findings demonstrate an improved prediction of patients' recovery when incorporating the information from the latent space. Moreover, we discovered that complexity metrics, such as brain signal reversibility, offer indicators that are associated with lesion severity and predict lesion recovery.

In the final chapter, General discussion, we summarize the main contributions of this dissertation, and discuss some open questions and possible future directions of investigation.

CHAPTER 2

2. Stroke dataset description

Work in this chapter is based on the following publications:

Idesis, S., Faskowitz, J., Betzel, R. F., Corbetta, M., Sporns, O., & Deco, G. (2022). Edge-centric analysis of stroke patients: An alternative approach for biomarkers of lesion recovery. *NeuroImage: Clinical*, 103055.

Idesis, S., Favaretto, C., Metcalf, N. V., Griffis, J. C., Shulman, G. L., Corbetta, M., & Deco, G. (2022). Inferring the dynamical effects of stroke lesions through whole-brain modeling. *NeuroImage: Clinical*, 103233.

2.1 Subjects

We used the Washington University Stroke Cohort dataset (Corbetta et al., 2015), a large prospective longitudinal (two weeks, three months, 12 months) study of patients with a first-time, single lesion stroke. Although patients were studied at 1-3 weeks (mean = 13.4 days, SD = 4.8 days), 3 months, and 12 months after stroke onset, the current study only analyzed data from the first time point. Furthermore, a group of age-matched control subjects was evaluated twice at an interval of three months. From this cohort, we selected 96 stroke patients and 27 healthy subjects.

Stroke patients were prospectively recruited from the stroke service at Barnes-Jewish Hospital (BJH), with the help of the Washington University Cognitive Rehabilitation Research Group (CRRG). The complete data collection protocol is described in full detail in a previous publication (Corbetta et al., 2015). Healthy controls were selected based on the same inclusion/exclusion criteria as previously done (Corbetta et al., 2015). This group was typically constituted of spouses or first-degree relatives of the patients, age- and education-matched to the stroke sample. Patients were characterized with a robust neuroimaging battery for structural and functional features, and an extensive (~2 hour) neuropsychological battery.

2.2 Neuroimaging acquisition and preprocessing

A complete description of the neuroimaging assessment is given in (J. C. Griffis et al., 2019). Neuroimaging data were collected at the Washington University School of Medicine using a Siemens 3T Tim-Trio scanner with a 12-channel head coil, specifically: 1) sagittal T1-weighted MP-RAGE (TR=1950 msec; TE=2.26 msec, flip angle = 90 degrees; voxel dimensions = 1.0x1.0x1.0 mm), and 2) a gradient echo EPI (TR=2000 msec; TE=2 msec; 32 contiguous slices; 4x4 mm in-plane resolution) resting-state functional MRI

scans from each subject. Participants were instructed to fixate on a small centrally located white fixation cross that was presented against a black background on a screen at the back of the magnet bore. Between six and eight resting-state scans (128 volumes each) were obtained from each participant (~30 minutes total) giving a total of 896 time points for each participant.

Resting-state fMRI preprocessing included (i) regression of head motion, signal from ventricles and CSF, signal from white matter, global signal (ii) temporal filtering retaining frequencies in 0.009 - 0.08 Hz band: and (iii) censoring of frames with large head movements, FD = 0.5 mm. The resulting residual time series were projected onto the cortical and subcortical surface of each subject's brain, which was divided into 234 regions of interests (200 cortical plus 34 subcortical). These regions were taken from the multi-resolution functional connectivity-based cortical parcellations developed by Schaefer and colleagues (Schaefer et al., 2018), including additional subcortical and cerebellar parcels from the Automated Anatomical Labeling (AAL) atlas (Tzourio-Mazoyer et al., 2002) and a brainstem parcel from the Harvard-Oxford Subcortical atlas (https://fsl.fmrib.ox.ac.uk/fsl/fslwiki/Atlases).

A structural connectome atlas was created using a publicly available diffusion MRI streamline tractography atlas based on high angular resolution diffusion MRI data collected from 842 healthy Human Connectome Project participants (Yeh et al., 2018) as described previously (Griffis et al., 2019, 2021). Briefly, the HCP-842 atlas was built using high spatial and high angular resolution diffusion MRI data collected from N=842 healthy Human Connectome Project participants. These data were reconstructed in the MNI template space using q-space diffeomorphic reconstruction (Yeh & Tseng, 2011), and the resulting spin distribution functions were averaged across all 842 individuals to estimate the normal population-level diffusion patterns. Whole-brain deterministic tractography was then performed on the population-averaged

dataset using multiple turning angle thresholds to obtain 500,000 population-level streamline trajectories.

2.3 Neuropsychological and behavioral assessment

The same subjects (controls and patients) underwent a battery of neuropsychological tests in the domains of motor, attention, language, visual, and memory functions at each time point. Briefly, the battery consisted of 44 measures across four domains of function: language, motor attention and memory (for a complete description of the tasks measures, see (Corbetta et al., 2015). A dimensionality reduction was applied to the individual test data in each domain using principal component analysis as in (Corbetta et al., 2015), yielding summary domain scores: Language, MotorR and MotorL (one score per side of the body), AttentionVF (visuospatial field bias), Average performance (overall performance and reaction times on attention tasks), and AttentionValDis (the ability to reorient attention to unattended stimuli), Memory V (composite verbal memory score) and MemoryS (composite spatial memory score). Finally, patients' behavioral scores were z-scored with regard to controls' scores, to highlight behavioral impairments.

In addition to domain-specific scores, the patients' clinical severity was assessed through the National Institutes of Health Stroke Scale (NIHSS) (Brott et al., 1989) that includes 15 subtests addressing: level of consciousness (LOC), gaze and visual field deficits, facial palsy, upper and lower motor deficits, limb ataxia, sensory impairment, inattention, dysarthria and language deficits. The total NIHSS score was used as an averaged measure of the clinical severity for each patient.

2.4 Lesions

Each lesion was manually segmented on structural MRI scans and checked by two board-certified neurologists. The location (cortico-subcortical, subcortical, white-matter only) of each lesion was assigned with an unsupervised K-means clustering on the percentage of total cortical/subcortical gray and white matter masks overlay. For a more extensive explanation on how the overlap of each lesion group with gray matter, white matter, and subcortical nuclei is calculated, see the work by Corbetta et al, 2015.

We summarize the lesion distribution and average of the used sample in **Figure A6**.

2.5 Lesion disconnection masks

The Lesion Quantification Toolkit (Griffis et al., 2021) produces a comprehensive set of atlas-derived lesion measures that include measures of grey matter damage, white matter disconnection, and alterations of higher-order brain network topology. Importantly, the measures produced by the toolkit are based on population-scale (e.g., N = 842) atlases of grey matter parcel boundaries and white matter connection trajectories that were constructed from high-quality resting-state functional MRI and diffusion MRI data using state-of-the-art methods.

Taking advantage of the Lesion Quantification Toolkit (LQT), the structural disconnection (SDC) masks consisted of a spared connection adjacency matrix where each cell quantified the percentage of streamlines connecting each region pair in the atlas-based structural connectome that were spared by the lesion. Therefore, the multiplication of each SDC with a template SC provides an atlas-based weight for each region pair corresponding to each

patient. For the mentioned cohort, DTI was not acquired during the subacute stage visit (~ 2 weeks), only during the two subsequent chronic visits (not included in the current study). Therefore, the estimates from the LQT were used.

Since many stroke lesions occur predominantly in the white matter, or include both a gray and white matter component, the SDC mask should provide an accurate description of the damage to the connectome. We computed the total amount of disconnection (J. C. Griffis et al., 2019) as a metric of anatomical impairment to assess the validity of the model.

CHAPTER 3

3. Functional effects: Exploring brain dynamics of stroke patients through Edge-centric analysis

Work in this chapter is based on the following publication:

Idesis, S., Faskowitz, J., Betzel, R. F., Corbetta, M., Sporns, O., & Deco, G. (2022). Edge-centric analysis of stroke patients: An alternative approach for biomarkers of lesion recovery. *NeuroImage: Clinical*, 103055.

Highlights

- We applied an edge-centric approach to a longitudinal stroke patient dataset
- Highest values of co-fluctuation were associated with stroke severity
- Normalized entropy increased across patient recovery time
- We demonstrate a novel direction for mapping the brain in a clinical setting

Abstract

Most neuroimaging studies of post-stroke recovery rely on analyses derived from standard node-centric functional connectivity to map the distributed effects in stroke patients. Here, given the importance of nonlocal and diffuse damage, we use an edge-centric approach to functional connectivity in order to provide an alternative description of the effects of this disorder. These techniques allow for the rendering of a metric such as normalized entropy, which describes the diversity of edge communities at each node. Moreover, the approach enables the identification of high amplitude co-fluctuations in fMRI time series. We found that normalized entropy is associated with stroke lesion severity and continually increases across the time of patients' recovery. Furthermore, high amplitude co-fluctuations not only relate to the lesion severity but are also associated with patients' level of recovery. The current study is the first edge-centric application for a clinical population in a longitudinal dataset and demonstrates how a different perspective for functional data analysis can further characterize topographic modulations of brain dynamics.

Keywords

Stroke; Edge-centric; Functional Connectivity; Normalized entropy; Co-Fluctuations; Longitudinal; Brain Dynamics

3.1 Introduction

The brain can be conceptualized as a system of regions that functionally influence each other, forming a complex network of interactions (Bassett & Sporns, 2017; H. J. Park & K. Friston, 2013). Stroke causes focal brain lesions that alter this network organization both locally and globally (Crofts et al., 2011; Wang et al., 2019). The tools of network science and graph theory allow for these changes to be quantified in various ways. Using fMRI, it has been shown that the functional synchronization between distinct regions of the brain, referred to as FC, is disrupted by stroke (Silasi & Murphy, 2014; Wodeyar et al., 2020). Commonly observed disruptions to this network organization include inter- and intra-hemispheric changes in FC (Crofts et al., 2011; J. C. Griffis et al., 2019; Siegel et al., 2016). Furthermore, using structural magnetic resonance imaging (sMRI) of the brain's white matter architecture, several studies have shown how structural disconnections explain brain network (such as modularity and synchronization) dysfunction after stroke (Corbetta et al., 2015; Joseph C Griffis et al., 2019; Siegel et al., 2016; Wang et al., 2019). These studies show how decreases in modularity and synchronization are strongly related to behavioral deficits.

Common to many network neuroscience investigations is a reliance on network analyses that results in measurements specific to each brain region. A recent study proposed that resting-state functional connectivity (rsFC) may not be fully representative of brain activation patterns underlying specific behaviors, which was shown to be constrained by the structural connectome (Honey et al., 2007; Honey et al., 2009; Olafson et al., 2021). Therefore, it could be the case that the observed modulations of functional connectivity following stroke represent an incomplete picture of the brain dysfunction linked to ipsi- and contralateral stroke. Along these lines, new analytical approaches should be explored to see if they can further expand our understanding of these fMRI-derived modulations. In particular, new network-

based analyses of fMRI that focus on the brain's functional connections, known as edges, could help to fill these gaps.

Recent studies have motivated an edge-centric approach, shifting focus onto the information that can be resolved on a per-edge level (Ahn et al., 2010; Faskowitz et al., 2020; Zamani Esfahlani et al., 2020). Using a straightforward unwrapping of the Pearson correlation, co-fluctuation time series (alternatively referred to as "edge time series") data can be estimated for each edge. Unlike sliding-window time-varying connectivity, which requires the parameterization of a window duration, kernel shape, and step size, edge time series have the same temporal resolution as the original functional data. Importantly, the time-averaged value of an edge time series is a correlation coefficient. This means that edge time series are a mathematically exact decomposition of a functional connection into its framewise contributions. Previous analyses of edge time series data have shown that transient periods of high-amplitude activity make disproportionately large contributions to the time-averaged functional connectivity (Allan et al., 2015; Cifre et al., 2020; Petridou et al., 2013; E. Tagliazucchi et al., 2012; Zamani Esfahlani et al., 2020). In other words, data selected from specific temporal slices can be used to reconstruct a similarity matrix with a high correspondence to the functional connectivity matrix constructed from the full dataset (Betzel et al., 2021; Greenwell et al., 2021). Like with co-activation pattern (CAP) analysis (Karahanoglu & Van De Ville, 2015; Liu & Duyn, 2013), the structure of high-amplitude activity forms distinctive spatial patterns that are transiently expressed and only partly resembles the canonical functional systems architecture (Sporns et al., 2021). What separates edge time series from previous methods is that it provides an exact mathematical relationship to the Pearson correlation.

Edge time series can be compared in a pairwise manner, creating an edge-by-edge similarity matrix of the brain that can be submitted to network

analyses. Clustering this data results in a community structure of edges, where communities represent groups of region pairs that similarly fluctuate across time (Chumin et al., 2021; Jo, Esfahlani, et al., 2021). When mapped to brain regions, these edge communities naturally form a pervasively overlapping structure, such that every node participates in multiple communities. The distribution of edge community affiliations can be conceptualized as an entropy that describes how dispersed the edge community distribution is at each node. Up until this point, this family of approaches has been applied to map fMRI data from young and healthy samples. Consequently, these approaches have not yet been applied to measure the impact of neural dysfunction and/or damage.

In the present study we explore the utility of edge-centric analytical approaches in a clinical setting, by using newly developed measures that disclose information at the edge level. More specifically, we measure the relation between edge-centric derived measures and metrics of post-stroke severity and classification. Additionally, this study examines how these edge measurements possibly change across time, in a longitudinal neuroimaging setting and its association with the level of patients' recovery. In this work, we used the Washington University Stroke Cohort dataset (See chapter 2). We found that normalized entropy of the edge community distributions increased globally across time, as patients recovered from stroke. Furthermore, we found that a marker of high amplitude co-fluctuation has a significant relation with lesion volume and an association with the patients' recovery after 1 year. In summary, the current study reveals how edge-centric analysis provides indicators that reveal lesion severity and reflect lesion recovery, making it the first study with edge-centric approach with clinical applications across time.

3.2 Material and methods

3.2.1 Edge-centric calculations: Normalized entropy and high amplitude co-fluctuations

Time series were extracted for each node (N=235 brain regions) of the parcellation by averaging the preprocessed fMRI BOLD signal within each node at each timepoint. Taking the statistical similarity, as commonly indexed by Pearson correlation, between each possible pair of nodal time series would result in a N-by-N (235-by-235) similarity matrix. This matrix is commonly referred to as a Functional Connectivity matrix. Recently, a new method has been proposed to represent the time series formed by comparing two nodes, by using an intermediate calculation of the Pearson correlation (Faskowitz et al., 2020; Zamani Esfahlani et al., 2020). The resulting edge time series are formed by first, z-scoring each of the two nodal time series independently. Then, the element-wise product of the z-scored time series is taken, forming an edge time series. Values of the edge time series reflect the co-fluctuation pattern between nodes. A positive co-fluctuation results when, at a specific point in time, both series are concordant relative to each of their mean signals. A negative co-fluctuation value results when, at a specific point in time, one time series is above the mean (a positive value) and the other is below the mean (a negative value). Notably, the mean of an edge time series equals the Pearson correlation.

Edge time series have the same temporal resolution as the original data, allowing for the analysis of instantaneous (i.e., a single time frame) co-fluctuation patterns. This data has the dimensionality of edge-by-time. At each frame, the overall co-fluctuation activity can be indexed by taking the root-sum-square (RSS) of all edge co-fluctuations. Then, using these RSS values, the time frames can be ranked. Here, we grouped time frames into 10 ordered deciles based on RSS co-fluctuation activity.

Edges can be clustered based on the similarity of their time course. Here, we applied the k-means algorithm (with normalized Euclidean distance metric) to partition the set of edges into 10 clusters with similar co-fluctuation amplitude. The number of clusters was set to match the presented results in a previous paper (Faskowitz et al., 2020). K-means was repeated 25 times and the partition that was least distant from all other clusters (as assessed by minimum variation of information) was taken to be the representative solution for a given dataset (Faskowitz et al., 2018). This procedure results in a community affiliation for each edge. That is, each edge is associated with one of k communities, where k is 10. By projecting this partition to the node level, we find that the 234 edges (excluding self-loops; therefore N-1 edges) emanating from each node are affiliated with edge communities. Summing edge communities of each node and dividing by 234 provides a probability distribution over the k communities. We can then take the entropy of this distribution, to obtain a measurement of how dispersed the distribution of edge clusters are at each node. A low entropy indicates a relatively even distribution of edge communities associated with a node, whereas a high edge community indicates a high concentration in relatively few communities. Here, we employ the normalized entropy, which is bounded to the interval [0,1].

3.2.2 Entropy localization

The difference between patients and controls was calculated for each node and then displayed in the brain surface plot (**Figure A1**).

3.2.3 Functional system interactions

To investigate the average correlations between canonical functional networks, we compared the within and between network average FC for both

patients and controls at the three distinct timepoints. The sum of weights of the connections between the networks was then Fisher z-transformed to be compared between them at the same scale expressing the co-activity of these networks after the stroke damage and this co-activity recovered across time. The connections displayed exceed the chosen threshold of 1.75 to emphasize the effect (**Figure 3.3b**)

3.2.4 Participation coefficient

We calculated the participation coefficient within each time window for each node using the Brain Connectivity Toolbox (BCT) (https://sites.google.com/site/bctnet/) (Rubinov & Sporns, 2010) function "participation_coef_sign.m", averaging across 500 trials of modularity maximization with the "negative_asym" null model option (Rubinov & Sporns, 2011). The participation coefficient in this study expresses the level at which a node is diversely associated with other nodes across all modules (Fukushima et al., 2018; Rubinov & Sporns, 2010). The (node) modules used for the participation coefficient were obtained by using the modularity undirected function (community detection technique from the BCT). As the normalized entropy did not reveal a significant relation with lesion metrics in an individual level at the acute stage of the injury, participation coefficient was calculated given its previous importance in the field (Warren et al., 2014).

3.2.5 High amplitude co-fluctuations: similarity with FC and principal component analysis

Using the RSS to sort the data (see 3.2.1. Edge-centric calculations section), we calculated a similarity matrix by averaging the top 10% RSS frames. The elements of this matrix represent the cofluctuation patterns that are expressed when the brain is in a high-amplitude state (i.e.: the first decile as

ranked by RSS). The chosen decile was based on previous literature (Zamani Esfahlani et al., 2020) while a comparison between the different deciles is described in **Figure A4**. The obtained similarity matrix was then compared to the full FC matrix (calculated from all frames) using the Pearson correlation (of the vectorized upper triangle for each matrix). This resulted in a coefficient for each subject, representing the similarity between a subject's high-amplitude values and the FC. This value was associated with lesion volume and used to reveal the number of recovered domains (**Figure 3.5a**) and to be compared with the lowest 10% scores (**Figure 3.5b**). Additionally, we calculated the first principal component (PC) of each edge time series matrix, for each patient, at the three different timepoints. This singular value partially describes the first axis of the edge-time series variance. With this addition, we can inspect and compare our results against a node-centric approach as discussed in previous literature (Novelli & Razi, 2021).

3.2.6 Distinction between left and right hemisphere

The normalized entropy calculation was performed in parallel for two subsets of patients according to the location of the stroke: 49 left hemisphere lesioned patients and 47 right hemisphere lesioned patients. In this way, the two groups were compared based on the entropy levels of the patients belonging to the corresponding subset. No classification model was assessed for this comparison.

3.2.7 Distinction between subcortical and cortical region

The normalized entropy calculation was performed in parallel for two subsets of patients according to the location of the stroke, with 33 patients with cortical area lesions and 23 patients with subcortical area lesions. For remaining patients, the lesion location was unspecific or a combination of both tissue

areas. As in the previous section, the entropy level of the subjects of each sample (in this case, patients with cortical vs patients with subcortical lesion) was compared to the other one without performing a classification model.

3.3.Results

We performed a series of analyses on the functional MRI data of stroke patients (**Figure 3.1a**). The first step consisted in obtaining the edge-time series (**Figure 3.1b**) which was calculated for the three distinct timepoints. After calculating co-fluctuation amplitude, the data was sorted and segmented to obtain the 10% of frames with the highest co-fluctuation amplitude (**Figure 3.1c**). Lastly, the edge community entropy was calculated per node to observe its relationship with stroke metrics, its relation with the lesion localization and its fluctuation across time both by node and network (**Figure 3.1d**)

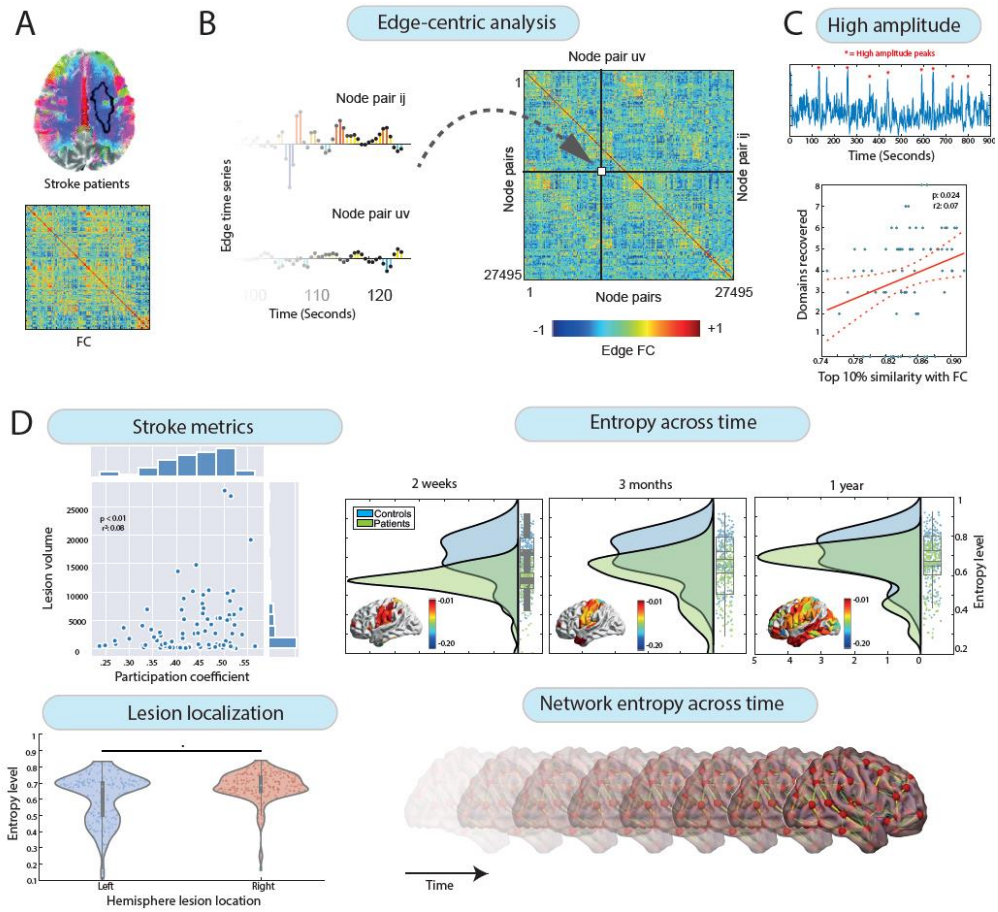

Figure 3.1 : Pipeline of brain dynamics exploration through edge-centric analysis

Figure 3.1: Pipeline of brain dynamics exploration through edge-centric analysis: **(A)** All the analyses were performed using the FC of the stroke patients. **(B)** Edge-FC is calculated by multiplying element-wise the product time series and normalizing the sum by the squared root standard deviations of both time series. **(C)** The elements of the co-fluctuation time series are the element-wise products of z-scored regional BOLD time series, from which the highest peaks are selected for further analysis. **(D)** Normalized entropy and participation coefficient were obtained in order to assess their fluctuation across time, their relation with stroke metrics and their collaboration with lesion localization

To measure the effect of time, we compared the first principal component (PC) singular value for each patient at the three different timepoints. There was not a significant effect of time on the first PC ($F(2,147) = 0.08$, $p = 0.91$). All p-values reported in the results section were corrected using False Discovery Rate. The same effect was observed on the top 10% high-amplitude values ($F(2,132) = 0.47$, $p = 0.62$). There was a significant difference when comparing the level of entropy at the three different time points [$F(2,702) = 30.64$, $p < 0.01$]. Timepoint 3 showed the highest value (mean = 0.74, std = 0.11) followed by timepoint 1 (mean = 0.66, std = 0.11) and timepoint 2 (mean = 0.67, std = 0.14) (**Figure 3.2**). Entropy level revealed an increasing trend across time that was not apparent in the other two metrics. Based on these results, we selected normalized entropy as the variable of interest to be used as a potential fMRI-based indicator of recovery by comparing it with the corresponding values in the control group (**Figure 3.3a**).

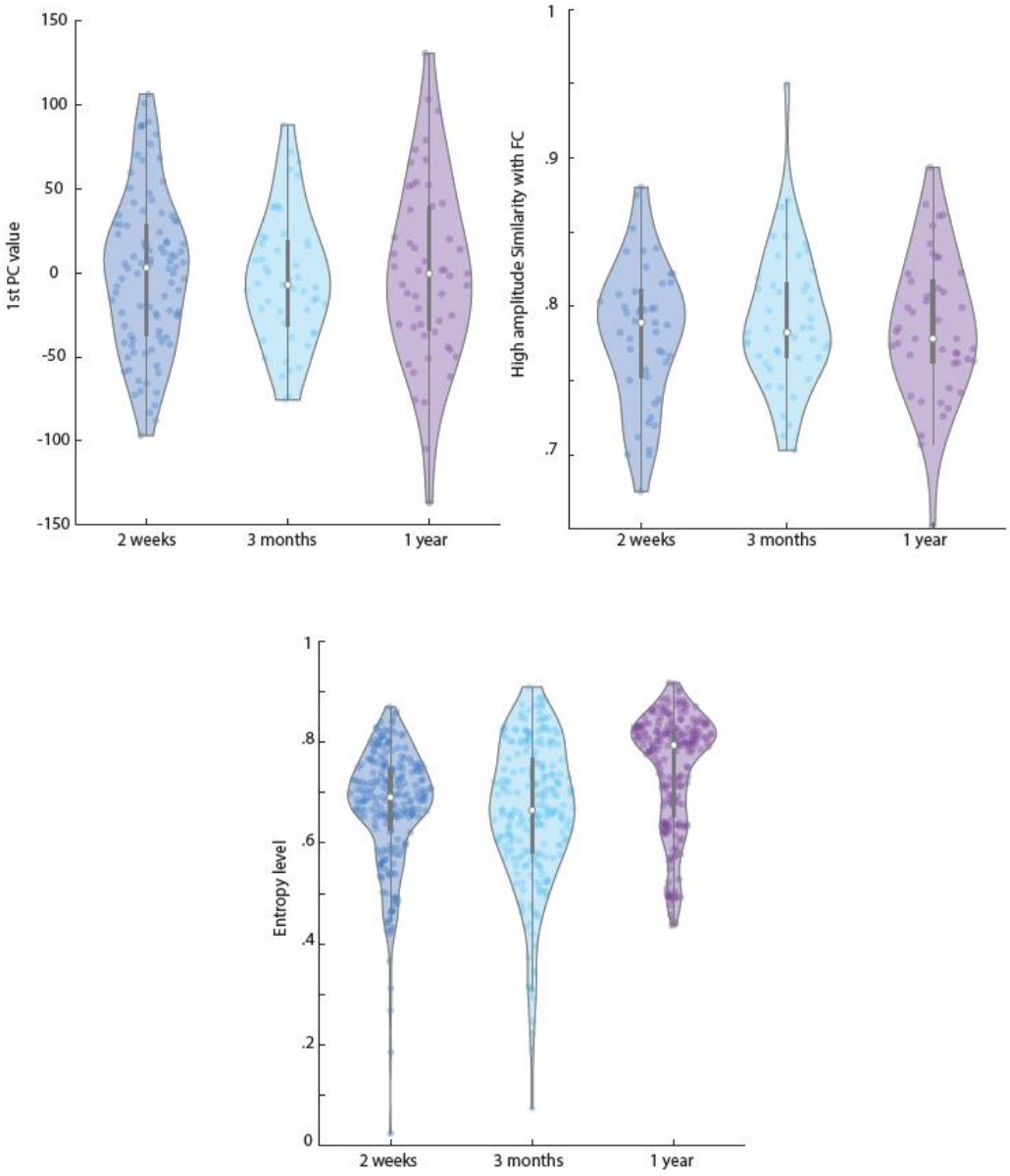

Figure 3.2: Fluctuation across time of principal components, high amplitude co-fluctuations, and entropy

Figure 3.2: Fluctuation across time of principal components, high amplitude co-fluctuations, and entropy: Representation of participants' values at three different time points after stroke (2 weeks, 3 months, and 1 year) for (top-left) the first PC of static nFC, (top-right) high-amplitude similarity with FC and (bottom) the entropy level.

In order to investigate the difference in entropy levels between controls and patients, we compared both groups at each time point. There was a significant difference between patients and controls at time point 1 ($t(468)= 13.78$, $p < 0.01$), timepoint 2 ($t(468)= 10.86$, $p < 0.01$) and time point 3 ($t(468)=5.45$, $p < 0.01$) with the magnitude of the difference between the two groups decreasing over time (**Figure 3.3a**). The increase in normalized entropy and the reduced difference with the control group across time could be interpreted as an indication of recovery.

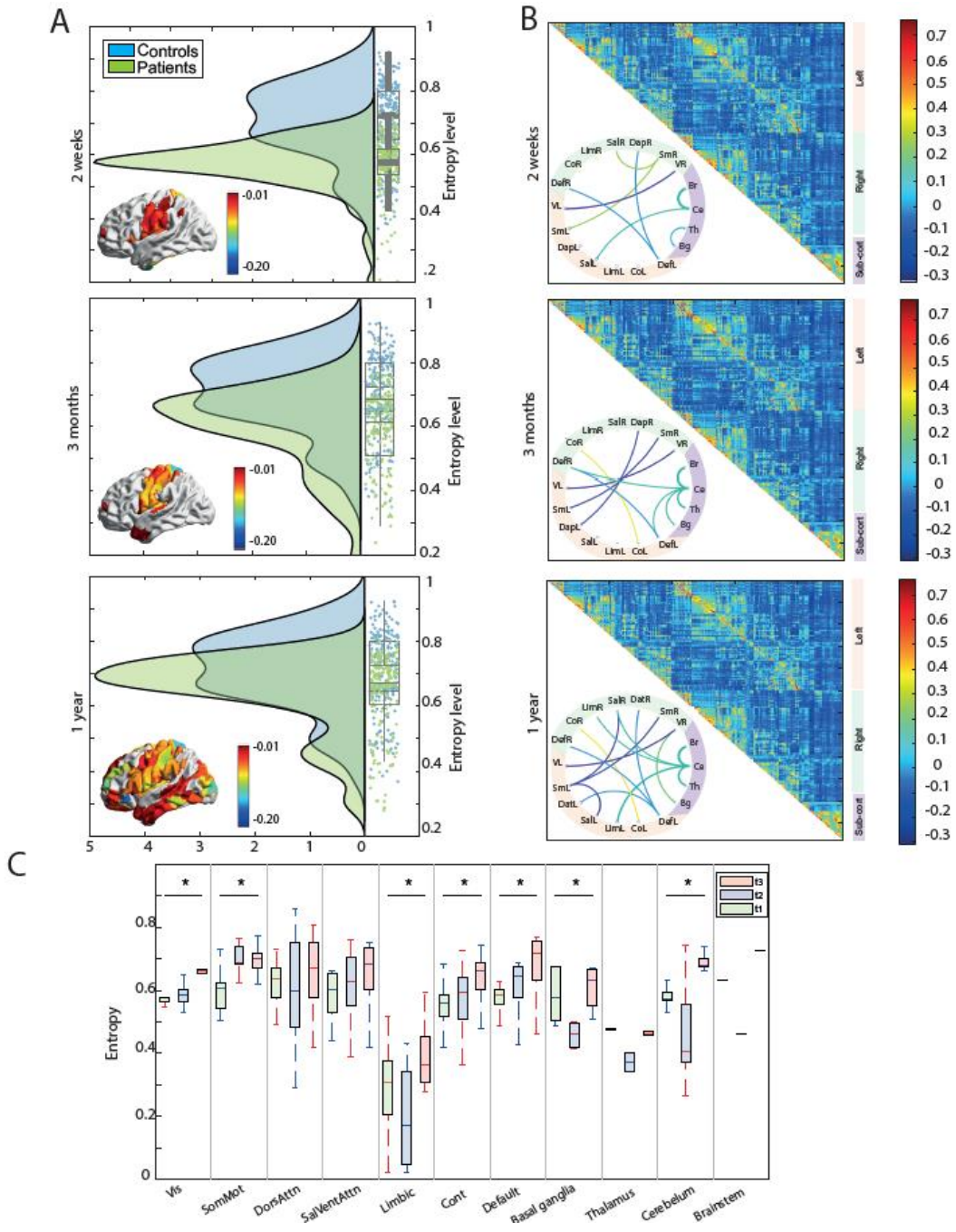

Figure 3.3: Entropy and functional connectivity across time

Figure 3.3: Entropy and functional connectivity across time: **(A)** Comparison of entropy between patients and control at each time point. The difference is visualized in each surface for each node. **(B)** FC at each timepoint with the corresponding communication between the networks. **(C)** Entropy across time segmented by network. Asterisk indicates when the comparison between the three time points is significant. Systems labels: V = Visual; Sm = Somato-motor; Dat = Dorso-attentional; Sal = Salience; Lim = Limbic; Co= Control; Def = Default; Bg = Basal Ganglia; Th = Thalamus; Ce = Cerebellum; Br = Brainstem

When visualizing the difference between patients and controls by node, there were 83 nodes in which the patients had a higher value than the controls in the acute stage (time point 1), 68 at time point 2, and 169 at time point 3 (**Figure 3.3a**). We explored the surface projection of entropy values for each group and both combinations of differences (controls minus patients and patients minus controls) to observe both patterns (**Figure A1**). The localization of differences to individual nodes could prompt future exploration of this topographic pattern. Especially meaningful might be to explore the relationship between these maps and maps that index other topographic properties of the brain including cortical expansion or gene expression. When visualizing the average functional correlation between the networks, 8 connections were preserved at time point 1, 10 connections at time point 2 and 14 connections at time point 3 (**Figure 3.3b**) indicating the recovery of the patients across time.

To analyze the within-network fluctuation of the entropy level, we compared it for each individual network. Several of them revealed a significant difference across time: Visual ($F(2,84) = 6.21$, $p < 0.01$), Somato-Motor ($F(2,102) = 77.45$, $p < 0.01$), Limbic ($F(2,33)=5.87, p < 0.01$), Control ($F(2,87)=4.72, p = .01$), Default ($F(2,135)=13.57, p < 0.01$), Basal ganglia ($F(2,15)=9.26, p < 0.01$) and Cerebellum ($F(2,75)=39.3, p < 0.01$). In contrast, the remaining ones did not expose a significant difference between the different timepoints: Dorsal-Attention ($F(2,75) = 1.58, p = 0.21$), Salience-Ventral ($F(2,63) = 1.47, p = 0.23$), Thalamus ($F(2,3) = 9.43, p = 0.05$), Brainstem ($F(2,1) = 1.32, p = 0.36$)

(**Figure 3.3c**). The majority of the networks revealed an increase across time, indicating that the phenomena could be studied in both global and local ways.

Normalized entropy was found to be negatively associated with stroke metrics although these relations were not significant (lesion volume: R^2 = 0.02, p = 0.37, NIHSS score: R^2 = 0.05, p = 0.163) (**Figure A2a**). Therefore, the participation coefficient was explored as it was shown to have a strong statistical relationship with normalized entropy (Faskowitz et al, 2020).

The participation coefficient was calculated for each patient in order to see its correspondence with the basic stroke severity metrics. Average participation coefficient was related in a significant manner with the lesion volume (R^2 = 0.08, p < 0.01). The same occurred for the NIHSS score (R^2 = 0.05, p =0.04) (**Figure 3.4**). Furthermore, the participation coefficient relation with the stroke metrics was also analyzed in the other two time points showing no significant effect (timepoint 2: lesion volume: R^2 = 0.04, p = 0.13, NIHSS score: R^2 = 0.01, p = 0.63, timepoint 3: lesion volume: R^2 = 0.01, p = 0.47, NIHSS score: R^2 = 0.01, p = 0.42) indicating that this effect is only visible at the acute stage (**Figure A2b**). When comparing participation coefficient between patients and controls, no difference was found for any of the 3 timepoints (**Figure A3**) as opposed to the increasing trend exposed previously by normalized entropy.

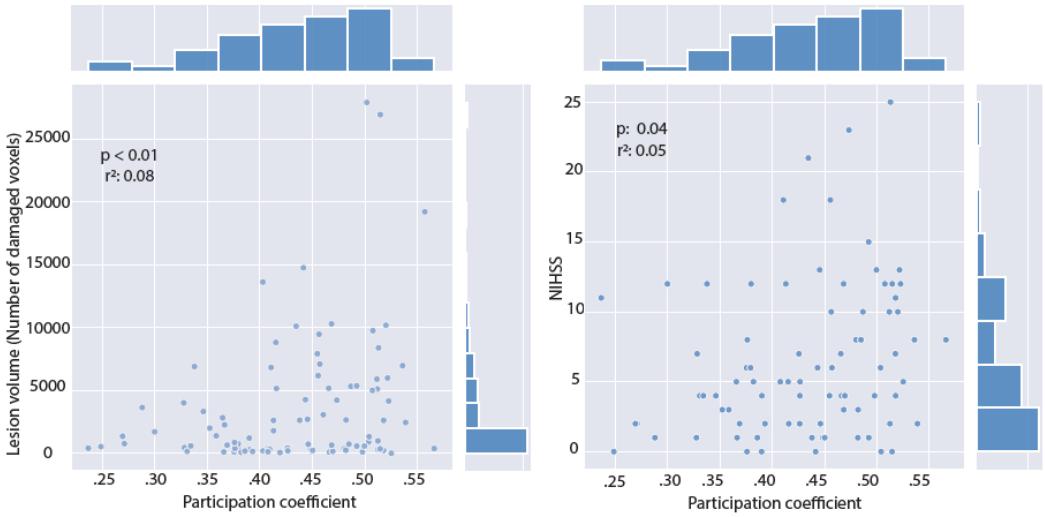

Figure 3.4: Relation of Participation coefficient with stroke metrics

Figure 3.4: Relation of Participation coefficient with stroke metrics: Relationship between the participant coefficient of each patient, (left) their lesion volume (Number of damaged voxels) and (right) their NIHSS score. Lesion volume was calculated based on the topography of the stroke damage using a voxel-wise analysis of structural lesions in order to quantify the amount of damaged voxels. The National Institutes of Health Stroke Scale (NIHSS) includes 15 subtests and was used as a clinical measure of severity for each patient.

The level similarity of the highest 10% data points (ranked by the RSS. For more detail see methods section) with the FC were associated with a significant percentage of the lesion volume ($R^2 = 0.05$, $p = 0.03$). Furthermore, they relate to a significant number of domains recovered ($R^2 = 0.07$, $p = 0.02$) (**Figure 3.5a**). When comparing the correlation with the complete FC, the top 10% data points showed a significantly higher correlation value than the bottom 10% ($t(190) = 39.31$, $p < 0.01$)) (**Figure 3.5b**). We explored the correlation of each decile of data points (i.e.: first 10%, 10% to 20%, and so on) to show the decaying effect of the correlation with the FC (**Figure A4a**). Furthermore, when compared to the other deciles, the highest 10% revealed to have the highest clustering coefficient, global efficiency and assortativity, next to the lowest distance (**Figure A4b**). The relation between each decile

with lesion volume revealed that the only decile with a significant relation is the top 10% (R^2 = 0.05, p = 0.03) while all the others present no significant association (p > 0.2) (**Figure A5**)

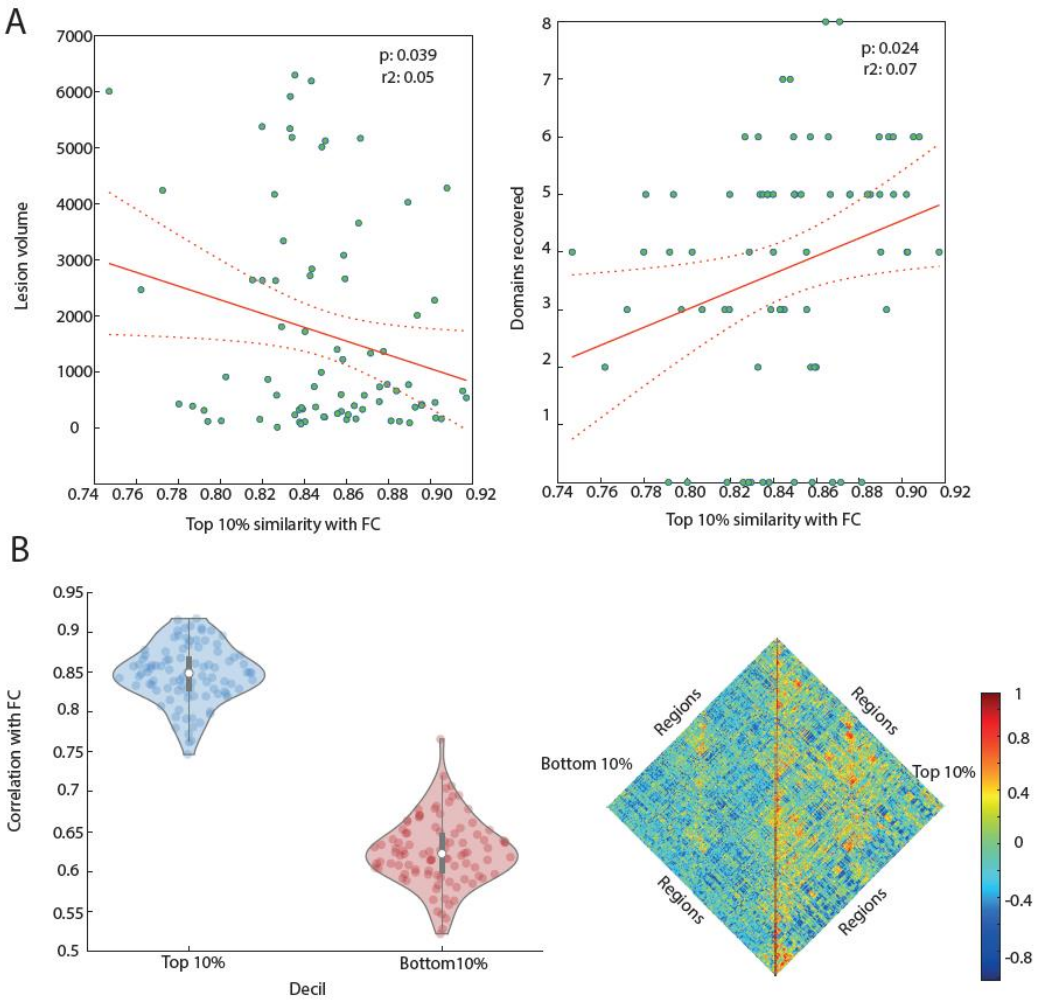

Figure 3.5: High amplitude co-fluctuations' informative value

Figure 3.5: High amplitude co-fluctuations' informative value: **(A)** Association between the 10% highest value of each patient with their corresponding (left) lesion volume and (right) amount of domains recovered after a year. **(B)** Comparison between the top and the bottom 10% FC.

When comparing patients' entropy level according to lesion localization, we found a significant difference between patients with cortical lesions (M = 0.74, SD = 0.12) when compared with the ones with subcortical ones (M = 0.68, SD = 0.12) ($t(468) = -5.13$, $p < 0.01$). In the same way, there is a significant difference between patients with right hemisphere lesions (M = 0.67, SD = 0.09) when compared with the ones with left hemisphere ones (M = 0.60, SD = 0.14) ($t(468) = -6.09$, $p < 0.01$) (**Figure 3.6**), which further illustrates how the topography of normalized entropy can be modulated by clinical factors.

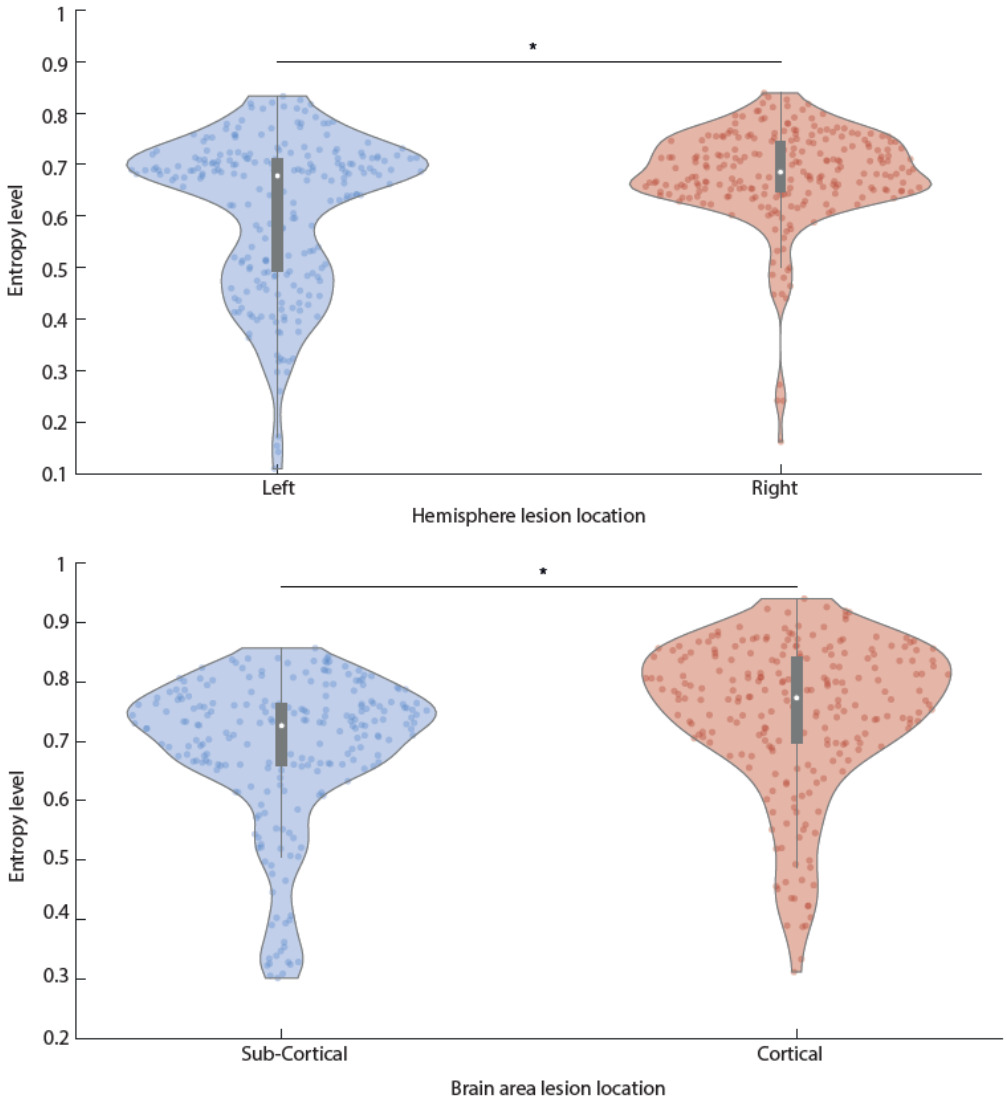

Figure 3.6: Entropy level according to lesion location

Figure 3.6: Entropy level according to lesion location: Comparison in entropy level according to (top) the injured hemisphere and (bottom) the brain area (sub-cortical vs cortical)

3.4 Discussion

In the current study we applied an edge-centric approach to a longitudinal stroke patient dataset. The analysis revealed a relation between the highest values of co-fluctuation with stroke severity and correlated with the number of domains recovered. Furthermore, normalized entropy was shown to increase across patient recovery time, suggesting a potential utility as an indication of recovery. Moreover, normalized entropy was shown to differentiate patients according to the lesion location. Lastly, the participation coefficient's significant relation with stroke metrics adds another useful metric for further exploration. Collectively, this series of edge-centric network analyses demonstrate a novel direction for mapping the brain in a clinical setting. These analyses could potentially point towards improving diagnostic and treatment planning strategies.

3.4.1 Discussion of results

We employ an edge-centric analysis to calculate the normalized entropy of each node (Faskowitz et al., 2020) across stroke recovery. First, we show that the global average of this measure changes across time significantly differently in our stroke sample, relative to the matched healthy control sample (**Figure 3.3a**). Furthermore, these changes in normalized entropy are differentially expressed within a set of canonical functional networks (Schaefer et al., 2018) (**Figure 3.3c**). Regarding the localization of the entropy level, previous studies associated the highest levels of entropy to specific networks (e.g., dorsal-attention or visual networks; (Faskowitz et al., 2020)). In this study we found that the difference between patients and healthy controls (i.e., where patients displayed more evenly distributed edge communities) is localized around the somatosensory cortices for the first two time points, whereas this difference is more diffuse in the third time point. We could speculate that as the stroke recovery process unfolds, edge community

patterns might reconfigure in such a way to promote globally higher entropies. It could be the case that in recovery, edge communities span many nodes more evenly, possibly creating higher entropy at more nodes.

Another factor to take into consideration is the neurovascular coupling disruption produced by stroke (Lin et al., 2011). Therefore, the entropy increase across time could reflect the vascular coupling stabilization, potentially signaling a return to pre-stroke levels, as seen in previous literature (Blicher et al., 2012).

While analyzing the individual normalized entropy scores at the first time point, no significant relationship was found between the patients' globally averaged normalized entropy and stroke metrics. Nevertheless, previous studies showed a strong relationship between this measure and participation coefficient (Faskowitz et al., 2020). It has been found that stroke lesions with damaged gray matter regions and high participation coefficient, had a weak association with cognitive outcomes (Reber et al., 2021; Warren et al., 2014). Previous studies have shown that the participation coefficient reflects, at an areal level, the balance between intra- and inter-modular connections (Sporns et al., 2007). As the participation coefficient was shown to be significantly related with edge community entropy (Faskowitz et al., 2020), we used the measure here to relate to the aforementioned stroke metrics. We found that the participation coefficient was related with the lesion volume and the NIHSS score, revealing its connection with the post-stroke effects. However, in contrast to normalized entropy, we did not find an increasing trend across time of the participation coefficient, exposing one limitation of this specific metric. The fact that normalized entropy correlated with NIHSS score in the expected direction of the effect but not in a significant way, opens the door to debate if the metric might not be beneficial for this specific brain disorder. One possibility would be that participation coefficient is only applied to positive weights whereas the normalized entropy is based in edge communities that

annotate all edges regardless of their sign. In order to answer this question, further studies should be developed using other clinical populations to demonstrate the relation between their severity metrics and normalized entropy and/or participation coefficient.

Previously, studies have tried to localize the spatial components of normalized entropy. In those studies, the brain systems associated with the highest levels of normalized entropy included visual, attentional, somatomotor and temporoparietal systems (Faskowitz et al., 2020). These findings were replicated in another study finding that overlap is greatest in primary sensory and attentional systems and lowest in association cortices (Jo, Esfahlani, et al., 2021). The current study is the first one to examine the distinct entropy pattern regarding stroke lesion by comparing subjects with lesions in different hemispheres (left vs right) and lesion depth (cortical vs subcortical). The findings presented here open the way for further research to explore the use of these metrics to explore brain organization of this disorder.

3.4.2 Relationship to other methods

Recent works has shifted the attention from regions to networks damaged under stroke circumstances (Boes, 2015). Along these lines, we explore the edge-centric brain dynamics and its fluctuation across time in the different functional networks (**Figure 3.3c**). The shift from node communities to edge communities provides a novel, and complementary, approach to inspect the brain dynamics in a disorder that not only affects the brain locally, but globally. In order to compare the obtained results with existing literature of the field, we analyze widely used metrics from a previous study (Pustina et al., 2017) and assessed their modulation across time (**Figure A7**). As the current study uses functional data, a threshold was needed to calculate these corresponding network metrics.

One of the metrics used in this study, normalized entropy, was previously compared to other measures of overlap, like flexibility and versatility (Bassett et al., 2011; Betzel et al., 2020; Faskowitz et al., 2020; Shinn et al., 2017). Furthermore, a previous study linked structural lesions in simulated stroke networks by measuring the diversity of weights at each node (Saenger et al., 2018). Here, we added to this understanding by constructing a topographic map of entropies derived from the range of edge community affiliations at each node. The entropy metric here provides a time-averaged index of the diversity of dynamic edge co-fluctuation patterns emanating from each node. Future work should focus on the intersection between these dynamic patterns and the underlying anatomical structure (Davison et al., 2015; Liu et al., 2021), particularly in a clinical context.

Previous literature introduced related approaches such as quasi-periodic patterns (QPPs), which represent repeating spatiotemporal patterns of neural activity of predefined temporal length (Adhikari et al., 2020). The QPP involves propagation of activity in the default mode and task positive networks of the brain (Abbas et al., 2019). As in similar approaches (Petridou et al., 2013) they require picking a seed for its analysis, adding a subjective component to the process in contrast to the edge-centric approach which requires no seed. A similar technique showed that fMRI signals could be represented by a sparse spatiotemporal point process where the inflection points contained most of the signal's information (Cifre et al., 2020) in a similar way as presented in the high amplitude co-fluctuations on this study.

Previous studies proposed the use of obtained fine-scale dynamics by observing brief and intermittent episodes of high-amplitude co-fluctuations involving large sets of brain regions (Rabuffo et al., 2021; Zamani Esfahlani et al., 2020). In a similar way, a common approach to extract and cluster voxel- or vertex level activity during high-activity frames is the co-activation

patterns, also known as CAPs (Karahanoglu & Van De Ville, 2015; Liu & Duyn, 2013). It is relevant to mention that while RSS co-fluctuations and CAPs are similar in some ways, our method is nonetheless distinct and has unique advantages. Most importantly, our method is built upon a mathematically exact decomposition of static rsFC into its frame-wise contributions. This decomposition enables us to quantify, precisely, how individual time points impact static rsFC. Furthermore, our method does not rely on sliding time windows nor step-size parameters. Even more, the decomposition does not require that we select a seed region or brain system in advance. Rather, our decomposition method considers all activity levels and the entire network simultaneously (Liu et al., 2021; Zamani Esfahlani et al., 2020). These studies show how dynamic information could be utilized to analyze case-control differences in a clinical neuroimaging setting.

Nevertheless, a remaining open question concerns the neurobiology underlying high-amplitude co-fluctuations, and how the resultant topography of the observed changes relates to stroke recovery at the neurological level. On one hand, their infrequent occurrence could reflect a dynamic strategy for limiting the consumption of metabolic resources. On the other hand, high-amplitude frames are suggested to be, to some extent, a mathematical necessity emerging in correlated, modular systems (Novelli & Razi, 2021). Another study presented a generative model for high-amplitude co-fluctuations in silico using computational simulations of whole-brain dynamics and demonstrated that such high-amplitude patterns have an origin in modular structural connections (Pope et al., 2021). This leads to the suggestion that these intermittent events are partly shaped by modular organization of structural connectivity indicating a potential overlap of functional and structural information (Liu et al., 2021; Pope et al., 2021; Rabuffo et al., 2021; van Oort et al., 2018). There is a concern that the high-amplitude co-fluctuations in the cortical activity that drive the nFC could be artifacts, potentially specific to fMRI. This has been mitigated by evidence

showing that the high-amplitude events in the RSS of the edge time series are not systematically related to confounding variables including in-scanner motion, respiratory and heart rate (Zamani Esfahlani et al., 2020), and they readily appear in computational simulations (Pope et al., 2021; Rabuffo et al., 2021; Wang et al., 2018).

Based on these conclusions, we performed the analysis using this approach and we found how the highest ten percent of the data values, (sorted based on the RSS co-fluctuations) not only were associated with the lesion volume after stroke but also related to the number of cognitive domains in the patients' recovery (**Figure 3.5**). The ability to inform about the recovery of the subjects suggests that the information contained in this subset of the data could be more explanatory than previously believed.

While its contributions compared to the nFC are still debated, it has been proposed that the RSS peaks not only occur when the Euclidean norm of the BOLD signal is large but, most likely, when the expressed spatial mode is well aligned with the leading eigenvector of the nFC. The leading eigenvector of the static nFC matrix could also be obtained as the first component of the BOLD activity, being mathematically equivalent (Novelli & Razi, 2021). The fluctuation of the first principal component value at each time point and the edge-centric derived metrics (top amplitude co-fluctuations and normalized entropy) reveals how the first two stages maintain consistency across time while the third stage has an increasing trend across time (**Figure 3.2**). The similarities between the edge-centric approach and the principal components analysis of the node-centric approach reveal the strengths of the first one such as its simplicity or not needing any assumption used in sliding-window approaches (Novelli & Razi, 2021; van Oort et al., 2018). The normalized entropy fluctuation across time could refine our theoretical understanding of the patients' recovery after suffering a stroke.

3.4.3 Limitations

Even though **Figure A8** shows possible variations in the results, an assumption of the bootstrap procedure is that population variation can be estimated from resampling from the available data. However, the present dataset contains, in general, relatively small lesions. With this in mind, we note that we are not able to make a confident prediction about how these results could be extrapolated to a dataset consisting of patients with larger lesions.

The edge-centric approach involves a much larger dimensionality than the most-common node-centric methods. In particular, clustering a full eFC matrix, of size edge-by-edge, is impractical on personal computing hardware. To circumvent this, the edge time series, of size edge-by-time, can be clustered directly using k-means. However, this computational “shortcut” precludes the usage of other community detection methods, such as modularity maximization that operate on networked data (i.e., a “square” adjacency matrix).

Furthermore, the interpretation of the edge-community structure remains open to interpretation, and the cognitive relevance of these communities has yet to be established. Lastly, throughout this study, the comparison of functional signals was done in an undirected manner. Measures such as correlation cannot determine the directionality of influence between signals. Further studies could analyze the effect of these metrics in asymmetrical networks to benefit from their directionality, such as the ones used in effective connectivity.

3.4.4 Future directions

Even if the current study is not focused on improving predictability of stroke recovery, we provide novel fMRI connectivity methods that could be used in the future for that purpose. Given that the eFC matrix can be employed to boost the identifiability of fMRI data (Jo, Faskowitz, et al., 2021), future work could explore if similar improvements to predictive models could be obtained using eFC and related edge-centric data structures.

The current study demonstrates that relations derived from computational and theoretical research on the human connectome can help to advance our understanding of how focal brain lesions are modulated across time. Additionally, these data show the emerging possibility of how network neuroscience and connectomics can contribute to clinical advances. By using the same techniques, future studies could try to replicate these results by studying similar brain disorders in which a typical recovery pattern is expected.

The inclusion of animal models could also add more robustness to the edge-centric approach providing a natural bridge for testing external manipulations and measuring how these metrics are affected by different system complexities. Furthermore, computational models could contribute to this goal by simulating whole-brain connectivity and adding additional information of network interactions.

3.5 Conclusions

In conclusion, this study added new evidence for the role of the edge-centric approach as a promising bridge between structure and function. Also, it revealed how edge-centric analysis provides indicators that relate to lesion severity and reveal lesion recovery, making it the first study taking an edge-centric approach with clinical applications across time.

CHAPTER 4

4. Function and anatomy integration: Inferring the dynamical effects of stroke lesions through whole-brain modeling

Work in this chapter is based on the following publication:

Idesis, S., Favaretto, C., Metcalf, N. V., Griffis, J. C., Shulman, G. L., Corbetta, M., & Deco, G. (2022). Inferring the dynamical effects of stroke lesions through whole-brain modeling. *NeuroImage: Clinical*, 103233.

Highlights

- We derived a causal mechanistic generative whole-brain model to explain the functional and behavioral consequences of stroke lesions
- The model got enhanced by adding structural disconnection masks
- The model classified behavioral impairment severity with higher accuracy than empirical data
- We showed how network dynamics changes emerge after a stroke injury

Abstract

Understanding the effect of focal lesions (stroke) on brain structure-function traditionally relies on behavioral analyses and correlation with neuroimaging data. Here we use structural disconnection maps from individual lesions to derive a causal mechanistic generative whole-brain model able to explain both functional connectivity alterations and behavioral deficits induced by stroke . As compared to other models that use only the local lesion information, the similarity to the empirical fMRI connectivity increases when the widespread structural disconnection information is considered. The presented model classifies behavioral impairment severity with higher accuracy than other types of information (e.g.: functional connectivity). We assessed topological measures that characterize the functional effects of damage. With the obtained results, we were able to understand how network dynamics changes emerge, in a nontrivial way, after a stroke injury of the underlying complex brain system. This type of modeling, including structural disconnection information, helps to deepen our understanding of the underlying mechanisms of stroke lesions.

Keywords

Dynamical effects; Generative model; Stroke; Structural Disconnection mask; Whole-brain model

4.1 Introduction

In the last two centuries, the study of patients with focal brain lesions has been the main approach for understanding brain organization and localization of function (Bates et al., 2001; Broca, 1861; Corbetta et al., 2015; Karnath et al., 2018; Mesulam, 1981). More recently, nonetheless, it has become apparent that focal lesions cause widespread abnormalities of brain network activity that correlate with cognitive deficits and recovery of function (Corbetta et al., 2018; He et al., 2007; Ovadia-Caro et al., 2013; Siegel et al., 2016; Wang et al., 2019). In parallel new methods have been developed to map lesion-related patterns of disconnection, either structural (Foulon et al., 2018) or functional (Boes, 2015), not directly, but using clinical scans and normative connectomes. However, which signals provide the most accurate prediction of cognitive impairments and recovery of function remains controversial (Bowren et al., 2022; J. C. Griffis et al., 2019; Salvalaggio et al., 2020; Weiss Cohen & Regazzoni, 2020).

Correlational studies as those discussed above do not provide a clear mechanistic understanding of how brain lesions affect information processing. A recent development -whole-brain models- use biologically plausible structural connectivity coupled with a local model of activity as the input for the generation of global dynamics, and can thus be used to understand the effect of damage on global (whole brain) dynamics (Adhikari et al., 2017; Cabral et al., 2012; Cofré et al., 2020; Kringelbach et al., 2020; Saenger et al., 2018). Early attempts used volume and location information to modify a healthy structural connectome to approximate the effect of lesions and fitted the yielded global dynamics to the patient's own blood oxygenation level-dependent (BOLD) signals measured with functional magnetic resonance imaging (fMRI) (Adhikari et al., 2017; Saenger et al., 2018). These studies showed that focal lesions cause a decrease in both segregation and

integration at rest, as well as a decrease in neural state variability or entropy during stimulation.

In this study, we innovate whole-brain models of stroke lesions in two ways. First, we optimize the whole brain model (Deco et al., 2017; Jobst et al., 2017) by converting it into a generative model to yield a Generative Effective Connectivity (GEC). We described the model as 'generative' since the underlying BOLD signals are generated from the model. In contrast to functional connectivity (FC) that describes the statistical interactions between regions, and structural connectivity (SC) that describes the undirected anatomical links between two brain regions, GEC describes causal pairwise interactions that show the influence one region exerts over another in a directed way (Gilson et al., 2016). EC links are directional and provide information on asymmetrical regional pairwise temporal interactions. Second, crucially, we take into consideration the effect of lesions on the structural connectome that are driven by direct damage to the white matter, rather than focusing solely on the connections of damaged grey matter regions. On average, a stroke is expected to cause disconnection in about 20% of all brain connections based on diffusion imaging connectomes (Joseph C Griffis et al., 2019). Moreover, lesions that directly disconnect brain regions and/or interrupt intermediate links between brain regions are the main sources of FC abnormalities after stroke (J. C. Griffis et al., 2019; Griffis et al., 2021). Hence, the whole brain model is adjusted in terms of its input connectivity by the pattern of SC disconnection computed in each patient.

To validate the use of GEC whole-brain models, we compare GEC to SC or FC models for the prediction of stroke-related deficits. Recent studies have reported a higher predictive value of GEC over FC in normal or pathological conditions, such as epilepsy or addiction (Hejazi & Nasrabadi, 2019; Pallarés et al., 2018; Wei et al., 2021). Other studies have used machine learning to compare the prediction of neurological deficits (motor, language, attention,

etc.) based respectively on lesion location, SC, or FC disconnection computed indirectly in normative atlases (Pini et al., 2021; Salvalaggio et al., 2020). These studies found fairly accurate predictions for lesion and SC disconnection, not for FC disconnection. More clinically oriented studies have applied automatic classification methods to grade the severity of the stroke lesion (Acharya et al., 2019; Govindarajan et al., 2020; Sprigg et al., 2007).

In the current study, we implemented a classifier to distinguish the performance of stroke patients on different neuropsychological tasks by comparing prediction accuracy based on SC, FC, or GEC models. Furthermore, by taking advantage of the asymmetric property of the GEC, we measured the topology of graph measures in healthy and stroke patients. Treating the whole-brain models as a complex cluster of networks with nodes and edges characterized by global integration and local specialization (Tononi et al., 1994), we measured changes in graph topology to understand how network dynamics change after a stroke injury (Adhikari, Belloy, et al., 2021; Vecchio, Caliandro, et al., 2019). Overall, the results show the importance of white matter structural disconnection for the accuracy of whole brain models of dynamics in stroke.

4.2 Material and methods

4.2.1 FC measures

Based on previous work (J. C. Griffis et al., 2019; Siegel et al., 2016) we defined three measures that are consistently impaired in stroke patients:

1. Intra-hemispheric FC: average between pairwise FC of Dorsal attention network (DAN) and Default mode network (DMN) regions.
2. Inter-hemispheric FC: average homotopic inter-hemispheric connectivity within each network
3. Modularity: overall Newman's modularity among cortical networks, which is a comparison between the number of connections within a module to the number of connections between modules (Newman & Girvan, 2004)

4.2.2 Alternative lesion disconnection mask

In addition, for the analysis of the FC impairments metrics, a second mask (For the original mask, see chapter 2) based on gray matter damage, was tested as a control (gray matter in **Figure 4.2**). Inspired on a previous study (Adhikari et al., 2017) we applied a disconnection mask measuring all connections incoming or outgoing from the damaged cortical parcels. In other words, the mask for each patient included all links observed in healthy controls except those from and to a node with 100% grey matter damage (Adhikari, Griffis, et al., 2021). The two masks therefore capture damage of white matter connections to/from the damaged gray matter or capture more directly the disconnection induced by both gray matter and white matter damage. Since many stroke lesions occur predominantly in the white matter or include both a gray and white matter component, the SDC mask shall provide a more accurate description of the damage to the connectome. It is

important to realize that, for the lesions that were only subcortical, no gray matter damage was computed, revealing a huge limitation of the gray matter mask (See Section 2.5).

4.2.3 Whole-brain Hopf model parameter estimation

We simulated the BOLD activity at the whole-brain level by using the Hopf computational model, which simulates the dynamics emerging from the mutual interactions between brain areas, considered to be interconnected based on the established graphs of anatomical SC (Deco et al., 2017; Kringelbach et al., 2015). The structural connectivity matrix was scaled to a maximum value of 0.2 (Deco et al., 2017), leading to a reduction of the parameter space to search for the optimal parameter. We calculated the global scale coupling value factor, G, which assesses the influence of the SC on the model. We selected the optimal value in which the model phases were more like the empirical data. The model consists of 235 coupled dynamical units (ROIs or nodes) representing the 200 cortical and 35 subcortical brain areas from the parcellation. The local dynamics of each brain area (node) are described by the normal form of a supercritical Hopf bifurcation, also called a Landau–Stuart oscillator, which is the canonical model for studying the transition from noisy to oscillatory dynamics (Kuznetsov, 1998). When coupled together using brain network anatomy (Explained above in the “Neuroimaging acquisition and preprocessing” section), the complex interactions between Hopf oscillators have been shown to successfully replicate features of brain dynamics observed in fMRI (Deco et al., 2017; Kringelbach et al., 2015).

The calculation of the local dynamics of each individual node is able to describe the transition from asynchronous noisy behavior to full oscillations. Thus, in complex coordinates, each node j is described by following equation: (For more information, see Deco et al., 2019)

$$\frac{dz_j}{dt} = z(a_j + i\omega_j - |z_j|^2) + g \sum_{k=1}^{N} C_{jk}(z_k - z_j) + \beta\eta_j, \qquad (4.1)$$

Where

$$z_j = p_j e^{i\theta} = x_j + iy_j \qquad (4.2)$$

α and ω are the bifurcation parameters and the intrinsic frequencies of the system, respectively. This normal form has a supercritical bifurcation at a_j = 0. Within this model, the intrinsic frequency ω_j of each node is in the 0.04–0.07Hz band (i=1, …, n). The intrinsic frequencies were estimated from the data, as given by the averaged peak frequency of the narrowband BOLD signals of each brain region. The variable g represents a global coupling scaling the structural connectivity C_{jk}, and η is a Gaussian noise vector with standard deviation $\beta = 0.04$. This model can be interpreted as an extension of the Kuramoto model with amplitude variations, hence the choice of coupling $(z_k - z_j)$, which relates to a tendency of synchronization between two coupled nodes. We insert equation 4.2 in equation 4.1 and separate real part in equation 4.3 and imaginary part in equation 4.4 (Deco et al., 2017).

$$\frac{dx_j}{dt} = (a_j - x_j^2 - y_j^2)x_j - \omega_j y_j + G \sum_{\iota} C_{jk}(\chi_j - x_j) + \beta\eta_j(\tau) \qquad (4.3)$$

$$\frac{dy_j}{dt} = (a_j - x_j^2 - y_j^2)y_j + \omega_j x_j + G \sum_{\iota} C_{jk}(y_j - y_j) + \beta\eta_j(\tau) \qquad (4.4)$$

It is important to clarify that for the GEC+SDC model, the SDC information was added to the structural connectivity in order to enhance the optimization of it (See section “Lesion disconnection mask” in Chapter 2).

4.2.4 Generative Effective Connectivity calculation

The analysis of GEC incorporates an indirect metric (as it is derived from other presented metrics) into the whole-brain model to replace the existing descriptive metrics of FC and SC. Previous studies have shown how GEC is fundamental to understand the propagation of information in structural networks (Gilson et al., 2016; Jobst et al., 2017). Methods for estimating GEC are explained in detail in a previous publication (Deco et al., 2019). Briefly, we computed the distance between our model and the empirical grand average phase coherence matrices (as a measure of synchronization of the system) of the healthy controls group. In the stroke patients' group, we adjusted each structural connection separately using a greedy version of the gradient-descent approach. In order to work only positive values for the algorithm, all values are transformed into a mutual information measure (assuming Gaussianity). Therefore, the individual subject information is introduced by means of its disconnection (SC + each subject SDC) derived with the LQT. The equation of the optimization is as follows (For more information, see Deco et al., 2019)

$$C_{ij} = C_{ij} + \varepsilon\left(FC_{ij}^{phases\_emp} - FC_{ij}^{phases\_mod}\right) \quad (4.5)$$

Where "C" is the anatomical connectivity and is updated with the difference between the grand-averaged phase coherence matrices (Empirical: $FC_{ij}^{phases\_emp}$ and model: $FC_{ij}^{phases\_mod}$, scaled by a factor ε < 0.001). The prediction, therefore, is based on the current estimation of the structural connectivity, which gets updated optimizing the phase FC in each iteration. In summary, the model was run repeatedly with recursive updates of GEC until convergence was reached.

The distinction between functional and effective connectivity is crucial here: FC is defined as the statistical dependence between distant neurophysiological activities, whereas GEC is defined as the influence one neural system exerts over another providing directionality in the relations making the matrices asymmetrical (Friston, 2011; Friston et al., 2003).

In the current study, we also added the structural disconnection masks (previously mentioned in this section) to the structural connectivity information provided by the simulations. Therefore, different models were used in the analysis (**Figure 4.1a**).Only using the structural information (SC-based model), using the effective connectivity information (GEC-based model) and lastly, using the effective connectivity information plus the structural disconnection mask information (GEC with SDC mask model). For the last one, the optimization benefited from the information of the SDC when optimizing the model.

4.2.5 GEC correlation with clinical and behavioral variables

Based on the work of (Favaretto, 2022) , we tested whether the GEC measures added some significant information to the obtained results from the static FC and dynamical FC combination in describing the behavioral outcome. We calculated the dynamical functional states (DFSs) using a sliding—window temporal correlation (window width=60s, window steps=2s) followed by eigenvector decomposition and clustering to establish the connectivity states that continuously activate across time. By construction, only one of the DFSs was active for each sliding window. The dynamic of the FC for each patient could be described in terms of a single time series of discrete values that alternate across time. In other words, a DFS is a spatial map of the edges between brain regions which shows consistent co-modulation in time (Cabral, Kringelbach, et al., 2017; Cabral, Vidaurre, et al.,

2017). Only a subset (n=44) of the subjects was used for the DFSs analysis. The subset was made in order to use patients that were not employed for the principal components analysis. For more information, see (Favaretto, 2022). For each domain score, lesion volume, and total NIHSS score, we estimated the parameters of a Generalized Linear Model (GLM) with the Effective connectivity static principal components (SPCs) as the regressor and each behavioral score as output. We retained only SPCs which explained at least 5% of the total variance, and that corresponded to an eigenvalue of the covariance matrix larger than 1, yielding to 2 SPCs. Therefore, for the regressor, we used the first two PCs (explaining 32% and 12% of the variance of the original data, respectively) adding to a total of 44% of the variance explained. Then, we estimated the GLM with both SPCs from the GEC and three dynamical PCs scores obtained from the above DFSs as regressors. The dynamical PCs scores capture numerous measures related to dynamical functional connectivity (Favaretto, 2022). It is relevant to clarify that the DFSs were added to the result of the models and were not computed every time.

The behavioral domains' assessment was described more in detail in the "Neuropsychological and behavioral assessment" section. We used all the regressors (static in combination with dynamic) at the acute stage to estimate the behavioral scores. No adjustments were necessary as the number of regressors was kept constant. In other words, as the comparison was made within the SPCs and within the SPCs + dyn PC, but not between them, the amount of regressors was the same in each comparison and therefore, not requiring any correction to solve difference in their quantity of variables.

4.2.6 Classification procedure

We tested how GEC classification differs from other models using SC and FC as division criteria. The subjects were split into two equal groups by using the

corresponding medians of SC lesion (number of damaged voxels in the lesion) and FC principal components. Therefore, our results could be compared with those of previous studies. The same procedure was performed with the principal components of two different models (GEC and the GEC + SDC mask) to end up with the four separation criteria (SC, FC, GEC, and GEC + SDC). To achieve this classification, we used the neuropsychological scores to classify patients who were divided based on their median split, applying a random forest algorithm.

Briefly, the random forest algorithm builds upon the concept of a decision tree classifier, where samples are iteratively split into two branches depending on the values of their features (Breiman, 2001; Sanz Perl et al., 2021).

We trained and evaluated a random forest classifier to distinguish different levels of severity, estimated based on the neuropsychological test results. We used the neuropsychological scores (see “Neuropsychological and behavioral assessment” in chapter 2) as features to classify using a random forest algorithm whether patients belonged to the low severity or high severity group based on the above criteria (SC, FC,EC, GEC+SDC). Dividing the dataset by using the median of:

1) The lesion volume obtained from the SC segmentation (from the lesion itself) indicating the number of voxels affected by the lesion.
2) The summation of the singular values of the first two PCs obtained from the FC information.
3) The summation of the singular values of the first two PCs obtained from the GEC information.
4) The summation of the singular values of the first two PCs obtained from the GEC information (with the SDC mask).

We trained random forest classifiers with 1000 decision trees using 80% of the subjects through cross-validation analysis. Different training criteria were calculated and presented in **Figure B5**. All accuracies were determined as the area under the receiver operating characteristic curve (AUC) (For more information, see (Sanz Perl et al., 2021)).

4.2.7 Topological measurements

The directionality of GEC opens the field to explore various topological attributes that cannot be done or are less informative in symmetrical and undirected networks such as the FC. In the current study we introduce a small group of these metrics:

1) Broadcasters' percentage was calculated as the mean of the number of successors (number of nodes forming directed edges from which the node is the source, without counting the reciprocal relations) divided by the amount of the neighbors (all the nodes connected, disregarding the directionality). A connection is labeled as reciprocal when the number of successors and receivers are the same, while a connection is directed when these values are not identical.

$$Broadcasters'percentage = \frac{Succesors(excluding\ reciprocal\ relations)}{Amount\ of\ neighbors} \quad (4.6)$$

2) Receivers' percentages were obtained in the same way but with predecessors (number of nodes forming directed edges from which the node is the target, without counting the reciprocal relations) instead of successors.

$$Receivers'percentage = \frac{Predecessors(excluding\ reciprocal\ relations)}{Amount\ of\ neighbors} \quad (4.7)$$

3) Broadcasters' amount was calculated by counting how many nodes were having a higher weight of outgoing information than incoming and then average across patients.

$$Brodcasters'amount = \sum nodes\,, if\ Succesors > Predecessors \quad (4.8)$$

4) The receivers' amount was calculated by counting how many nodes were having a higher weight of incoming information than outgoing and then average across patients.

$$Receivers'amount = \sum nodes\,, if\ Succesors < Predecessors \quad (4.9)$$

5) Reciprocity was calculated by obtaining the ratio between reciprocal connections and the total amount of neighbors of the corresponding node. Since the GEC estimation procedure set some directional connections to zero, reciprocity is present in fewer connections than in FC calculations.

$$Reciprocity = \frac{Reciprocal\ relations}{Amount\ of\ neighbors} \quad (4.10)$$

6) Average path length was calculated as the mean distance of the nonzero values of the network. of the Effective Connectivity Matrix (ECM)

$$Distance\ matrix = \min\left(Distance(ECM)\right) \quad (4.11)$$

7) Communicability was used to calculate the relation between different nodes by using the shortest path of the Effective Connectivity Matrix (ECM)

$$Communicability\ matrix = \frac{ECM - Min(ECM)}{\max(ECM) - \min(ECM)} \quad (4.12)$$

4.2.8 Lesion assessment based on region interaction

To analyze the interaction between brain regions, each patient's structural connectivity matrix was segmented into three different groups: The intersections connecting cortical nodes with other cortical nodes, cortical nodes with sub-cortical nodes, and finally subcortical nodes with other subcortical nodes. The association between each of three different groups and other variables of interest was inspected. For assessing the value of each group, three different approaches were used, giving similar results. These approaches consisted of total disconnection (how many nodes were completely disconnected), partial disconnection (percentage of disconnection of nodes that were not completely disconnected), and the combination of both. As in previous sections, the relationship between the variables was assessed without performing any type of prediction.

4.3 Results

We derived a whole brain model to infer the dynamical effects of stroke lesions two weeks after onset. We calculated four different models: First, a healthy control model (without GEC) and a healthy control model (with GEC) based on a healthy atlas structural connectome (see methods) in combination with individually measured fMRI BOLD signal. A variation of the second one was calculated for a posterior comparison using the stroke patients' fMRI BOLD signal instead of the previously mentioned healthy control fMRI BOLD signal (referred as SC-model). Also, a stroke model with GEC (referred as GEC-Model) integrates the healthy connectome with each patient fMRI BOLD signal in order to use the resulting GEC as input for the model. Lastly, the Stroke model with GEC + SDC (referred as GEC+SDC model) integrates the healthy connectome weighted for stroke patients, by the structural disconnection produced by each individual lesion (one connectome per patient) next to each patient fMRI BOLD signal as input for the model. In contrast, one structural connectome was used for the healthy subjects as an average for the entire group based on the Yeo atlas (Yeo et al., 2011). To render the connectome directional, it was adjusted by the phase differences between regions computed on group average functional connectivity data. Then, we estimate the computational model based on coupled Stuart Landau oscillators (**Figure 4.1a**). The presented model contains a global scale factor, also referred as the G coupling value, which assess the influence of the SC in the model. We selected the optimal value in which the model phases were more similar to the empirical data. As the optimal model fit (simulated FC to empirical FC) is dependent on the global coupling, in the current study, we use the healthy control dataset to calculate this parameter. The result was a value of 3.1 as the most efficient for the used model, obtained by a parameter sweep of the homogeneous parameter space (a, G) around the Hopf bifurcation (a ≈0). It is important to clarify that the G value is a scaling factor

of the SC, which was adjusted in the model through iterations for each subject.

We developed an effective connectivity (GEC) model in healthy controls and adjusted it in stroke patients to account for different descriptions of the structural damage. GEC captures directional interactions between regions of the brain. In the healthy control group, we computed the distance between the model and the empirical grand average phase coherence matrices obtained from the empirically measured fMRI signals. In stroke patients' group, we adjusted each structural connection separately using a greedy version of the gradient-descent approach. The resulting GEC (**Figure 4.1a**) reveals the influence of one region over another in a direct way and provides information of asymmetrical regional pairwise temporal interactions. The model fitting was assessed for each patient in order to represent the similarity between the simulated and the empirical data at the subject level (**Figure 4.1b**).

By using a principal component analysis (PCA) of the resulting GECs, we calculated the relation between the main components and behavioral performance of the stroke patients (**Figure 4.1c**). Furthermore, we classify the level of damage severity using a machine learning algorithm (Random Forest classifier), revealing the enhanced performance compared to approaches used in previous studies. Finally, we calculated graph topological metrics in order to show how network dynamics change after a stroke injury.

The presented mechanistic generative whole-brain model reveals the consequences of the stroke lesions by benefiting from structural disconnection maps revealing the importance of the anatomical connectivity disruption at the subject level.

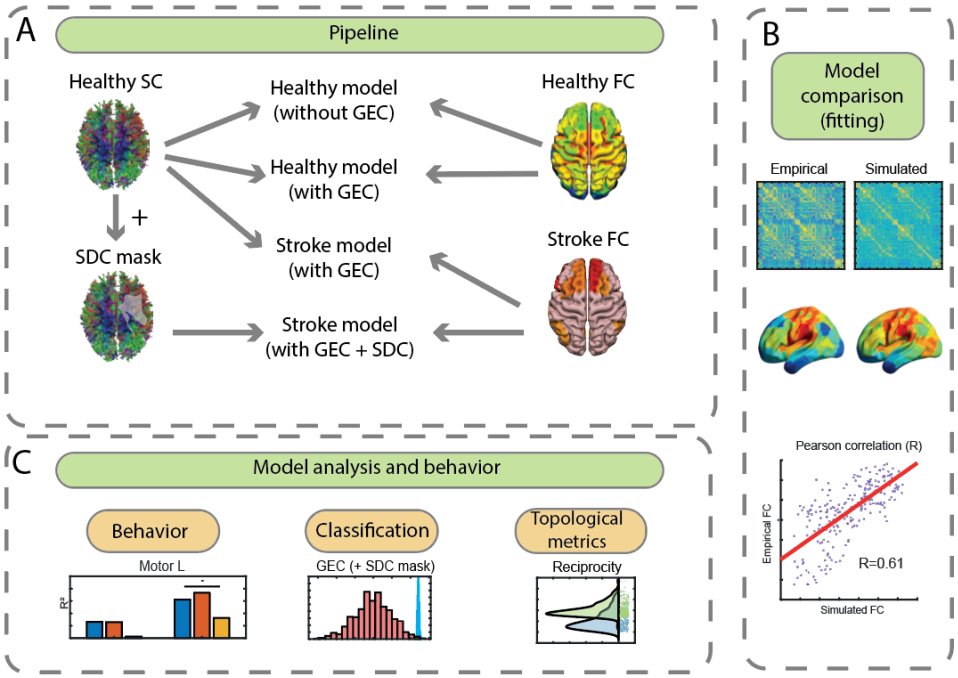

Figure. 4.1: Pipeline of whole-brain models' calculation and the corresponding derived analysis

Figure 4.1: Pipeline of whole-brain models' calculation and the corresponding derived analysis. **(A)** Pipeline: Four different models were created: Healthy model without effective connectivity (GEC) and Healthy model with GEC, both composed of healthy controls SC and healthy controls FC; Stroke model with GEC, composed by healthy controls SC and stroke patients FC; Stroke model with GEC plus SDC mask, composed by Stroke patients SC (Healthy SC + SDC mask) and stroke patients FC. A variation of the second model (Healthy model with GEC) was calculated as a comparison, later called as SC-Model where instead of the healthy controls FC, the stroke FC was used. The control parameters of all the models were tuned using the grand average FC derived from the healthy controls' fMRI BOLD data. For modeling local neural masses, it was used the normal form of a Hopf bifurcation. GEC is calculated by optimizing the effectiveness of the synaptic connections between brain regions as specified by the SC. **(B)** Model comparison (fitting): The model fitting was assessed for each subject and the Pearson correlation was calculated to check similarity between the empirical and the simulated models. **(C)** Model analysis and behavior: To analyze the properties underlying the GEC, we performed a Principal Component Analysis (PCA), with which results, we measure their associative strength with the neuropsychological assessment (behavior) and their sensitivity to classify the severity of the stroke in each patient. Furthermore, topological metrics were calculated taking advantage of the asymmetric feature of the GEC.

4.3.1 GEC-based whole-brain models with disconnection masks reproduce FC impairments in stroke patients

In the first analysis, we intend to test how different whole brain models predict the most common FC abnormalities found in stroke patients, specifically: 1) a decrease of negative intra-hemispheric FC between regions of the Dorsal attention networks (DAN) and Default mode network (DMN); 2) a decrease of inter-hemispheric homotopic FC; 3) a decrease of modularity. We compared models that simulated FC or GEC, each with different kinds of information: no lesion information, gray matter damage and white matter SDC.

We first considered the Intra-hemispheric FC, i.e., the average pairwise correlation between regions of the DAN and DMN. We only considered the damaged hemisphere to avoid diminishing the effect with the preserved hemisphere. As in previous work (J. C. Griffis et al., 2019; Siegel et al., 2016), the empirical FC in healthy controls shows a negative correlation that is decreased (less negative) in stroke ($t(121)= -2.08$, $p= .03$). In contrast, the model FC, both without or with gray matter or SDC mask, is not significantly different between healthy and stroke ($t(121)= .2$, $p= .83$). However, the simulated GEC, only when the SDC mask is applied, showed a significantly less negative correlation than controls, in agreement with empirical data ($t(121)=-10.5$, $p<.01$) (**Figure 4.2a**). It should also be noted that all FC and GEC model measures have a much smaller variability than the empirical measures. This is due to the optimization of the model that used the same parameter value (G-coupling). Therefore, the only source of variability in the model for all the patients was the noise, losing variability information through the process.

Next, we consider the Interhemispheric FC measured in healthy and stroke patients. As in previous work, interhemispheric homotopic FC was

significantly stronger in healthy subjects than stroke patients (t(121)=3.84, p<.01). Using SC-based models there was no significant FC difference between groups (t(121)=-1.09, p= .27). Again, the GEC-based model only when using the SDC mask replicated the normal pattern (t(121)=68.60, p<.01)(**Figure 4.2b**).

Thirdly, we consider modularity. In stroke, when considering a given functional parcellation, modularity is decreased and recovers over time (Siegel et al., 2018). This result was replicated in our study: controls showed a significantly higher modularity value than patients (2 weeks post-stroke) (t(121)=2.98, p< .01). Again, the FC models with or without masks failed to replicate the empirical pattern (t(121)=2.05, p= .06), while GEC models that included the SDC mask did replicate (t(121)=53.14, p<.01)(**Figure 4.2c**).
In Summary, this analysis shows that whole brain GEC models that include structural disconnection information resemble the empirically observed FC abnormalities in stroke patients including intra-hemispheric, inter-hemispheric, and modularity. Other models that do not include lesion information or only gray matter damage, do not resemble empirical results.

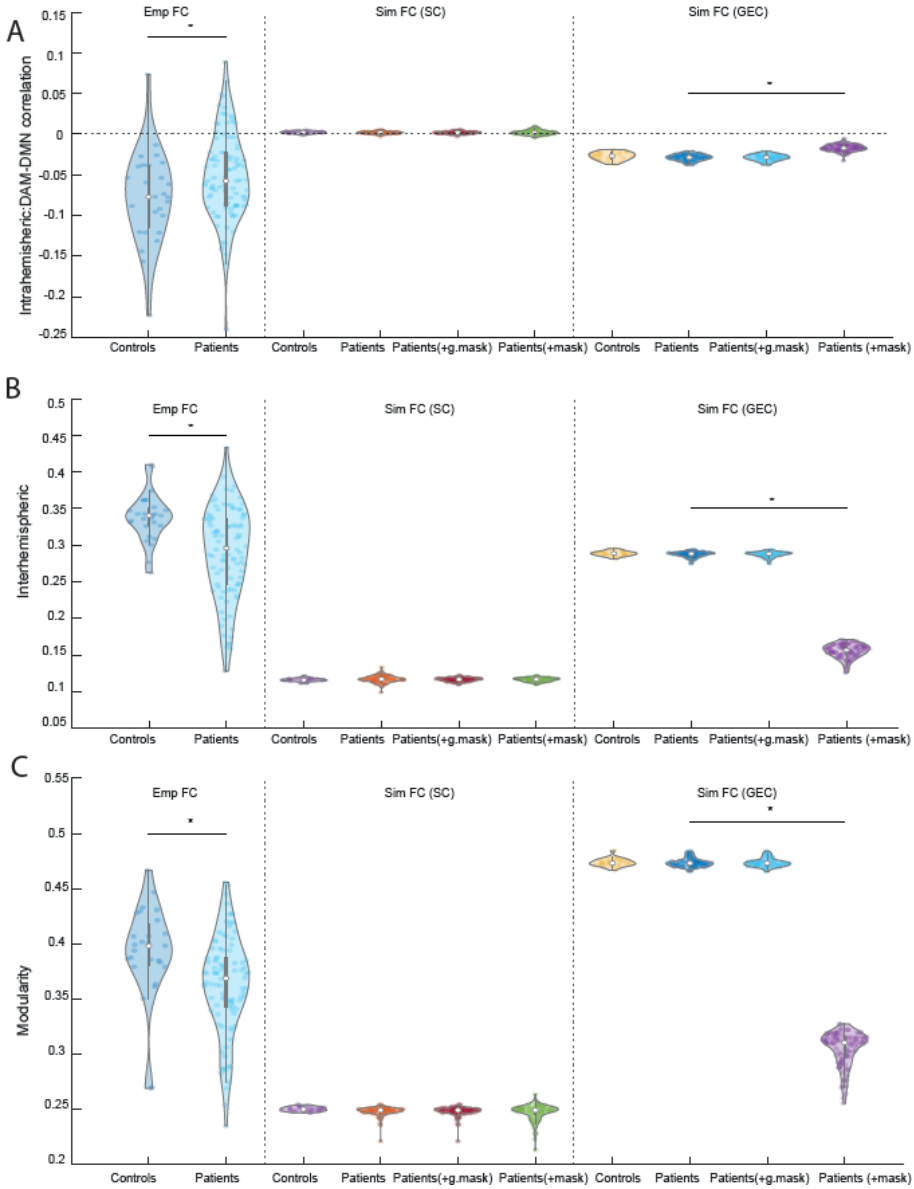

Figure 4.2: FC impairment in stroke and replication with whole-brain mechanistic model

Figure 4.2: FC impairment in stroke and replication with whole-brain mechanistic model: Comparison between patients and controls in their empirical FC (left), SC-based model (center), and GEC-based model (right) in **(A)** intrahemispheric value, **(B)** interhemispheric value, and **(C)** modularity value. Both models are performed with and without mask including the comparisons between the SDC mask and the gray matter mask (See Methods). The model based on GEC showed to be more like the empirical FC (compared to the model based on SC) because it was trained to optimally fit the empirical data.

4.3.2 GEC-based whole-brain models show the best fitting to the empirical data when including structural disconnection information

Next, in order to inspect the validity of the models, we checked how the different models fit the empirical data. Therefore, we assessed the quantitative similarity between empirical FC and simulated FC from different models (SC, GEC, and GEC with SDC mask) in stroke patients.

The GEC-based model with SDC masks showed the highest correlation with the empirical data (mean = 0.52), followed by the GEC-based model without SDC masks (mean = 0.32), and lastly the SC-based model (mean = 0.27). **Figure 4.3a** displays the topology of the empirical and simulated FCs. **Figure 4.3b** reveals the group analysis of this phenomenon (top) including the correlation by node of one example subject (bottom). This result shows the validity of the presented model and the importance of the SDC mask. The same analysis was run on the control group model showing that the level of correlation in healthy controls is similar to that obtained in stroke patients (**Figure B9).** In summary, this analysis shows that whole brain models that include SDC information have the highest resemblance to the empirical data showing the value of the lesion information in the presented models.

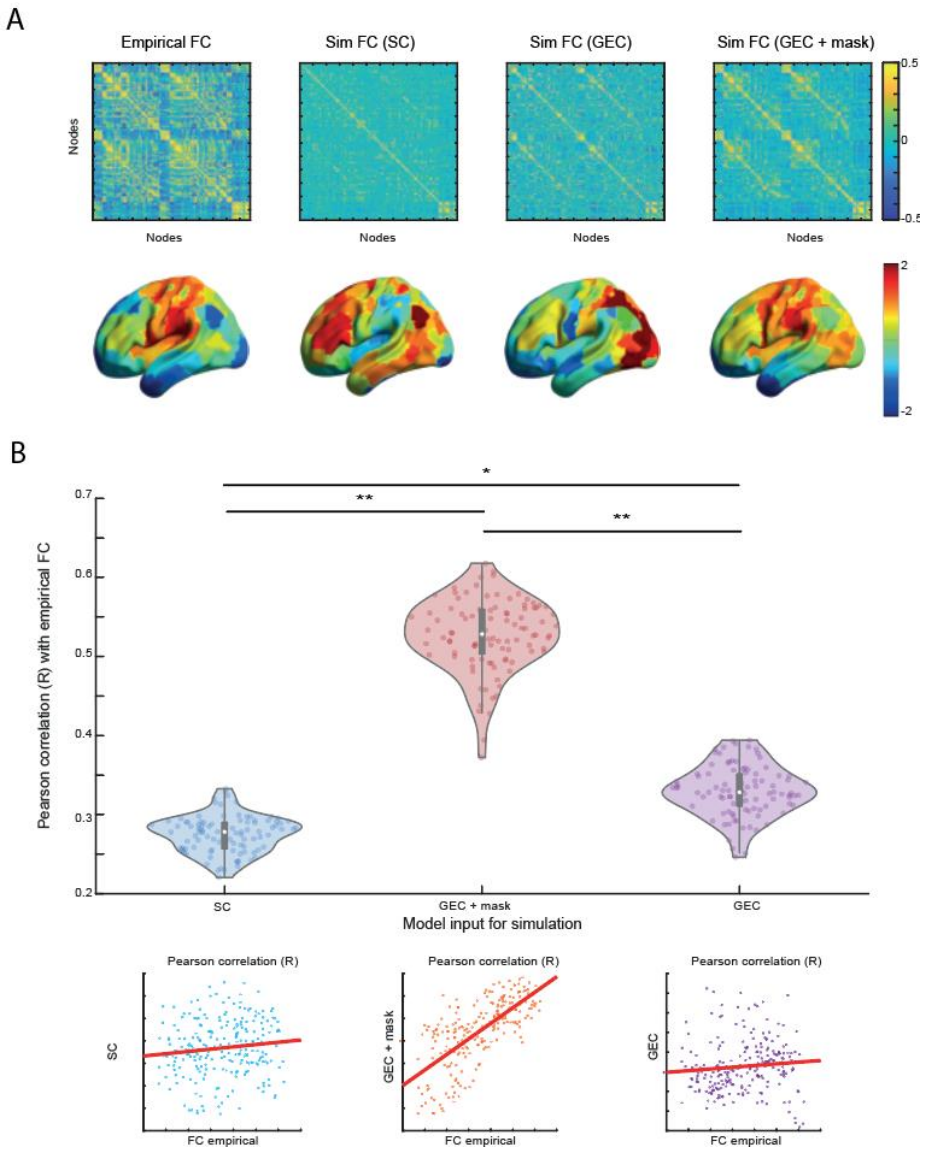

Figure 4.3: Whole-brain models similarity with empirical data

Figure 4.3: Whole-brain models similarity with empirical data: **(A)** FC matrices for empirical data (top), Simulated FC using SC (center-top), Simulated FC using GEC (center-bottom) and Simulated FC using GEC plus the SDC mask (bottom). Matrices were illustrated in brain surfaces to help visualization revealing the topological localization of the effects. **(B)** The correlation between the empirical data and each of the aforementioned models. The highest correlation was observed in the model based on GEC plus SDC masks. Group results are displayed (top) while also an individual result from one example subject is shown (bottom)

4.3.3 GEC-based whole-brain models show abnormalities of network communication in stroke

Having established that GEC-based whole brain models replicate the most common FC abnormalities in stroke, and that are the most accurate in replicating empirically measured FC, it is now possible to examine deficits in communication, specifically differences in directional interactions both within stroke patients and between stroke and controls.

Hence, we compared within and between network communication of GEC in both patients and controls (**Figure 4.4a)**. The sum of weights of the connections was Fisher z-transformed to show the difference. The matrix is organized with sender nodes on the vertical axis and receiving nodes on the horizontal axis. In controls there are strong within-network and inter-hemispheric homotopic interactions. There are also strong interactions between networks. It is apparent that the DMN is the strongest sender (left: [F (6,119) = 7.78, p<.01]; mean=1.28, SD = 1.25; right hemisphere: ([F(6, 119)=2.73,p=.01]; mean=0.53, SD =0.77). DMN therefore appears to be the network with the strongest influence on other networks (See Discussion).

Stroke patients seem to maintain robust within-network homotopic interactions, but much weakened between-network interactions. This can be observed clearly in the difference matrix in **Figure 4.4a** (GEC difference)**.** Statistical comparisons among networks are shown in **Figure B8** with the strongest differences in DMN, somatomotor, brainstem and basal ganglia. However, more information emerges when all lesions are flipped to one side and then comparing healthy to damaged hemisphere (**Figure 4.4b).** These matrices indicate that regions in the damaged hemisphere do not communicate with the homotopic healthy hemisphere regions, while such influence is maintained in the opposite direction from healthy to damaged

hemisphere (compare off-diagonal interaction for healthy (upper) and damaged (lower) hemisphere networks). Between network interactions seem to be damaged in both healthy and damaged hemispheres.

In summary the GEC models show interesting impairments in communication from the lesioned to the healthy hemisphere, and a loss of interaction between networks which is especially evident in the DMN and a few other networks. This approach will be discussed in relation to other methods to study interactions, e.g., Granger causality.

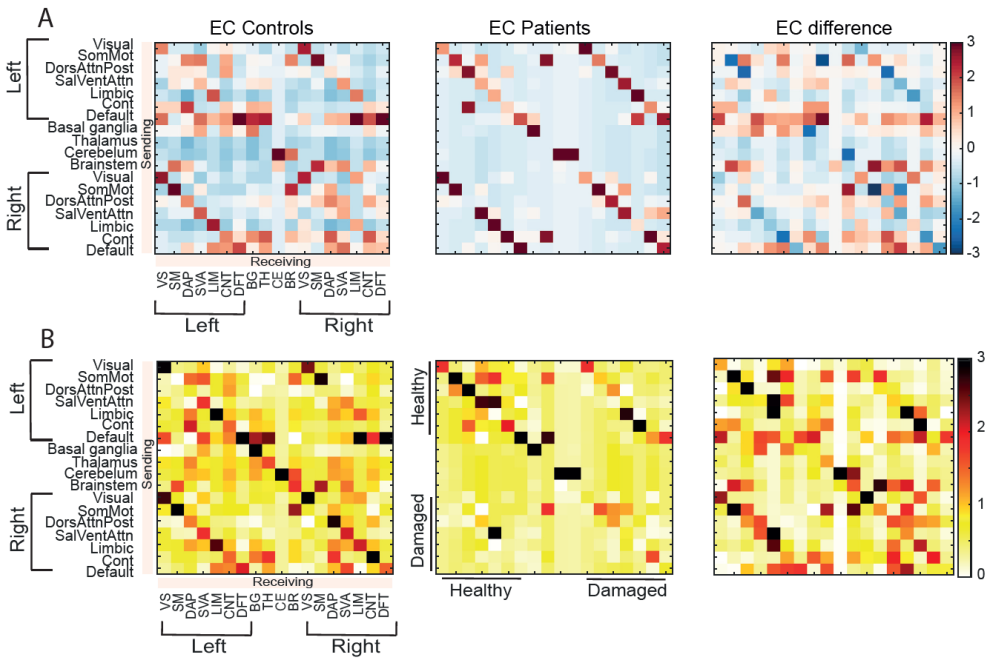

Figure 4.4: Network interactions derived from the whole-brain models

Figure 4.4: Network interactions derived from the whole-brain models: **(A)** Network interactions for the GEC of (left) controls, (center) patients. The right panel exposes the difference for each interaction between the two groups. **(B)** Network communication comparing damaged from healthy hemisphere: In center and right panels, the matrices were re-organized to have all the damage hemispheres together on one side and all the healthy hemisphere on the other.

4.3.4 GEC-based whole-brain models and correlation with clinical variables

In the next analysis, we explored the correlation between (simulated FC from) GEC-based models and lesion, clinical, and behavioral variables. The analysis aims to shed light on the relation between lesion metrics (such as lesion volume and NIHSS score) and behavioral variables (such as motor tasks). Furthermore, we compared the obtained outcome with previously reported results in order to show the robustness of the presented models.

To reduce the spatial variability across all brain regions, we first computed the PCs (calculated as the singular value of the first two principal components) from the GEC model. Two static PCs explained 44% of the total variance (see methods) and explained a significant percentage of the lesion volume variability (R^2 = .17, p < .01), and clinical severity based on the NIHSS score (R^2 = .12, p < .01) (**Figure 4.5a**).

Next, we explored how these PCs were related to behavioral deficits using a subset of patients from (Favaretto, 2022), in contrast to the complete set used in the previous analysis. Here we considered both static components (computed on the time-averaged data) or dynamic components based on a state decomposition analysis (see Methods) (Favaretto, 2022). It is important to clarify that the comparison was made only with the subjects for which we obtained the SPCs and Dynamic PCS.

The GEC static principal components (SPCs) did not show any significant association with behavior (**Figure 4.5b**). However, the behavioral association in some domains improved when static and dynamic GEC components were combined: Motor-Left (R^2 = .36, p < .01), Motor-Right (R^2 = .23, p = .05) and Attention Visual Field-effect (AttentionVF) (R^2 = .41, p < .01). In all domains,

except for Attention validity/Disengagement, PCs from GEC associative value were higher when performed with the damage mask (**Figure B3**).

In summary, not only the PCs from the GEC model were related to lesion metrics but also outperformed previously reported metrics in existing literature, in their relation to clinical variables such as behavioral impairment.

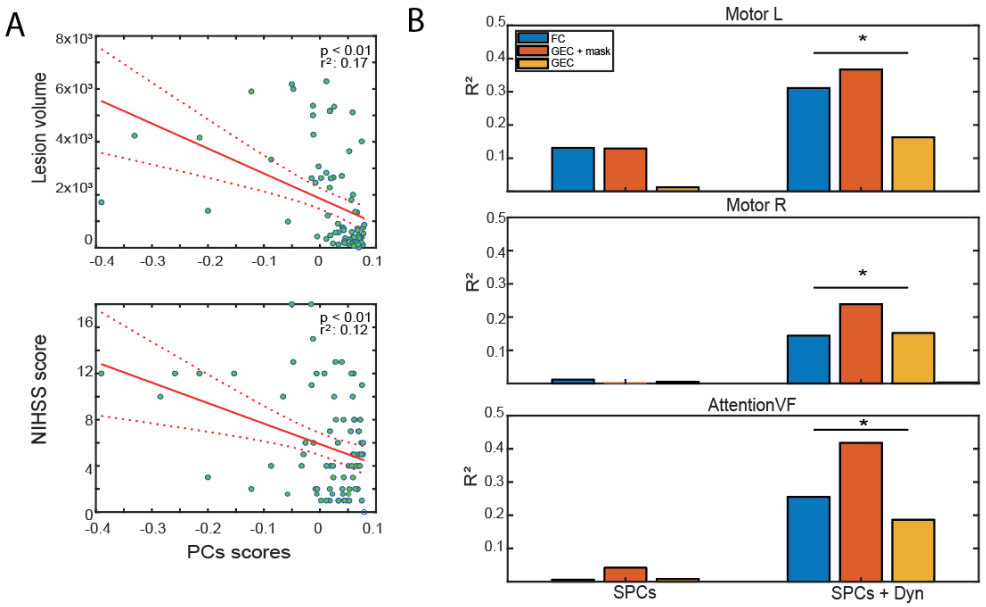

Figure 4.5: GEC-based whole-brain models and correlation with clinical variables

Figure 4.5: GEC-based whole-brain models and correlation with clinical variables:
(A) Relation between the values obtained from the PCA of the GEC and (top) the lesion volume (Calculated in voxels from the SC), and (bottom) the NIHSS score. **(B)** Associative strength of three behavioral domains given by the static PCA (SPCs) of the three approaches (FC, GEC with the SDC mask and GEC without the SDC mask) and with their corresponding interaction with the dynamical components (see Methods for details). Asterisk indicates when only one regressor shows a significance relationship of the three measurements.

4.3.5 GEC-based whole-brain models and classification of behavioral impairment

In the next analysis, we intend to test the utility of the whole brain models for the classification of patients' lesion severity in order to contribute to their diagnosis. Hence, we implemented a classification algorithm in order to distinguish patients' lesion severity using as input the results of the behavioral tests. The division of patients according to their structural disconnection was based on the median value of their lesion volume, separating the sample into two equal groups.

Given the heterogeneity in lesion location and behavioral deficits across patients, we infer that FC dynamics would be differently affected depending on the severity of the static FC impairment. Therefore, we applied a Principal Component Analysis (PCA) to the static FC of acute patients (after z-scoring to the average FC of controls subjects) to split into a low and high severity group. Then, we used the same logic to divide the sample using the PCs of the previously mentioned models. As a result, the prediction of behavioral impairment is based on a median split of the subjects' singular value (Derived from PCA analysis) according to different criteria (SC, FC, GEC, GEC with SDC mask). By using a random forest classifier, we obtained the area under the curve (AUC) representing the accuracy of the classifier for high and low severity injury values, according to the median score. We used the performance in the neuropsychological tests, including all the behavioral domains (explained in the methods section), of the patients to test the algorithm and assess the classification. The scores were z-scored to get one score across domains. The outcome is visualized as histograms (**Figure 4.6**). Each row represents classification based on different signals (SC, FC, GEC, GEC with SDC mask). The histograms in blue correspond to the AUC values obtained using the real data, while the histograms in red indicate the AUC

values obtained after shuffling the data labels. Label shuffled is used as a null model to obtain the p-values shown in the insets.

To measure the statistical significance of the accuracy values, we trained and evaluated a total of 1000 classifiers using the behavioral scores of the patients but scrambling the class labels. Afterward, we produced an empirical p-value by counting how many times the accuracy of the classifier with scrambled class labels was greater than that of the original classifier. All accuracies were determined as the area under the receiver operating characteristic curve (AUC). The GEC (with SDC mask) showed the highest performance (mean= .73, SD<.10, p<.01) followed by GEC (mean=.65, SD <.1, p=.26), FC (mean=.65, SD<.11, p=.029) and SC (mean=.63, SD<.10, p=.028) (**Figure 4.6**). The presented result is obtained by using 80% of the subjects during the training of the cross-validation classification. For an exploration of other ratios of training, see **Figure B5**.

In summary, the highest performance to classify behavioral impairment was obtained by using the GEC-model including the disconnection information, showing another contribution of the presented models for stroke patients' diagnosis.

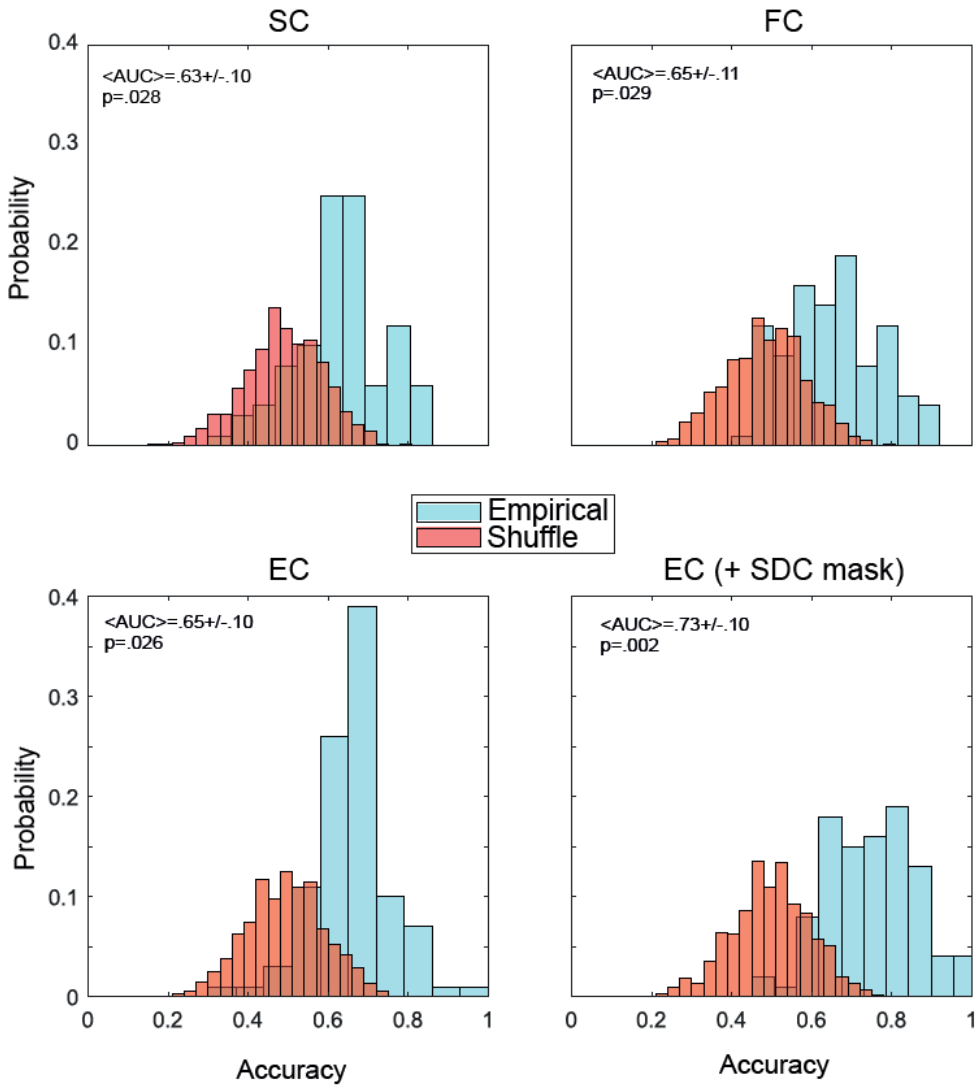

Figure 4.6: : Improving classification of lesion severity by using GEC-based whole-brain models

Figure 4.6: Improving classification of lesion severity by using GEC-based whole-brain models: Each plot represents a different criterion of classification of the two groups. Histograms of AUC values for the random forest classifiers trained to distinguish low from high severity behavior impairment using as division criteria: the lesion volume of the SC (top-left), the PCs of the FC (top-right), the PCS of the GEC (bottom left) and the PCs of the GEC with the SDC mask applied (bottom-right). All classifiers were tested using the neuropsychological assessment performances. Histograms in blue correspond to data without label shuffling, while red indicates AUC after label shuffling

4.3.6 Topological measures in GEC-based models

Since the GEC represents the directed non-symmetrical interactions between brain regions, it is possible through graph metrics to describe differences in the topological organization between healthy controls and stroke patients by means of a group level analysis. Following that line, the next analysis will explore a diverse range of graph metrics in order to show how they reflect the difference between the two groups.

In the comparison between stroke patients and healthy subjects, patients have a significant higher degree ratio per node, both in broadcasters ($t(121)=113.04$, $p < .01$), and in receivers ($t(121)=123.16$,$p < .01$). Moreover, when comparing broadcasters to receivers, all patients had a larger number of broadcasters than receivers (**Figure 4.7a**). It should be noted that the difference in **Figure 4.7a** with healthy controls is somehow exaggerated by the fact that all reciprocal connections were excluded for the calculation of broadcasting and integration. Metrics calculations are explained in detail in the Methods section.

In addition, the average path length was higher in patients than in the control group ($t(121)=28.5$,$p < .01$), while the effect was the opposite for reciprocity and communicability where controls showed significantly higher values than patients ($t(121)=-14.59$, $p < .01$ and $t(121)=-41.13$, $p < .01$ respectively.

To examine the influence of lesions on these metrics, the damaged hemispheres were aligned on the same side. Broadcasters' percentage was higher in the healthy hemisphere compared to the damaged one ($t(190)=67.01$, $p<.01$)). The same effect was visible in the reciprocity level ($t(190)=31.54$, $p<.01$)), while the reverse direction was observed in the

receivers' percentage ($t(190)=-49.09$, $p<.01$)) where higher values occurred in the damaged hemisphere (**Figure 4.7b**).

These findings suggests that communication is less efficient in stroke patients (longer path length, lower reciprocity, and communicability), and this depends on a topological organization in which the integration among regions is abnormally high (higher broadcasters and receivers). Interestingly, this overall topological organization reflects an asymmetry between the damaged and healthy hemisphere, where the latter sends abnormally more to the damaged one.

Next, it is interesting to ask how this topological organization relates to the canonical FC abnormalities reported in previous work (Baldassarre et al., 2016; J. C. Griffis et al., 2019; Siegel et al., 2016). Hence, the relation between FC impairments in stroke (intrahemishperic, interhemispheric, and modularity) and the topological metrics of the GEC (Broadcasters' amount, receivers' amount, and reciprocity) was investigated giving as a result 9 combinations (3 FC x 3 topological) (**Figure 4.7d**). Using the empirical FC, 6 out 9 correlations were significant, using the simulated FC from the GEC model with SDC masks 5 out of 9 correlations were significant, while using the GEC model without any mask, only one correlation was significant.

Interestingly all topological measures (broadcasters, receivers, and reciprocity) correlated significantly with the strength of inter-hemispheric FC and modularity, much less with intra-hemispheric FC. The model that includes only SC correlated significantly with the modularity, and since it did not contain any directional information, did not correlate with broadcasters or receivers.

There was a significant difference between patients with cortical lesions when compared with those with subcortical lesions: cortically damaged patients

showed a lower value of broadcaster amount ($t(54)= -2.5$, $p= .013$), a lower value of receivers' amount ($t(54)= -2.42$, $p= .018$) and a higher value of path length ($t(54)= 2.28$, $p= .026$) (**Figure B6**). This result implies that the topological measures capture prevalently cortico-cortical communication and less subcortical-cortical communication.

Conversely, we did not find any significant differences when comparing the patients with lesions in the left hemisphere and the right one ($t(94) = -.5$, $p =.6$). Left and right hemisphere lesion produced topological measures that were strongly correlated: Broadcaster percentage: $r=.98$, $p<.01$; Receivers percentage: $r=.98$, $p<.01$; Reciprocity degree: $r=.92$, $p<.01$. This result implies that lesions on either side produce bilateral effects that are similar irrespective of the side of the lesion.

In summary, topological differences between stroke patients and healthy controls can be obtained by the means of graph metrics, indicating how brain dynamics are modified due to the stroke incidents. Those differences got enhanced when the healthy and damaged hemispheres were aligned across all stroke patients.

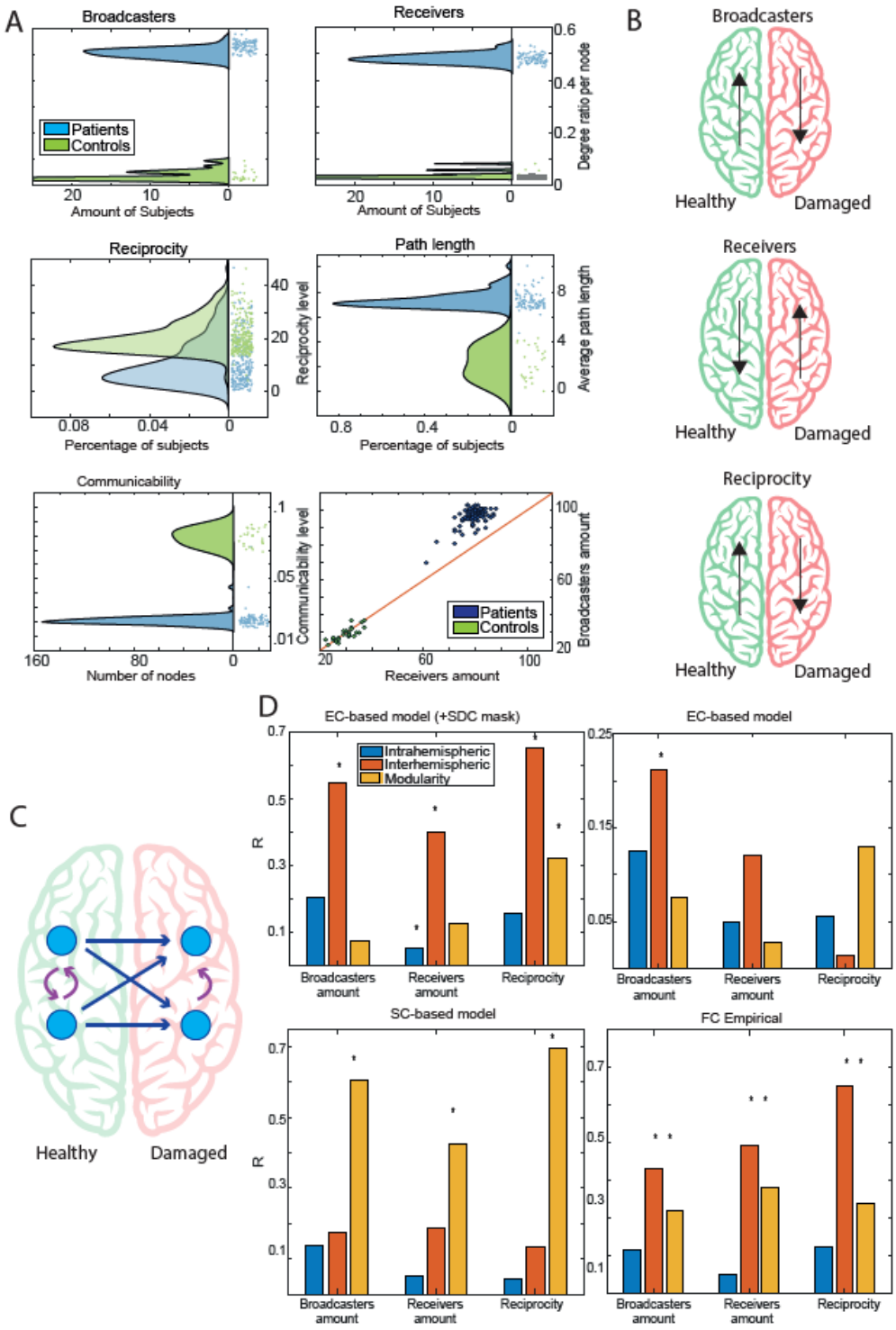

Figure 4.7: Topological measures benefitted from GEC-based whole-brain models

Figure 4.7: Topological measures benefitted from GEC-based whole-brain models: **(A)** Comparison between stroke patients and healthy controls in (top-left) the amount of broadcasters per node, (top-right) the amount of receivers per node, (center-left) reciprocity per node, (center-right) average path length and (bottom-left) communicability. At the bottom-right graph, it is visible the relation between both the number of receivers and broadcasters in both sample groups. **(B)** Hemispheres were flipped when corresponded to align the damaged and healthy hemispheres. Differences in ratio of Broadcasters (top), receivers (center) and reciprocity (bottom) are represented with arrows. **(C)** Visualization of connections in both healthy and damaged hemisphere indicating the relevance of interhemispheric communication. Blue arrows show the broadcasting increase in the healthy hemisphere and the receivers increase in the damaged hemisphere. Purple arrows indicate the superior reciprocity in the healthy hemisphere compared to the damaged one. **(D)** Relation between the FC impairments in stroke (Intrahemishperic, interhemispheric, and modularity) and the topological metrics of the GEC (Broadcasters, receivers, and reciprocity) in (top-left) GEC model with SDC mask, (top-right) GEC model without SDC mask, (bottom-left) SC model, (bottom-right) empirical FC.

4.3.7 Relation between regions interaction and stroke-related metrics

For the final analysis, we explored the nodes communication by inspecting the areas they are communicated to. Therefore, the edges of the corresponding nodes can be distinguished in different groups in order to observe which interactions are most associated with previous studied metrics. In order to localize which regions were involved in the affected nodes, we labeled the nodes based on which areas were being communicated. Each patient structural connectivity matrix was segmented into three different groups, edges that communicate two nodes from Cortical-Cortical (CC), nodes from Subcortical-Cortical (SC), and nodes from Subcortical-Subcortical (SS) (**Figure 4.8a**). We performed correlations between the amount of lesion of each group and previously reported metrics. The relations between them are presented here (**Figure 4.8b**).

Relation with behavior:

- There was a significant association between the CC group with Language (r^2=.36, p<.01), MotorL (r^2=.10, p<.01), MemoryS (r^2=.11, p<.01) and Motor IC T1 (r^2=.10, p<.01) while no significant relation with the remaining behavioral domains (p>.1)
- There was a significant association between the SC group with Language (r^2=.16, p<.01), MotorL (r^2=.33, p<.01), MemoryS (r^2=.20, p<.01) and Motor IC T1 (r^2=.35, p<.01) while no significant relation with the remaining behavioral domains (p>.1)
- There was no significant association between the SS group with any of the behavioral domains (p>.2)

Relation with FC abnormalities

- There was a significant association between the CC group and interhemispheric level (r^2=.23, p<.01) and modularity (r^2=.07, p<.01) while there was no significant difference with intrahemispheric level (r^2=.01, p=.19)
- There was a significant association between the SC group and interhemispheric level (r^2=.33, p<.01) and modularity (r^2=.14, p<.01) while there was no significant difference with intrahemispheric level (r^2=.001, p=.38)
- There was no significant association between the SS group and any of the three FC abnormalities (p>.1)

Relation with Topological metrics:

- There was a significant association between the CC group and the number of broadcasters (r^2=.20, p<.01), number of integrators (r^2=.33, p<.01), and reciprocity level (r^2=.26, p<.01)
- There was a significant association between the SC group and the number of broadcasters (r^2=.22, p<.01), number of receivers (r^2=.19, p<.01), and reciprocity level (r^2=.37, p<.01)

- There was no significant association between the SS group and any of the topological metrics (p>.3)

Relation with Lesion volume:

- There was a significant association between the CC group and lesion volume
  (r^2=.72, p<.01)
- There was a significant association between the SC group and lesion volume
  (r^2=.51, p<.01)
- There was no significant association between the SC group and lesion volume (r^2=.01, p=.8)

Relation with NIHSS:

- There was a significant association between the CC group and NIHSS
  (r^2=.10, p<.01)
- There was a significant association between the SC group and NIHSS
  (r^2=.51, p<.01)
- There was no significant association between the SC group and NIHSS (r^2=.01, p=.9)

In summary, this analysis shows that region interaction in the structural disconnection information is related to previously reported metrics across this study. This provides an extra benefit for the inclusion of this information into the whole-brain models.

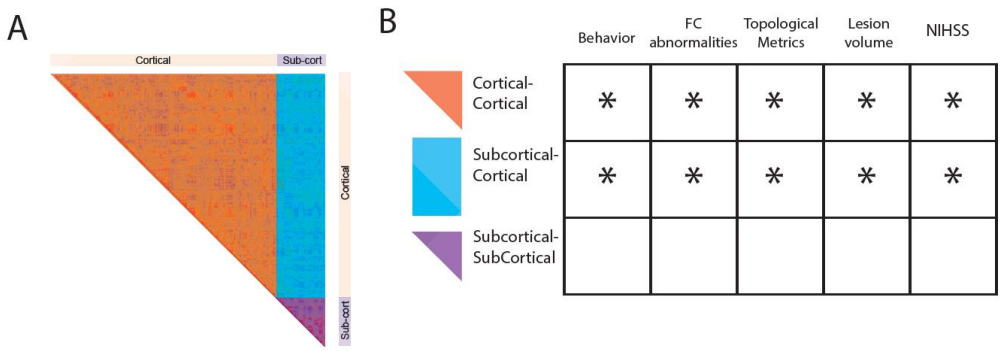

Figure 4.8: Relation between regions interaction and stroke-related metrics

Figure 4.8: Relation between regions interaction and stroke-related metrics: **(A)** Distinction between three different types of lesions regarding the involved regions, Cortical-Cortical, Subcortical-Cortical and Subcortical-Subcortical. Color is used as a reference to distinguish the three different groups in a visual way. **(B)** Association between the lesion classification and behavior domains, FC abnormalities, topological metrics, lesion volume, and NIHSS. It is important to note that the lower amount of nodes in the SS group is influencing the reported results.

4.4 Discussion

In the current study, we created a generative model based on effective connectivity (GEC) as a mechanistic answer to calculate post-stroke effects. The model replicates the most common FC impairments observed in previous literature by making use of the white matter structural disconnection caused by each patient's lesion (SDC mask). The GEC model proves to be more strongly associated than previous models when relating to subjects' behavioral performance. More importantly, we demonstrate that the GEC shows a higher performance when classifying the severity of the lesion. Finally, due to its asymmetrical property, it provides topological metrics useful for further analysis. All the presented methods and results contribute to shed light on the brain dynamics after stroke incidents, including the relevance of the structural disconnection information.

4.4.1 FC impairment in stroke

As reported in previous literature, there is a visible pattern of alterations in the FC of patients after stroke. These include an increase in the correlation of the intrahemispheric level (bringing it closer to zero), a decrease in the interhemispheric level, and a decrease in the modularity level (Arnemann et al., 2015; Baldassarre et al., 2016; Gratton et al., 2012; Siegel et al., 2016). While many studies focus on the concepts of integration and segregation (Adhikari et al., 2017; Bullmore & Sporns, 2009; Deco et al., 2015; H.-J. Park & K. Friston, 2013; Sporns, 2013), their reduction poststroke could be the result of a single disruptive process such as the previously observed reductions in network modularity in the brain (Gratton et al., 2012). Moreover, modularity could be considered as a quantification of the ability of the brain to differentiate into separable subnetworks and is an essential property found in many complex systems that allows the system to develop dynamic behaviors (Meunier et al., 2010).

By using simulated models, the Hopf model that included only the SC information did not accurately replicate the empirical FC abnormalities (**Figure 4.3**), while the model optimized with GEC did, but only when the SDC mask was added. Notably, the model replicated the empirical FC effects only when the degree of white matter disconnection was taken into account, not the gray matter (parcel) damage as in (Adhikari et al., 2017). This illustrates the critical importance of white matter damage not only for understanding the physiological effects of stroke (Corbetta et al., 2015; Joseph C Griffis et al., 2019; Griffis et al., 2020), but also for accurate modeling and prediction as illustrated in this work.

The current study underlines the validity of whole-brain computational models by complementing previous results (Joseph C Griffis et al., 2019) with the information of SDC masks. The inclusion of the SDC masks should be taken into consideration in the future when modeling data of stroke patients.

Regarding the lesion localization, a clear distinction between cortical and subcortical patients is found when the SDC mask was included in the model, providing another advantage in using the presented model as a tool for future studies concerned about lesion localization and diagnostics.

4.4.2 Associative value of GEC and enhancement by using SDC mask

Previous literature suggests that the relationship between the structural disconnection and the functional connectivity patterns (FC) should be low-dimensional (Corbetta et al., 2015; Joseph C Griffis et al., 2019) as the components which explained most of the variance could provide useful information about cognitive and behavioral impairment (Bayrak et al., 2019). In comparison to a recent study (Favaretto, 2022) that focused on the

influence of the FC components and their interaction with dynamical features, this study aims to prove the enhanced associative value of the GEC components.

We investigated the associative power over all the described domains (**Figure. B3**). By comparing the dynamic components combined with the PC provided by the FC and GEC, the latest showed higher accuracy, especially for motor deficits. This is consistent with previous literature which claimed that functional alterations of brain networks are important for cognitive functions that rely on distributed networks (e.g., memory, attention, language), as compared to visual and motor functions for which structural damage is more sensitive (Corbetta et al., 2018). By performing a model which includes structural information, the relation over domains more sensitive to structural damage was more likely to be enhanced. It is important to underline that the present model combines both structural and functional information, providing more information compared to the analysis using only functional data (Favaretto, 2022). Future studies could introduce alternative models to control this issue.

4.4.3 Network communication reveal loss of interaction after stroke

Several studies have discussed the role of DMN as a brain hub (Power et al., 2013; van den Heuvel & Sporns, 2013). Here we found that the DMN is the network that exerts the main influence over other networks and that this influence is significantly decreased in stroke patients, both in the damaged and healthy hemisphere. A functional-anatomical gradient of cortical organization going from sensory-motor networks to polymodal tertiary association networks, with the DMN sitting at the top of this hierarchy has been described (Margulies et al., 2016), situating the default-mode network

along a principal gradient of macroscale cortical organization (Raut et al., 2020). Hierarchical dynamics as a macroscopic organizing principle of the human brain (Mitra & Raichle, 2016) and human cortical–hippocampal dialogue in wake and slow-wave sleep (Mitra et al., 2016) have also been described. This organization is exactly the one mandated by hierarchical generative models. Networks that occupy higher levels may continuously generate predictions to suppress prediction errors of lower brain networks, such as primary sensory and motor regions, which may be engaged when prediction errors cannot be readily cancelled out. The role of the DMN in exerting influence on other networks as shown here is consistent with this interpretation, and further suggest the testable hypothesis that stroke patients' deficits may partly reflect prediction errors in sensory-motor-cognitive processing.

This analysis also provides converging evidence on the alterations of directional interactions caused by focal stroke lesions. Allegra et al. (Allegra et al., 2021), measuring Granger causality (GC) on BOLD timeseries, found that focal lesions cause a relative decrease of GC from the damaged to the healthy hemisphere, as well as a decrease of interactions within the damaged hemisphere. Our results using GEC-based models converge on this empirical observation similarly showing a loss of 'sender' influence from the damaged to the normal hemisphere, as well as an overall decrease of interactions within the damaged one.

4.4.4 Improving classification of behavior severity level by using GEC

Previous studies (J. C. Griffis et al., 2019; Griffis et al., 2020; Wodeyar et al., 2020) showed, considering BOLD signals both at the voxel scale and ROI scale, that differences in structural connectivity were linked to changes in

functional connectivity. Thus, found that, in the brain, communication between different regions is mediated through anatomical connections. The damaging effects perceived in stroke patients' FC were evident when also inspecting their SC, but not evident when looking at FC only.

Furthermore, the GEC is calculated through simulations and modeling taking into consideration the anatomically restrained connections. In this study, the SC information was enhanced by the addition of the SDC mask. The classification using the GEC information when applying the SDC mask showed the highest accuracy of classification, followed by a similar value by the GEC without the SDC mask and afterward, with lower levels, the classification using only SC or FC. Despite providing a beneficial factor due to its enhanced classification power, further research is needed to know how this fluctuates across time and how the recovery of the patient is reflected on it.

The reported results by analyzing the z-abnormalities help to shed light on the relation between FC and SC. The generative model presented in the current study exposed how the effect changes in FC as a consequence of the stroke damage could be observed when the disconnection information is added. Nevertheless, in the damaged area and lesion severity classification, the direction of the effect was reversed between the empirical and the simulated data. Future studies could clarify the underlying reason for this discrepancy.

4.4.5 Topological measures benefited from GEC

Previous studies discussed the role of graph theory metrics in stroke patients (Han et al., 2020; Idesis, Faskowitz, et al., 2022; Sun et al., 2021; Vecchio, Tomino, et al., 2019) revealing how properties such as global efficiency

indicate the efficiency of integration of distributed information through the whole network. Nevertheless, the studies relied on FC to calculate the corresponding metrics. In the current study, the analysis profited from the asymmetricity of the GEC to calculate topological metrics that could better describe the difference between stroke patients and healthy subjects. The calculation of broadcasts and receivers, used in the current study, exclude the relations that are spared reciprocally (both directions with a different node). Excluding the reciprocal relations (which are the majority), the higher number of broadcasters and receivers in the patients (compared to the healthy controls where an even higher percentage of the connections were reciprocal) was expected. The fact that every single patient presented a higher number of broadcasters than receivers is a relevant and unexpected result. Previous authors discussed this as an implication of a loss of integration converting it into a good biomarker for stroke treatment (Adhikari et al., 2020; Pallarés et al., 2018). Furthermore, a previous study (Chen et al., 2021) tried to manipulate this phenomenon through transcranial alternating current stimulation (tACS) exposing the difference in integration capacity in stroke patients. As reciprocity was found higher in controls, this metric could be used as a biomarker of patients' recovery. By assessing the reciprocity across time of each patient, it could be observed if the networks tend to partially restore, or at least compensate for, the deficit provoked by the damage.

While the distinction between patients according to the hemisphere damaged did not reveal any significant information, the comparison between patients with cortical and subcortical lesions showed significant differences (when the corresponding SDC mask was applied) revealing that the measures presented could provide a novel method to assess distinctions in lesion localization.

The provided results open the possibility of using the metrics obtained in the current study to enhance the classification algorithms and create an even more accurate diagnosis.

4.4.6 Region interaction association with stroke metrics

Previous studies have reported the effects of after-stroke disconnections and their relation with global dynamic metrics such as modularity (Joseph C Griffis et al., 2019; Warren et al., 2014). In this study, we divided the disconnection matrix of each patient into different groups relative to which regions' communication was impaired. We found a strong relationship between all the variables of interest and the Cortical-Cortical and Subcortical-Cortical group while no association with the Subcortical-Subcortical group. These results support previous findings showing that stroke effects primarily disrupt whole-brain resting physiology by damaging interregional structural connections rather than only specific grey matter structures (J. C. Griffis et al., 2019). Based on these results, further studies could benefit from this approach to achieve more accurate analysis and reduce the amount of data used.

4.4.7 Limitations

The current study focuses on providing information about relationship with behavioral scores, classification of severity of the injury, and providing informative topological metrics to analyze the brain dynamics properties. Nevertheless, it is not clear how these parameters are modified through the process of the recovery of the patients. Future studies could benefit from this longitudinal dataset in order to address these types of questions. Localization of the top 5% weights in controls and patients is presented in **Figure B7** to allow comparisons in future studies which focus on the recovery after stroke.

Lastly, as beneficial as it was found, the GEC consists of a bidirectional matrix instead of the typical symmetrical matrices obtained by analyses of FC and SC. Therefore, computational processes may be more time demanding and computationally costly.

4.5 Conclusion

The current study illustrated how the application of generative models provided a mechanistic explanation of the stroke effects in patients. We presented an approach to combine structural and functional data from stroke patients. The proposed model can also be used to compare different existing SDC masks to determine the one that produces the best fit to empirically observed FC. Together with the relevance of the SDC mask for the whole-brain models of stroke, the current study replicates the existing biomarkers of stroke damage and provides evidence that the proposed model can improve the classification accuracy of behavioral deficits after stroke, revealing the strong influence of SDC in the observed effects. The present study opens a vast number of possibilities for further analysis providing a mechanistic explanation for stroke injuries and metrics due to its ability to model asymmetric interactions among brain regions.

CHAPTER 5

5. Function prediction from anatomy: Whole-brain dynamic modeling predicts function from structure in stroke

Work in this chapter reflects a paper currently under review.

Highlights

- We derived a whole-brain model to infer the dynamical effects of stroke lesions two weeks after onset only using anatomical information.
- We contrast the model's accuracy with other predictive models and non-predictive patient-specific models, to make visible the high performance of the presented model
- We used the computational model to predict patient abnormalities in the whole-brain FC measures
- The generative aspect of the model allows for its generalization to new datasets and contributes to advancing the analysis on brain disorders' dynamics, as seen in stroke patients
- . With the presented model, it is possible to measure in silico recording and estimate the effect of the lesions in order to shed light to the treatment and recovery of stroke incidents.

Abstract

Computational whole-brain models describe the resting activity of each brain region based on a local model, inter-regional functional interactions, and a structural connectome that specifies the strength of inter-regional connections. Strokes damage the healthy structural connectome that forms the backbone of these models and produce large alterations in inter-regional functional interactions. These interactions are typically measured by correlating the timeseries of activity between two brain regions, so-called resting functional connectivity. We show that adding information about the structural disconnections produced by a patient's lesion to a whole-brain model previously trained on structural and functional data from a large cohort of healthy subjects predicts the resting functional connectivity of the patient

about as well as fitting the model directly to the patient's data. Furthermore, the model dynamics reproduce functional connectivity-based measures that are typically abnormal in stroke patients as well as measures that specifically isolate these abnormalities. These results show that the model accurately captures relationships between the structure and functional activity of the human brain.

Keywords

Whole-Brain models, Predictive, Stroke, fMRI, Dynamics

5.1 Introduction

The development of accurate whole-brain models is essential for the understanding of how the structural and functional organization of the brain affects its ability to process information (Deco, Hagmann, et al., 2014). Stroke-induced alterations in resting-state FC are largely caused by changes in the structural connectome which forms the backbone of computational whole-brain models (J. C. Griffis et al., 2019). Consequently, a valid whole-brain model should be able to predict how a large stroke-induced alteration in the structural connectome will change the topography of a patient's resting FC. We call such a model predictive as it is predicting the functional dynamics from structural information and its alteration. Yet, predictive whole-brain computational models have been rarely leveraged in the study of stroke. While whole-brain models have been applied to stroke patients' data, in previous work the model was fit explicitly to the functional data of each patient. In other words, the models could reproduce functional anomalies observed in patients, but not predicted from the structural alterations alone (Adhikari, Griffis, et al., 2021; Alstott et al., 2009; Idesis, Faskowitz, et al., 2022; Saenger et al., 2018). Here we propose a generative and predictive whole-brain computational model of the resting state that allows to predict abnormalities in brain function and behavior which result from a particular stroke-induced lesion. This approach is considered generative due to the underlying BOLD signals that are generated from the model. We demonstrate the model's high performance by contrasting its accuracy with other predictive models and non-predictive patient specific model that was fitted directly to a patient's functional data. Our results show that the predictive model reproduces in part the FC matrix of patients, patient-specific abnormalities in the FC matrix, summary FC-based measures that are typically abnormal following a stroke such as homotopic interhemispheric FC and FC between the dorsal attention

network (DAN) and default mode network (DMN), and patient specific abnormalities in those measures (Corbetta et al., 2015).

Importantly, our results show that the predictive model has the same degree of accuracy as previously reported models, even though the model fitting did not include the patients' functional information, indicating that the model captures a relationship between structure and functional activity. The generative aspect of the model allows for its generalization to new datasets and may advance our understanding of the altered brain dynamics observed in stroke patients.

5.2 Material and methods

5.2.1 FC measures

Based on previous work (J. C. Griffis et al., 2019; Siegel et al., 2016) we defined three measures that are consistently impaired in stroke patients:

- Intra-hemispheric FC: average pairwise FC between Dorsal attention network (DAN) and Default mode network (DMN) regions.
- Inter-hemispheric FC: average homotopic inter-hemispheric connectivity within each network
- Modularity: overall Newman's modularity among cortical networks, a comparison between the number of connections within a module to the number of connections between modules (Newman & Girvan, 2004)

5.2.2 Whole-brain Hopf model parameter estimation

We simulated the BOLD activity at the whole-brain level by using the Hopf computational model, simulating the dynamics emerging from the mutual interactions between brain areas, considered to be interconnected based on the established graphs of anatomical SC (Deco et al., 2017; Kringelbach et al., 2015). The structural connectivity matrix was scaled to a maximum value of 0.2 (Deco et al., 2017), in order to explore the range of the G parameter established in previous works. To calculate the Generative Effective Connectivity (GEC) of the healthy control group, we optimized the similarity between the phases of the simulated and empirical data by changing the value of the global coupling factor G (obtaining a value of G = 0.75 as the optimal one), which assesses the influence of SC in the model. The higher the value of the factor G, the bigger the influence of the system in each node. The model consists of 234 coupled dynamical units (ROIs or nodes) representing the 200 cortical and 34 subcortical brain areas from the

parcellation. When combined with brain network anatomy (explained above in the “Neuroimaging acquisition and preprocessing” section), the complex interactions between Hopf oscillators have been shown to successfully replicate features of brain dynamics observed in fMRI (Deco et al., 2017; Kringelbach et al., 2015).

In complex coordinates, each node j is described by the following equation: (For more information, see Deco et al., 2019)

$$\frac{dz_j}{dt} = z(a_j + i\omega_j - |z_j|^2) + g \sum_{k=1}^{N} C_{jk} (z_k - z_j) + \beta\eta_j, \qquad (5.1)$$

and

$$z_j = p_j e^{i\theta} = x_j + iy_j \qquad (5.2)$$

Where α and ω are the bifurcation parameters and the intrinsic frequencies of the system, respectively. This normal form has a supercritical bifurcation at a_j = 0 for which we used the homogeneous parameter space around the Hopf bifurcation (a = -0.01). Within this model, the intrinsic frequency ω_j of each node is in the 0.04–0.07Hz band (j=1, …, n). The intrinsic frequencies were estimated from the data, as given by the averaged peak frequency of the narrowband BOLD signals of each brain region. The variable G represents a global coupling factor scaling the structural connectivity C_{jk}, and η is a Gaussian noise vector with standard deviation $\beta = 0.04$. This model can be interpreted as an extension of the Kuramoto model with amplitude variations, hence the choice of coupling ($z_k - z_j$), which relates to a tendency of synchronization between two coupled nodes. We insert equation 2 in equation 1 and separate real part in equation 3 and imaginary part in equation 4 (Deco et al., 2017).

$$\frac{dx_j}{dt} = \left(a_j - x_j^2 - y_j^2\right)x_j - \omega_j y_j + G\ \sum_k C_{jk}\left(x_k - x_j\right) + \ \beta\eta_j(\tau) \quad (5.3)$$

$$\frac{dy_j}{dt} = \left(a_j - x_j^2 - y_j^2\right)y_j + \omega_j x_j + G\ \sum_k C_{jk}\left(y_k - y_j\right) + \beta\eta_j(\tau) \quad (5.4)$$

For all cases, we will compute the goodness of fit by the mean error (squared difference) between the upper triangular values of the empirical and simulated FC.

5.2.3 Generative Effective Connectivity calculations

Generative Effective connectivity (GEC) utilizes differences detected at different times in the signals connected pair of brain regions to infer what effects one brain region has on the other.

The analysis of GEC incorporates an indirect metric (as it is derived from other presented metrics) into the whole-brain model to replace the existing descriptive metrics of FC and SC. Previous studies have shown how GEC is fundamental for understanding the propagation of information in structural networks (Gilson et al., 2016; Jobst et al., 2017). Methods for estimating GEC are explained in detail in a previous publication (Deco et al., 2019). Briefly, we computed the distance between our model and the empirical grand average phase coherence matrices (as a measure of synchronization of the system) of the healthy controls group. In the stroke patients' group, we adjusted each structural connection separately using a greedy version of the gradient-descent approach. In order to work only positive values for the algorithm, all values are transformed into a mutual information measure (assuming Gaussian distribution). Therefore, the individual subject information is introduced by means of its disconnection (SC + each subject SDC) derived from the Lesion Quantification Toolkit.

We fit “C” such that the model optimally reproduces the empirically measured covariances

$FC^{empirical}$ (i.e., the normalized covariance matrix of the functional neuroimaging data) and the empirical time-shifted covariances $FS^{empirical}(\tau)$ where τ is the time lag, which are normalized for each pair of regions i and j by $\sqrt{KS_{jk}^{empirical}(0)KS_{jk}^{empirical}(0)}$. We proceeded to update the C until the fit is fully optimized. The equation of the optimization is as follows: (For more information, see (Deco et al., 2023))

$$C_{jk} = C_{jk} + \varepsilon(FC_{jk}^{emp} - FC_{jk}^{mod}) + \varepsilon(FS_{jk}^{emp}(\tau) - FS_{jk}^{mod}(\tau)). \quad (5.5)$$

Where C is the anatomical connectivity and is updated with the difference between the grand-averaged phase coherence matrices (Empirical: FC_{jk}^{emp} and model: FC_{jk}^{mod}) and the difference between the time-shifted covariance matrices, both scaled by a factor ε < 0.001. Where $FS_{jk}^{mod}(\tau)$ is defined similar to $FS_{jk}^{emp}(\tau)$. After this process, C is considered as a Generative Effective Connectivity (GEC) matrix. The prediction, therefore, is based on the current estimation of the structural connectivity, which gets updated optimizing the phase FC in each iteration. In summary, the model was run repeatedly with recursive updates of GEC until convergence was reached. The distinction between functional and effective connectivity is crucial here: FC is defined as the statistical dependence between distant neurophysiological activities, whereas GEC is defined as the influence one neural system exerts over another providing directionality in the relations making the matrices asymmetrical (Friston, 2011; Friston et al., 2003). A similar approach has already been used measuring the level of non-reversibility in order to classify and predict the recovery of stroke patients (Idesis et al, 2023).

5.2.4 Models

Full Predictive model:

We calculated a predictive model to capture the dynamical effects of stroke lesions two weeks after onset. First, we estimated the optimal value of global coupling for which the modeled Hilbert phases were most similar to the empirical data in the healthy controls group (G=0.75). Then, we computed the GEC (See previous section) on the same group **(Figure 5.1a)**. Lastly, we added the information of the SDC mask of each patient to the existing GEC to simulate fMRI BOLD data of the corresponding patient **(Figure 5.1b)**. As a result, the simulated time series (referred to as "Full Predictive model") contains structural information of the patient while not using the functional information, making it a predictive model, in contrast to the previously discussed non-predictive models.

For each patient, the simulated fMRI BOLD timeseries for each parcel pair were then correlated to construct the patient's simulated FC matrix. In order to isolate the degree to which the patient's FC between two parcels was abnormal relative to healthy controls, empirical and simulated FC matrices for each patient were z-scored with respect to the healthy controls' empirical and simulated FC matrices to create the patient's empirical and simulated z-scored FC abnormality matrices. Specifically, the healthy group-mean FC for a parcel pair was subtracted from the patient's FC for that parcel pair, and this difference score was then divided by the standard deviation of the healthy group FC for that parcel pair.

In addition, we separately averaged the homotopic interhemispheric FC entries and the DAN-DMN entries from a patient's z-scored FC abnormality matrix to create averaged abnormality scores for these two classes of FC, which are typically abnormal in patients.

Predictive comparative models

Two different predictive models were calculated in order to compare their performance with the full predictive model:

- **Predictive model without mask**: In order to assess the influence incorporating a disconnection mask (lesion information) in the predictive model, this model simply consisted of the healthy group model without any disconnection mask.
- **Surrogate mask model**: As the effect of the disconnection mask could simply reflect the overall magnitude of disconnection, we computed models in which each patient received the disconnection mask of another patient. As the lesion amount is similar on average but the pattern/location of the lesion is different, comparisons of the full predictive model vs. the surrogate mask model indicate how strongly the accuracy of a predictive model depends on incorporating the specific features of a patient's lesion. Therefore, the model without mask and the surrogate mask model serves as predictive controls for the full predictive model.

Non-predictive and patient-specific Model

A non-predictive patient-specific model was calculated in order to compare it with the full predictive model. The patient-specific model utilizes functional information instead of predicting it, which converts it into a non-predictive model. For the optimization of these models, we used the patient's functional information, in contrast to the predictive models where that information was estimated. Therefore, each patient GEC was used instead of the healthy group GEC, used in the previous models.

5.2.5 Assessment of model accuracy

Behavior impairment prediction

We explored how well subjects' behavioral scores (See chapter 2) were predicted by their empirical and simulated FC. We calculated two partial least-squares regression (PLSR) models using the empirical and simulated FC matrices as predictors (**Figure 5.2d**). As a control, we included a third model based solely on anatomical information (the SDC matrix), as reported in previous literature (J. C. Griffis et al., 2019; Siegel et al., 2016). PLSR is a multivariate regression technique (Wold et al., 2001) that is closely related to principal components regression (Hotelling, 1957). Both approaches are especially useful for situations where there are more variables than observations and/or when there is high collinearity among the predictor variables. Nevertheless, PLSR has important advantages that are primarily due to differences in the criteria used for decomposition of the predictor matrix (J. C. Griffis et al., 2019). Detailed descriptions of theory and algorithms behind the PLSR approach are explained in previous literature (Krishnan et al., 2011)

Global efficiency

Global efficiency was calculated as the average inverse shortest path length (Latora & Marchiori, 2001). Unlike path length, the global efficiency can be calculated on disconnected networks, as paths between disconnected nodes are defined to have infinite length, and correspondingly zero efficiency. Therefore, it is an ideal metric when investigating stroke data. In contrast to path length, which is primarily influenced by long paths, global efficiency is primarily influenced by short paths. Different authors have claimed that this may convert global efficiency into a superior metric of integration (Achard & Bullmore, 2007; Rubinov & Sporns, 2010). Global efficiency is calculated as follows (Latora & Marchiori, 2001; Rubinov & Sporns, 2010):

$$E = \frac{1}{n} \sum_{i \in N} \frac{\sum j \in N, j \neq i \; d_{ij}}{n-1}$$

(5.6)

Where N is the set of all nodes in the network, n is the number of nodes, and (ij) is a link between the nodes i and j.

FC Entropy

FC entropy is an information theoretical metric that measures the richness of the functional connections and therefore may be a relevant biomarker for many disorders (Rocha et al., 2022; Saenger et al., 2018; Zamora-López et al., 2016). Previous studies have reported abnormal FC entropy values when comparing healthy controls with stroke patients (Adhikari et al., 2017; Saenger et al., 2018). However, these models use generic anatomical connectomes based on group averages instead of personalized structural connectivity. Although the current study used an atlas-based structural connectome for modeling the healthy control subjects, this connectome was separately modified for each patient based on their lesion.

Entropy is calculated as follows (Rocha et al., 2022):

$$H = -\sum_{i=1}^{m} p_i \log p_i / log_m$$

(5.7)

Where m is the number of bins used to construct the probability distribution function of the upper triangular element of |FC|. The normalization factor in the denominator is the entropy of a uniform distribution, and it ensures that H is normalized between 0 and 1.

Average degree

Average degree is a measure of the overall network connectivity that provides information about the network segregation and integration (Rubinov & Sporns, 2010). Average degree is calculated as follows (Rocha et al., 2022):

$$K = \frac{\sum_v k_v}{N} \tag{5.8}$$

Where N is the number of nodes and k_v is the degree of the node v as defined above.

5.3 Results

To infer the dynamical effects of stroke lesions two weeks after onset, we used a computational model based on coupled Stuart Landau oscillators (**Figure 5.1a**). The model contains a global scale factor, also referred to as the G coupling value, which determines the influence of SC in the model. It also contains GEC parameters that capture directional interactions between regions. Both types of parameters are optimized to improve the model fit (similarity of empirical and model FC). In the current study, we use only the functional data of the healthy control dataset to optimize these parameters at the group level. Performing an exhaustive exploration of the homogeneous parameter space (a, G) around the Hopf bifurcation (a = -0.01), we found G = 0.75 as the optimal value of G for which the modeled FC of the Hilbert phases were most similar to those observed in the empirical data. Initializing the GEC to be equal to the SC, we iteratively adjusted its values to improve the similarity between the model and empirical FC at a group level. **Figure C1** shows the role of the structural connections between parcels by assessing the difference between the empirical and simulated FC.

To simulate the functional data of stroke patients, we added individual information about the structural damage to the healthy group GEC by using a structural disconnection mask. Therefore, the model (referred to as the full predictive model) generated a simulated version of a functional connectivity matrix for each stroke patient as an output (**Figure 5.1b**).

From the obtained simulations, several metrics were calculated in order to assess how well the model captured the functional effects of stroke. For this purpose, among other results, we considered the main FC-based metrics that are known to give abnormal values in stroke patients (mean intra-hemispheric FC between the DAN and DMN, mean homotopic interhemispheric FC, and modularity level). We used the accuracy of the model (the goodness of fit

level) to classify patients according to their severity level. Lastly, the fitting of the model was related to behavioral impairment in several cognitive domains (**Figure 5.1c**).

The full predictive model reproduces the functional consequences of the stroke lesions by exploiting individual structural disconnection maps for each patient. Importantly, in contrast to previously reported models, it predicts a patient's functional connectivity.

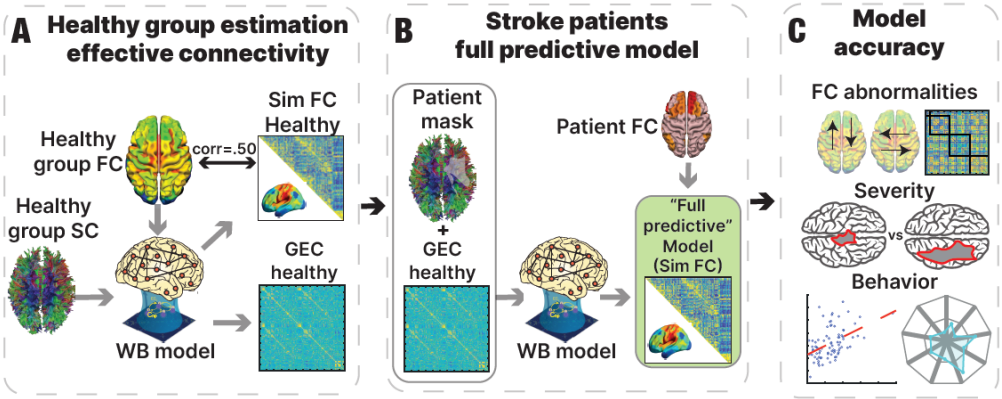

Figure 5.1: Pipeline of predictive model's analysis

Figure 5.1: Pipeline of the predictive model: **(A)** Healthy control generative effective connectivity (GEC) was calculated by using the healthy template SC with each healthy control fMRI time series. The model was optimized using a whole-brain (WB) model in order to create an average GEC for the healthy controls. **(B)** The predictive model used each patient's disconnection mask to modify the control GEC and obtain the patient's simulated FC, referred to in the figure as the full predictive model. **(C)** We determined the model's accuracy in predicting a subject's FC matrix (**Figures 5.2a**), FC-derived measures that are typically abnormal following a stroke (**Figure 5.2b**), patient abnormalities in FC **(Figure 5.2c**) ,and a patient's behavioral deficits (**Figure 5.2d**) . We also investigated the determinants of model accuracy by examining whether the accuracy of a patient's simulated FC matrix covaried with the

severity of their lesion-induced structural damage (**Figure 5.3a**), the magnitude of FC-based and graph-related functional measures that are typically abnormal following a stroke **(Figures 5.3b-5.3e**), and the magnitude of the patient's behavioral deficits (**Figure 5.3f**).

5.3.1 Model outcomes and their relationship with stroke effects

We assessed the validity and accuracy of the full predictive model by inspecting a wide range of metrics extensively reported in previous literature. In order to quantify the relationship between the empirical and simulated data (obtained from the model), we measured a goodness-of-fit level as the Pearson correlation between the empirical and simulated FC matrices and inspected if the obtained value gave an indication of impairment or abnormalities in any of the other metrics.

We first determined how well the model predicted each subject's empirical FC matrix by computing the Pearson correlation between the healthy control subject's predicted and empirical FC matrix. **Figure 5.2a** shows the distribution of correlation coefficients over the entire sample, indicating that the predictive model generated simulated FC matrices that consistently showed a moderate level of accuracy (group mean, r=0.43, std=.05; **Figure 5.2a**).

To assess whether the model accurately predicted specifically the abnormalities in a patient's FC that resulted from their stroke, we correlated each patient's empirical and simulated z-scored FC abnormality matrices. **Figure 5.2c** shows that the mean correlation across patients was significantly positive ($t(95)= 12.65$, $p< .01$), indicating that patient abnormalities in FC were significantly predicted.

Next, we analyzed how well the model predicted specific FC-based measures that are typically abnormal in stroke patients: 1) a decrease of negative intra-hemispheric FC between regions of the Dorsal attention networks (DAN) and Default mode network (DMN); 2) a decrease of inter-hemispheric homotopic FC; 3) a decrease of modularity. **Figure 5.2b** shows that the empirical and simulated values for these three signatures of stroke were significantly correlated across patients (intra-hemispheric: r=.47, p<.01; inter-hemispheric: r=.46, p<.01; modularity: r=.40, p=.03). Previous studies have shown that whole-brain GEC models preserve the same three FC-based measures, especially when they include structural disconnection information, revealing the key importance of incorporating this information into the models (Idesis, Favaretto, et al., 2022). In addition, for each patient we separately averaged the entries in their z-scored FC abnormality matrix for interhemispheric homotopic FC and DAN-DMN FC to assess whether the model specifically predicted patient abnormalities in these two FC measures. The results, shown in **Figure C9**, indicate that abnormalities in both FC measures were significantly predicted. Therefore, these results indicate that the predictive model reproduced to some extent the overall FC matrix, patient-specific abnormalities in that matrix, summary FC-based measures that are typically abnormal following a stroke, and patient-specific abnormalities in those measures.

Finally, we used Partial Least Squares Regression (see Methods) in order to separately assess how well the simulated FC matrices, the empirical FC matrix, the z-scored FC abnormality matrix (showing how abnormal was the matrix compared to the control) and the SDC matrix predicted the patients' behavioral scores. Although the simulated FC matrix was modestly predictive across behavioral domains, the model independent SDC matrix showed nominally better performance with the exception of the domains for Attention VF, Attention Ave, and Memory Verbal (**Figure 5.2d**). The empirical FC matrix

showed lower performance than the z-scored and simulated FC matrices across all domains, possibly because the predictive model that generated a patient's simulated FC matrix explicitly incorporated their structural disconnection matrix. Overall, these results indicate that although the predictive model partly accounted for behavioral abnormalities, the model did not generally perform better than a purely structural measure.

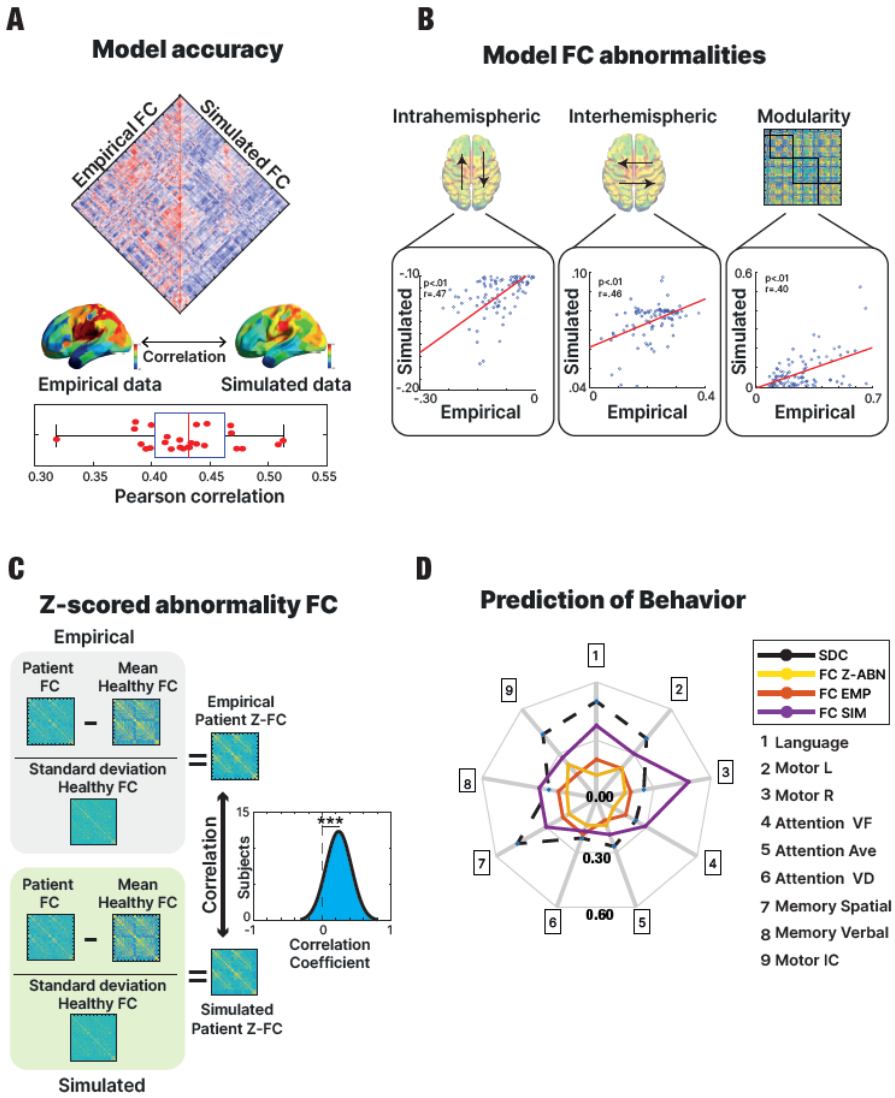

Figure 5.2: Model prediction of patient FC and behavior

Figure 5.2: Model prediction of patient FC and behavior. **(A)** The Pearson correlation between the empirical and simulated FC matrices of each subject was computed in order to assess model accuracy. **(B)** FC-based measures typically abnormal in stroke patients were calculated from the empirical and simulated FC matrices in order to compare their similarity. **(C)** The distribution across patients of the correlation between the empirical and simulated z-scored FC abnormality matrices for each patient. **(D)** Separate partial least squares regression (PLSR) analyses using the empirical, z-scored, and simulated FC matrices and the structural disconnection matrix as regressors were conducted to predict each domain of behavioral impairment.

5.3.2 Model accuracy in relation to structural damage and global metrics

In order to identify factors that determine how accurately a patient's FC matrix is simulated by the predictive model, we next investigated whether structural and functional features affect how accurately the model accounts for the data from individual patients. Specifically, we examined whether the accuracy of the model's simulation of a patient's FC matrix, as indexed by the correlation between the patient's simulated and empirical FC matrices, covaried with the structural damage from the patient's lesion, the values of the patient's graph-based functional metrics, and the values of the patient's simulated or empirical FC matrices.

We found that higher model accuracy was associated with lower values of total structural disconnection (r: -.58, p<.01), which served as a measure of overall lesion damage (**Figure 5.3A, left panel**). When splitting the sample in half by using the median value of total structural disconnection, patients with greater total disconnection showed significantly lower model accuracy ($t(94)$= 5.82, p< .01) (**Figure 5.3a, right panel**). A similar analysis using lesion volume (number of damaged voxels) as an alternative metric yielded similar results (**Figure C2**; an example of a patient lesion and the corresponding asymmetric effective connectivity matrix is shown in **Figure C3**).

The dependence of model accuracy on lesion severity was consistent with its dependence on the magnitude of graph-based metrics that are typically abnormal following a stroke (Rocha et al., 2022). We found significant positive correlations between model accuracy and global efficiency (r=.54, p<.01; **Figure 5.3b**), entropy (r=.30, p<.01; **Figure 5.3c**), and average degree (r=.58, p<.01; **Figure 5.3d**).

Furthermore, the Full Predictive whole brain model generated FC matrices whose correlation with empirical FC matrices (i.e., model accuracy) was significantly related to the magnitudes of intra-hemispheric FC (r=-.23, p=.02) and FC modularity (r=.33, p<.01) as seen in Figure **5.3e**. The sign of the relationship was consistent with the conclusion from **Figures 5.3a** and **5.3b-d** that the model poorly predicted the functional measures of patients that had more abnormal structural or functional measures. However, model accuracy was not correlated with the magnitude of inter-hemispheric FC, which is typically lower in stroke patients than controls.

Finally, separate PLSR analyses showed that model accuracy for a patient was well predicted by the full SDC matrix, next by the simulated FC matrix, the z-scored FC matrix and least by the empirical FC matrix (SDC: R^2=0.66, p<.01, Sim-FC: R^2: 0.37, p<.01, Z-scored Abnormality FC: R^2: 0.35, p<.01, and Emp-FC: R^2: 0.27, p<.01) (**Figure 5.3f**).

Overall, these results indicate that the model's ability to accurately reproduce a patient's FC matrix decreased as the patient's structural measures, and to a lesser extent functional measures, showed larger departures from those for healthy controls.

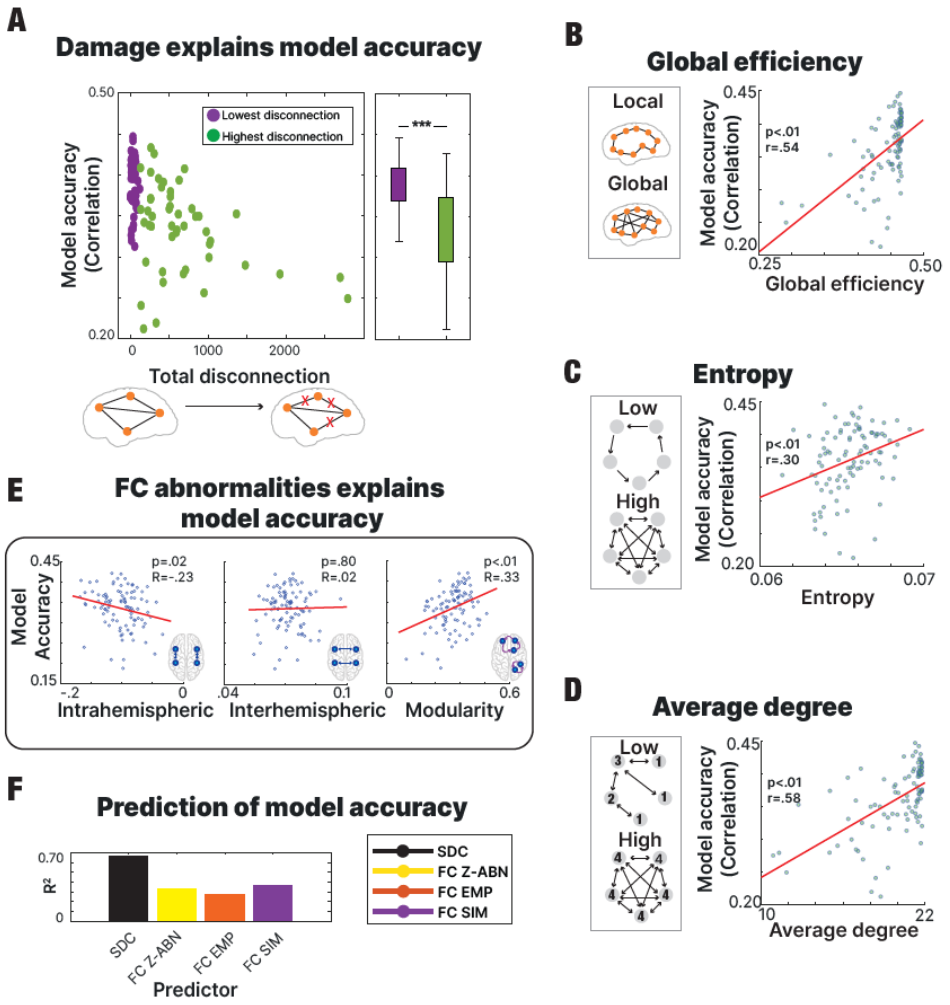

Figure 5.3: Structural and functional determinants of model accuracy for individual patients

Figure 5.3: Structural and functional determinants of model accuracy for individual patients **(A)** Subjects with lower levels of disconnection exhibited a higher correlation between the empirical and simulated FC matrices, indicating better model performance for patients with less severe lesions. **(B-C-D)** Higher global efficiency **(B)**, entropy (C) and average degree (D) were associated with higher model accuracy. **(E)** Model accuracy for FC-based measures typically abnormal in stroke patients was assessed for the presented model. Accuracy of the full predictive model was significantly associated with the magnitude of intrahemispheric FC and modularity but not interhemispheric FC. **(F)** Model accuracy predicted by each type of regressor (SDC matrix, FC empirical and FC simulated matrices, z-scored FC abnormality matrix) in a PLSR analysis of model accuracy.

5.3.3 Model comparison

Having established the accuracy with which the Full Predictive model reproduced measures that are typically abnormal in stroke patients (**Figures 5.2b and 5.2c**), we compared its performance with a patient-specific and non-predictive model reported in a previous study (Idesis, Favaretto, et al., 2022) that used both anatomical and functional information to simulate a patient's time series (referred to as the Non-predictive patient specific model) (**Figure 5.4a**).

Secondly, two comparative predictive models were chosen to assess how much model accuracy depended on the disconnection mask that was incorporated in the Full Predictive model. The model without mask allowed us to assess the accuracy gain obtained by incorporating the patient's lesion information, with respect to not incorporating any lesion information (i.e., using the healthy group GEC for all patients). The surrogate mask model allowed us to assess the accuracy gain obtained by incorporating specifically the patient's lesion information, with respect to using a lesion from a different patient (**Figure 5.4b**).

We compared the performance of all models by computing the correlation of the simulated and empirical FC matrices. The Full Predictive model showed roughly equivalent accuracy to the Non-predictive patient specific model (Idesis, Favaretto, et al., 2022), while the Model with surrogate mask and the model without mask showed lower accuracy (**Figure 5.4c**).

An ANOVA indicated that the main effect of model type (non-predictive, full predictive, no mask, surrogate mask) on accuracy was significant ($F(3,378)= 30.74$, $p<.01$). Post-hoc tests indicated that the patient-specific and full predictive models did not significantly differ in accuracy ($p<.36$) but were

significantly more accurate than both the surrogate mask and no mask models (p<.01 in all cases). Model accuracy relative to the accuracy of the healthy control group model is shown in **Figure C4**. The influence of the global coupling parameter (GC) is presented in **Figure C5**. The relation between the accuracy of each model and the magnitude of FC measures typically abnormal in stroke patients is presented in **Figure C6**. Comparisons of dynamical metrics between the models are presented in **Figure C8** (see figure caption for explanation of metrics).

Overall, the results show the efficacy of the full predictive model, which does not use a patient's functional BOLD data, allowing its predictions to be generalized to new patient datasets, and opening the door for predicting the expected effects of a simulated lesion or external stimulation of a patient's brain.

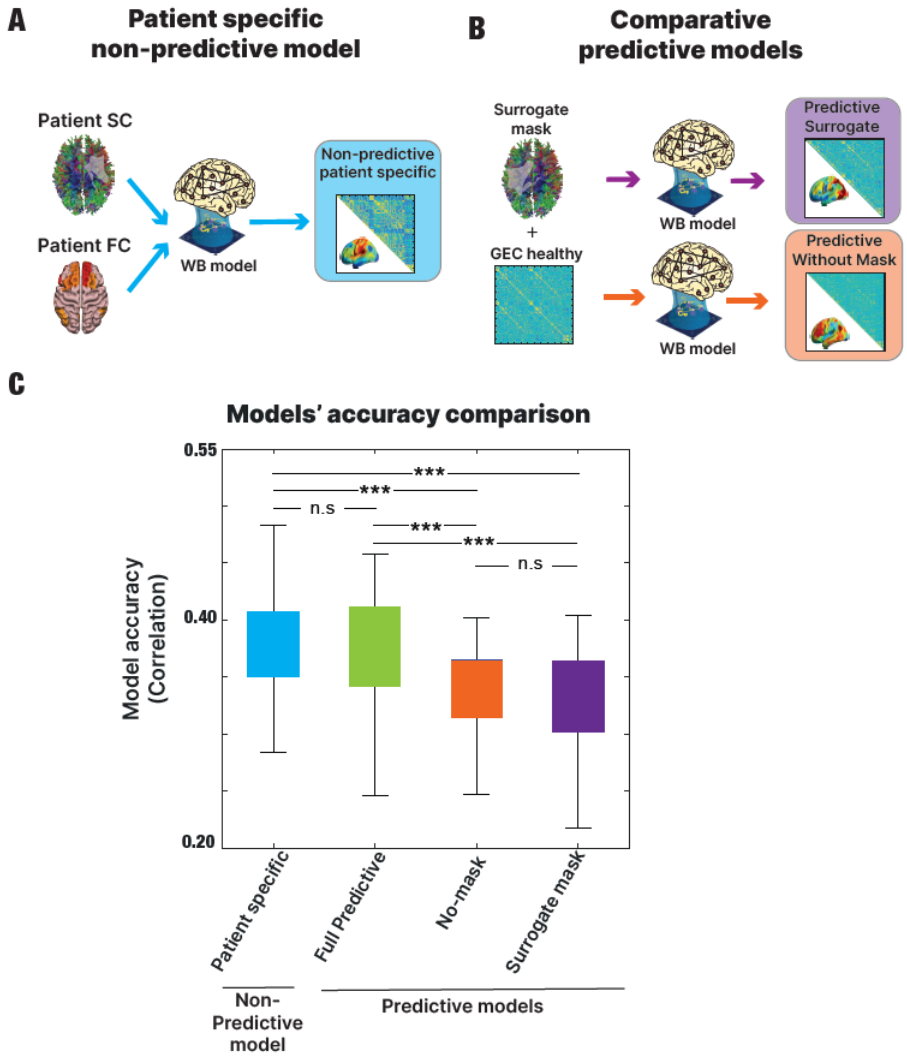

Figure 5.4: Model comparisons

Figure. 5.4: Model comparisons: **(A)** We calculated the Non-predictive patient specific model using both the anatomical and functional data of each patient. This model was not predictive since it was fit to the patient's functional data. **(B)** We calculated two comparative predictive models to compare with the full predictive model. The Predictive No-mask model was built using only the healthy GEC while the predictive surrogate mask model was calculated by modifying the healthy GEC via the disconnection mask of a different patient. **(C)** The similarity between the empirical and simulated FC matrices was assessed for each model. The non-predictive patient specific model and full predictive model showed similar levels of performance that exceeded performance for the surrogate and no-mask models.

5.4 Discussion

The results show that functional connectivity in patients could be predicted by a whole-brain computational model strictly from the structural disconnection caused by patient's lesion, suggesting that the model mechanistically captured to some degree the relationship between anatomical structure and functional activity. Moreover, the model significantly predicted abnormalities in patient FC with respect to the FC of the healthy control group Although the model also predicted the behavioral abnormalities of patients, prediction was no better than that obtained using a purely structural measure, the structural disconnection matrix. While previous work has examined how well computational models can reproduce FC when model parameters are directly fitted using functional and structural data from healthy controls or stroke patients (Adhikari, Griffis, et al., 2021; Idesis, Favaretto, et al., 2022), the current study moves fundamentally beyond such work by determining whether these models can in fact predict the effects of a stroke based solely on the structural information associated with a patient's lesion (Rocha et al., 2022).

We first fit the model to data from age- and education-matched healthy controls based on a healthy structural connectome and the healthy controls' functional imaging data. For each patient, we then determined how the patient's lesion has modified the healthy structural connectome and made corresponding changes to the structural connectivity parameters in the healthy model (the GC parameters) without additional model fitting or recourse to the patient's functional data. Finally, the modified healthy model specific to the patient generated the patient's predicted FC, which was compared against the empirically measured FC. Specifically, model accuracy was evaluated by assessing the correlation between the patient's empirical and predicted FC matrices. Because FC matrices specify the functional interactions between each pair of brain regions, the predicted matrices

potentially provide information concerning which functional connections are particularly vulnerable in the patient, a possibility also raised by the prediction of patients' z-scored FC abnormality matrices.

Perhaps the most surprising result was that the accuracy of the full predictive model was essentially equivalent to the accuracy obtained by fitting the model directly to the patient's functional and structural data. Moreover, the accuracy of the full predictive model depended on incorporating the structural disconnection specific to that patient's lesion, as shown by the significantly poorer performance obtained by substituting the structural disconnection for a different patient. However, the accuracy for predicting a patient's FC matrix tended to be less the more a patient's structural connectome and functional measures differed from the structural connectome and functional measures of healthy control subjects. Specifically, accuracy decreased with the magnitude of the total structural disconnection caused by the lesion. Similarly, measures of modularity and intra-hemispheric FC and graph-based measures that are typically abnormal following a stroke tended to be more poorly predicted the more they differed from healthy control values (surprisingly, a similar relationship was not observed for inter-hemispheric FC, an important signature of stroke-induced dysfunction). One interpretation is that the model tended to better predict patients that were more similar to healthy controls since it was initially based on a model computed from healthy control data. Another possibility is that similar relationships are also present for the non-predictive patient-specific model, i.e., the dependence of model accuracy on structural and functional measures is not related to prediction per se. The results in **Figures C6 and C7** provide some support for this alternative explanation. For example, the accuracy of the patient-specific non-predictive model tended to decrease with the magnitude of a patient's inter-hemispheric FC (**Figure C6**). However, the results do not rule out the first explanation as a contributing factor.

Previous computational work based on concepts from statistical mechanics has shown that resting-state organization conforms to a state of 'criticality' that promotes responsiveness to external stimulation, i.e., resting state organization facilitates task-based processing (Deco & Jirsa, 2012; Deco, Ponce-Alvarez, et al., 2014; Sanz Perl et al., 2022; Senden et al., 2017). The rich body of empirical work on resting-state organization has facilitated an important testing ground for evaluating computational whole-brain models. In these models, neural modules or elements are connected by 'structural' links that mirror the empirical structural connectivity of the human brain as assessed using diffusion-based MRI (Deco & Jirsa, 2012; Deco et al., 2011; Deco, Ponce-Alvarez, et al., 2014), resulting in resting-state dynamics that respect critically. Initial applications of whole-brain computational models to stroke populations (Adhikari et al., 2017; Saenger et al., 2018) used the biophysically-based model of Deco et al. (Deco, Ponce-Alvarez, et al., 2014), which involves a mean field approximation of populations of spiking neurons with realistic NMDA, AMPA, and GABA synaptic dynamics. However, the authors subsequently developed the mesoscopic Hopf model (Deco et al., 2019) used in the current study, which provides a better fit to healthy control data and runs two orders of magnitude faster, allowing the use of higher-resolution functional parcellations that likely increase model accuracy.

The whole-brain computational models presented in recent studies that involve stroke patients included a global coupling parameter and GEC parameters that encoded directional interactions between nodes that had direct structural connections (Adhikari, Griffis, et al., 2021; Idesis, Favaretto, et al., 2022). The resulting generative effective structural connectivity weights allowed a better fit between the empirical and modeled FC than that achieved by models that only varied the global coupling parameter. In both papers, however, the model was fit directly to a patient's functional data, and therefore was not a predictive model.

The mesoscopic Hopf model (Deco et al., 2019) includes global coupling and GC parameters that affect the connectivity between nodes of the model and bifurcation parameters that affect the dynamics of the nodes. Specifically, the bifurcation parameter for a node governs the transition between noise-dominated and oscillatory behavior. The current work assumed that strokes do not affect the bifurcation parameters/nodes, only the connections between nodes, yet prior studies indicate that delta waves are prominent perilesional and propagate to directly connected regions (Russo et al., 2021; Sarasso et al., 2020). Therefore, nodes for perilesional/partly damaged parcels and perhaps directly connected parcels may have abnormal bifurcation parameters. Evaluating this possibility is beyond the scope of this work but is currently in progress. On the positive side, properly accounting for abnormal bifurcation parameters/nodes may improve model accuracy. On the negative side, it is unclear how node abnormality might be incorporated into a fully predictive model.

The presented full predictive model could be applied in future work to other focal and non-focal pathologies that damage the structural connectome. Also, the current study focused on predicting FC in sub-acute stroke patients, but future studies could examine whether changes in structural connectivity during recovery produce predicted changes in FC. Because the dataset consisted mostly of ischemic patients; however, model predictions will need to be tested in hemorrhagic stroke patients before concluding that the model applies more generally to stroke.

In conclusion, the current study shows that the effect of stroke-induced perturbations in structural connectivity on functional dynamics can be captured by a fully predictive whole-brain computational model. Therefore, adding lesion information to a model trained on healthy functional data is sufficient to reproduce functional anomalies, even though the accuracy of prediction worsens for patients showing greater structural damage and

functional deficits. Despite this limitation, the predictive model can provide unique insights into how strokes disrupt resting brain organization.

CHAPTER 6

6. Recovery prediction: Latent information contribution to the prediction of stroke patients' recovery

Work in this chapter reflects a paper currently under review.

Highlights

- We found a low-dimensional representation encoding the fMRI data which preserves the typical FC anomalies known to be present in stroke patients
- We enhanced patients' diagnostics and severity classification.
- We showed how low-dimensional representation increased the accuracy of recovery prediction.
- We revealed how complexity metrics such as brain signal reversibility provided indicators that relate to lesion severity and lesion recovery

Abstract

Large-scale brain networks reveal synchronization between distinct regions of the brain, referred to as functional connectivity (FC), which can be observed through neuroimaging techniques such as functional magnetic resonance imaging (fMRI). FC studies have shown that brain networks are severely disrupted by stroke. However, since FC data are usually large and high-dimensional, extracting clinically useful information from this vast amount of data is still a great challenge, and our understanding of the functional consequences of stroke remains limited. Here, we propose a dimensionality reduction approach to simplify the analysis of this complex neural data. By using autoencoders, we find a low-dimensional representation encoding the fMRI data which preserves the typical FC anomalies known to be present in stroke patients. By employing the latent representations emerging from the autoencoders, we enhanced patients' diagnostics and severity classification. Furthermore, we showed how low-dimensional representation increased the accuracy of recovery prediction.

Keywords

Stroke – fMRI - Dimensionality reduction – Reversibility - Recovery prediction

6.1 Introduction

There is a growing amount of evidence that neural activity is low-dimensional, at various scales, in agreement with theoretical work arguing that low-dimensional dynamics exist in the brain because neural circuits operate more effectively in low dimensions (Dubreuil et al., 2020; Schuessler et al., 2020). This suggests that the huge dimensionality of functional neuroimaging data (millions of voxels or hundreds of regions) may be highly redundant, and that it may be possible to find low-dimensional representations, or "latent signals" (Humphries, 2020) preserving most of the relevant information content. However, evidence that a low-dimensional representation can actually retain the most prominent dynamical features, including, crucially, clinically relevant features, is still weak.

In this work, we use dimensionality reduction, which maps high-dimensional data into a new space whose dimensionality is much smaller (Shalev-Shwartz & Ben-David, 2014), to investigate low-dimensional representations of fMRI data in normal subjects and stroke patients. This is an ideal testbed to assess the clinical relevance of low-dimensional representation. At the population level there is strong evidence that post-stroke neurological impairments have a low-dimensional structure (Corbetta et al., 2018). Moreover, stroke produces dysfunction in distributed brain networks (Carrera & Tononi, 2014), which are commonly identified as low-dimensional abnormalities in functional connectivity (FC) that predict behavioral deficits after stroke. These include reductions in interhemispheric network integration, ipsilesional network segregation, and network modularity (Arnemann et al., 2015; Baldassarre et al., 2016; Crofts et al., 2011; Gratton et al., 2012; Joseph C Griffis et al., 2019; J. C. Griffis et al., 2019; Meunier et al., 2010; Siegel et al., 2016).

Classic dimension reduction techniques, such as PCA, are linear. When applying a linear method to neural activity data and keeping d dimensions,

one is implicitly assuming that the neural activity sits on a d-dimensional plane. However, the actual shape – the manifold – on which the neural activity sits is generally a curved nonlinear surface (Cunningham & Yu, 2014). Machine learning can be employed to find low-dimensional, nonlinear representations of complex data with only a small set of latent variables. While several previous studies have applied deep learning in fMRI data (Firat et al., 2015; Han et al., 2015; Huang et al., 2017), they have mainly focused on classification accuracy, rather than low-dimensional representations. Here, we apply deep learning methods directly to functional time series to extract a nonlinear low-dimensional representation of brain dynamics. In addition, we leverage the power of the recently proposed Temporal Evolution NETwork (TENET) framework (Deco et al., 2021; Deco et al., 2022) to analyze the asymmetry, or "reversibility" in the flow of the brain signals. TENET offers critical insight about the degree of non-equilibrium in brain dynamics, a variable that has been shown to be severely altered in consciousness disorders (Deco et al., 2022) and could be of high clinical significance in other neurological conditions. TENET requires to compare cross-correlation matrices, whose estimation is affected by large error in high dimensional spaces, and therefore is expected to significantly profit from a dimensionality reduction step.

Here, we will demonstrate that the latent non-linear components of brain dynamics found by machine-learning approaches retain the most important dynamical features that are usually identified from the high-dimensional original data. Furthermore, we will demonstrate that the latent representation is more powerful, both for diagnostic and for prognostic purposes. Diagnostically, the latent representation yields a better classification of clinical status (healthy/mild stroke/severe stroke) at the acute stage, and a better prediction of behavioral deficit. Prognostically, it improves the prediction of recovery after 1 year of the incident, as compared to other methods.

6.2 Material and methods

6.2.1 FC abnormalities

Local ischemia, which damages cells and neural connections at the site of injury, primarily affects white matter, thus altering long-range FC between cortical areas. Three types of large-scale FC alterations affect Resting State Networks (RSNs) (Siegel et al., 2016): i) within-network interhemispheric FC (Crofts et al., 2011; Joseph C Griffis et al., 2019; J. C. Griffis et al., 2019; Siegel et al., 2016) ii) between-network intra-hemispheric FC (Arnemann et al., 2015; Baldassarre et al., 2016; Gratton et al., 2012; Siegel et al., 2016); and iii) Modularity (Gratton et al., 2012; Meunier et al., 2010; Siegel et al., 2018).

6.2.2 Autoencoder

An autoencoder takes an input with a high dimensionality, processes it through a neural network and tries to compress the data into a smaller representation (Huang et al., 2017). In order to achieve this, the procedure takes two steps: encoding (embedding) and decoding (reconstruction). The autoencoder, therefore, consists of a deep neural network with rectified linear units as activation functions and dense layers, which bottlenecks into the d-dimensional layer (Sanz Perl et al., 2021). Gradient descent was implemented to backpropagate the errors, with the purpose of training the network. The minimized loss function consists of a canonical reconstruction error term (calculated from the output layer of the decoder).

Subsequently, to acquire training and test sets, we produced 80/20% random splits. We employed the training set to optimize the autoencoder parameters.

The training process involved batches with 256 samples and 100 training epochs (if needed) making use of the loss function and an Adam optimizer (Sanz Perl et al., 2021)

The encoder network applies a nonlinear transformation to map the input signal into Gaussian probability distributions in latent space, and the decoder network mirrors the encoder architecture to produce reconstructed matrices from samples of these distributions. By observing the reconstruction loss (comparison between the output and input signal), the performance of the autoencoder could be tuned to the appropriate hyperparameter configuration (**Figure D2a**). Autoencoders have proven to be effective even when applied on small sample sizes (Lin et al., 2022), such as the one considered here (time points x subjects = 48384). In order to avoid overfitting, we applied 10 iterations of cross-validation (80/20) and early stopping techniques (as the performance of the model increases to a peak point, training can be stopped). As input for the autoencoder we used the BOLD signal of both healthy controls and stroke patients (**Figure 6.1a**). Therefore, the input (and the output) of the autoencoder consists of a matrix with the number of ROIs as the number of rows and the concatenated time points of the subjects' time series as columns (every subject provides 896 samples for the AE training). This results in a 235-by-896 matrix of data representing each subject. Nevertheless, for the classification and prediction analyses, different metrics were used as input (See methods).

6.2.3 Edge-centric analysis

Using a straightforward unwrapping of the Pearson correlation, co-fluctuation time series (alternatively referred to as "edge time series") data can be estimated for each edge. Unlike sliding-window time-varying connectivity, which requires the parameterization of a window duration, kernel shape, and

step size, edge time series have the same temporal resolution as the original time series data. Importantly, the time-averaged value of edge time series is the correlation coefficient. This means that edge time series are a mathematically exact decomposition of a functional connection into its framewise contributions. Previous analyses of edge time series data have shown that transient periods of high-amplitude activity make disproportionately large contributions to the time-averaged functional connectivity (Cifre et al., 2020; Petridou et al., 2013; Enzo Tagliazucchi et al., 2012; Zamani Esfahlani et al., 2020). In other words, data selected from specific temporal slices can be used to reconstruct a similarity matrix with a high correspondence to the functional connectivity matrix constructed from the full dataset (Betzel et al., 2021; Greenwell et al., 2021).

In the current study, we applied a peak detection algorithm as described previously (Pope et al., 2021). The collective co-fluctuations of brain regions were estimated as the root sum square (RSS) of co-fluctuations between all pairs of brain regions (edges) at every time point. Next, BOLD time series were randomly shifted (using MATLAB's circshift operator), hence approximately preserving each node's autocorrelation, while randomizing the cross-correlation across nodes. This null model was iterated 1,000 times. Time points in the original time series for which the empirically observed RSS amplitude exceeded the null model (P<0:001) were maintained. The resulting peaks in the original RSS at the corresponding time points were considered as significant events. RSS peaks that exceed extreme z-score values (above or below 4.5 deviations) were excluded from the analysis. These peaks do not occur frequently (at most once per 1,100 frames). The correlation between the FC created by the timepoints containing peaks, and the original FC, gives an indication of how much information is contained in these specific points (Idesis, Faskowitz, et al., 2022).

Edge-centric analysis has been applied to stroke datasets in a previous study referenced in chapter 3 (Idesis, Faskowitz, et al., 2022). This work demonstrated that edge-centric measures, such as normalized entropy or high-amplitude co-fluctuations (transient periods of high-amplitude activity), can be used as indicators of lesion severity and recovery (Idesis, Faskowitz, et al., 2022).

6.2.4 Dynamic features preserved/enhanced in latent space

6.2.4.1 FCD

Time versus-time matrix representing the functional connectivity dynamics (FCD), where each entry FCD(t1, t2) is defined by a measure of resemblance between FC(t1) and FC(t2) (Cabral, Kringelbach, et al., 2017; Deco et al., 2017). Therefore, the FCD captures the spatiotemporal organization of FC by representing the coincidences between FC(t) matrices. It results in a symmetric matrix where an entry (ts1, ts2) is defined by the Pearson correlation between FC(ts1) and FC(ts2) (Deco & Kringelbach, 2016)

6.2.4.2 Edge metastability

We calculated the standard deviation of the edge time series which represents the temporal metastability. This metric gives information about temporal variability in the level of synchronization (Capouskova et al., 2022; Piccinini et al., 2022).

6.2.4.3 Modularity

Overall Newman's modularity was calculated, making a comparison between the number of connections within a module to the number of connections

between modules (Newman & Girvan, 2004). We adopted a constant null derived from the Potts model (Traag et al., 2011). We retained the full FC matrix, including its negative entries, for the purpose of community detection by applying the Louvain algorithm. Louvain bipartitions are identified by first inspecting a wide range of the resolution parameter, selecting upper and lower boundaries within which a two-community structure occurs, followed by a finer sampling of the range to retrieve bipartitions.

6.2.4.4 Functional Complexity

Functional complexity was calculated based on previous literature (Zamora-López et al., 2016). According to this definition, complexity emerges when the collective dynamics are characterized by intermediate states, between independence and global synchrony (Tononi et al., 1994). Thus, the authors choose to define complexity as the difference between the observed distribution of the functional connectivity and a uniform distribution. Hence, functional complexity is quantified as the integral between the two distributions. The latter is estimated by approximating the distributions with histograms and replacing the integral with the sum of differences over the bins. The equation for the functional complexity is given below; for more information, see (Zamora-López et al., 2016).

$$C = 1 - \frac{1}{c_m} \sum_{\mu=1}^{m} \left| p_\mu(r_{ij}) - \frac{1}{m} \right| , \qquad (6.1)$$

Where |.| means the absolute value and $C_m = 2\,\frac{m-1}{m}$ is a normalization factor that represents the extreme cases in which the p(r_{ij}) is a Dirac-delta function δ_m.

6.2.5 Classification

A random forest classifier (Breiman, 2001; Sanz Perl et al., 2021) was used in order to classify the participants. Briefly, the random forest algorithm builds upon the concept of a decision tree classifier, where samples are iteratively split into two branches depending on the values of their features (Breiman, 2001; Sanz Perl et al., 2021). For the classification procedure, there were two different division criteria:

1) Distinction between controls and stroke patients
2) Distinction between patients with high vs low lesion volume (see chapter 2). As an alternative, we calculated the distinction using thee NIHSS as division criteria, showing similar results (**Figure D10**)

We trained random forest classifiers with 1000 decision trees using 80% of the subjects through cross-validation analysis. All accuracies were determined as the area under the receiver operating characteristic curve (AUC).

The same procedure was applied both in source and latent space, having as possible features either the upper triangle of the corresponding FC, or the upper triangle of the reversibility matrix (See Reversibility Section). The latent space information used was obtained from the latent dimension 6 due to the results obtained in **Figure 6.2c** and **Figure D2**.

The reversibility matrix is calculated as defined in previous literature (Deco et al., 2021; Deco et al., 2022) in which the difference is calculated between the signal in the “real arrow of time” compared to the “reversed arrow of time”. The resulting measure captures how different, or “asymmetrical”, the signal is across time. Key demographic variables such as age and gender may strongly affect our findings. Therefore, we verified that the two groups (patients/controls) were matched in terms of these variables (**Supp. Table D1**). In addition, to further control for the possible confounding influence of

these factors, we checked that the two metrics showing a significant patients/control difference did not present any significant age or gender effect. To this aim, we divided subjects by age (using the corresponding median) and gender. In both cases, we found no significant differences ($p>.2$) between the groups (**Figure D13**).

6.2.6 Latent space visualization through 2D-Projection Association dimension with each behavioral domain

In order to visualize the distribution of the subjects and obtain a more intuitive understanding of their variability, we converted the data in the latent space into a two-dimensional plane. In order to achieve this goal, we used t-Distributed Statistic Neighbor Embedding (t-SNE) (De Filippi et al., 2021; Van der Maaten & Hinton, 2008). The proposed approach aims to preserve the local and global data structure while visualizing all samples in a two-dimensional plane. The higher-dimensional data is transformed into a set of pairwise similarities and embedded in two dimensions such that similar samples are grouped together (Van der Maaten & Hinton, 2008). **Figure 6.3d** shows this approach performed both in the separation of controls versus patients, and patients with high versus low severity of damage. It is relevant to clarify the different amount of participants in both figures, as the first scatterplot is a comparison between a subset of patients (to have the same amount of subjects per group) against the healthy controls (the dataset consists of 27 healthy controls) while the second is a comparison within all the patients presented in the dataset (96 patients).

6.2.7 Association of reduced dimension with each behavioral domain

The relation between each of 9 behavioral tasks and the features used for the subjects' classification (See 6.2.5: Classification Section) was assessed by

means of Pearson correlation. The presented result in **Figure 6.3f** was performed with 6 dimensions. Furthermore, **Figure D3** shows the same analysis with 10 dimensions in order to demonstrate the influence of higher dimensions when using dimensionality reduction approaches.

6.2.8 FC distance

In order to measure the similarity or distance between the stroke patients FC (at each time point) and the healthy controls FC, we used the Frobenius norm of the difference between the two FC matrices. The higher the FC Distance, the higher the damaging impact of the lesion on the FC. Similarly, the lower the FC Distance, the lower is the impact (Vattikonda et al., 2016). As an alternative approach to calculate the FC, we used the pairwise co-classification of nodes for a consensus clustering procedure **(Figure D4).** Co-classification yields a full matrix of pairwise affinities between nodes (scaled between 0 and 1) and one can thus use existing community detection algorithms for the consensus clustering step (Jeub et al., 2018). This analysis was added as a control as it has proven to overcome existing problems while identifying community structures (Jeub et al., 2018).

6.2.9 Correlation FC/SC

For each subject, the structural–functional coupling metric was quantified using Pearson's correlation between structural (healthy control anatomical template, see methods) and functional connection strengths as reported in previous studies (Liégeois et al., 2020; Tsang et al., 2017; Zhang et al., 2017). Previous work has shown how the acute stages after stroke incidents reveal a low relation between the two matrices while the strength of their relation increase as the patients recovered, which enables its use as a metric of recovery across time (Zhang et al., 2017). As reported in previous studies

(Coletta et al., 2020), we calculated the correlation between the SC and FC values for each network in order to assess how the stroke incident altered the structural-functional coupling in the corresponding areas. (**Figure D5**)

6.2.10 Prediction of recovery

A random forest classifier was used in order to classify the participants based on their recovery, comparing the ones with high level (better recovery) against low level (worse recovery). For more details, see section 6.2.5: "Classification". The same procedure was applied both in source and latent space, using as possible features either the upper triangle of the corresponding FC, or the upper triangle of the reversibility matrix. The latent space information used was obtained from the latent dimension 6 due to the results obtained in **Figure 6.2c**.

The division between high vs low recovered was made by splitting the sample in two using the median of three distinct metrics.

1) Behavior: Amounts of domains recovered after 1 year.
2) FC Distance: Distance between the subjects FC after 1 year and the healthy control FC
3) Correlation FC-SC: FC-SC correlation of each subject after 1 year.

As an alternative for the behavioral metric, we applied a principal component analysis of the behavioral recovery scores ($\frac{1\text{ year score} - 2\text{ weeks score}}{2\text{ weeks score}}$) as used in previous literature (Ramsey et al., 2017). We used the first component's median as a separation criterion **(Figure D6).**

6.2.11 Relationship of each dimension with FC abnormalities

We estimated the relation between previously explained anatomical and functional features (See Chapter 2) with the mean and standard deviation of each time-pattern in the latent space giving as a result 30 possible associations (5 features x 6 dimensions). Results are presented in **Figure D7.**

6.2.12 Latent FC means per dimension

The Pearson correlation was calculated at the latent space with all the estimated dimensions giving as an output a matrix of DxD (Dimensions). The mean of the resulting matrix was obtained in order to compare across the different dimensions of the latent space. (**Figure D2b**)

6.3 Results

We derived a low-dimensional embedding of the BOLD signal of a group of healthy controls and stroke patients and analyzed the latent information contained in it (**Figure 6.1**). The technique calculates the reconstruction error at each latent space dimension (2 through 10) to identify the point at which the error stabilizes (**Figure D2a**). The correlation between the source and the latent space exceeds the value of 0.9 at dimension 6. Once obtained the latent representation, the resulting matrix of size DxT (Dimensions by time points) of the testing set is used to analyze the embedded properties of the signal. As a first step, several functional features were calculated in both source and latent space to determine whether the information is preserved after the dimensionality reduction. Next, the latent representation was used to classify healthy controls vs patients at the acute stage (2 weeks after the stroke incident). Last, the low-dimensional embedding at the acute stage was used to predict recovery, in order to compare the recovery prediction accuracy with that obtained with the source space signal. The present study shows how the embedded information obtained through autoencoders can improve over well-studied metrics of diagnostic and prediction of recovery.

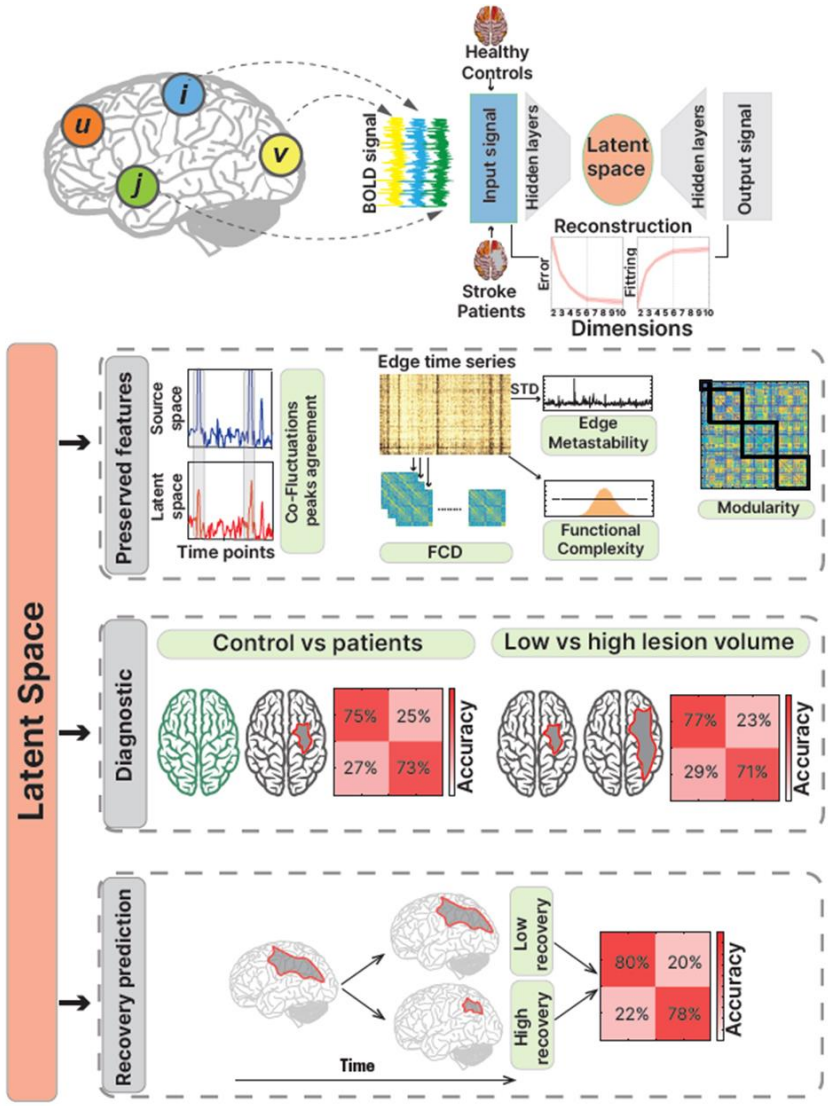

Figure 6.1: Pipeline of diagnostic and predictive analyses through latent space calculations

Figure 6.1: Pipeline of diagnostic and predictive analyses through latent space calculations: fMRI signals from both groups (healthy controls and stroke patients) were used as input signals for the autoencoder. Reconstruction error was calculated by assessing the difference between the output and the input signal. The latent information was used to perform three different analyses: **Top segment** shows the features both in source and latent space to verify if the information was preserved after the dimensionality reduction. **Middle segment** shows the accuracy of the classification used to separate healthy controls from stroke patients and to separate stroke patients with low and high severity.

Lower segment shows how the latent representation is used to predict the recovery after one year after the stroke.

6.3.1 Preserved features in latent space

The latent representation obtained through the autoencoder exposed how non-trivial dynamic features were preserved. To illustrate this point, we selected 5 different metrics that demonstrate various time series attributes (Co-fluctuations peak agreement, Functional Connectivity Dynamics, Edge metastability, Modularity, and Functional complexity). In all cases, the features were maintained, and in some cases, even enhanced. For some of the analysis, we focus on a specific dimensionality, with 6 dimensions, based on the results provided by the reconstruction error calculation (**Figure D2a**). It is worth clarifying that, as the latent reduction requires a division between training and testing dataset, the amount of subjects used for the latent space is slightly lower, as visible in the different degrees of freedom.

The same analyses were performed using a classical linear dimensionality reduction method, principal component analysis (PCA). To compare PCA with the latent representation obtained through the autoencoder, we used the same number of dimensions for the two methods, considering the 6 first principal components. These components accounted for only 85 percent of the total variance, implying that the autoencoder achieved a more efficient degree of dimensional compression. The results showed a higher performance of the autoencoder compared to PCA in preserving the dynamical features and discriminating between healthy controls and stroke patients (**Figure D14**). This suggests that the non-linear dimensionality reduction achieved though the autoencoder is much more efficient at capturing relevant dynamical features.

In order to assess the amount of temporal information that was preserved after the dimensionality reduction, we first calculated the edge time series (See methods section) **(Figure 6.2a)**. Furthermore, we compared how many

time points classified as peaks coincided in both spaces (peak agreement). The metric was normalized by dividing it by the sum of Peak Hits (coincidence) plus Peak Miss (not coincidence) **(Figure 6.2b)**. We calculated the metric across all latent dimensions. There is a significant increase in the peak agreement between dimensions 5 and 6 ($t(170)= -8.75$, $p < .01$), while no other consequent dimension exhibited significant differences revealing, how the level of agreement stabilized after reaching dimension 6 (**Figure 6.2c**). Remarkably, the stabilization of the peak agreement coincided with the one observed in the reconstruction error. These findings support the selection of 6 as the optimal dimension for performing the following analysis.

We compared the co-fluctuation high-amplitude peaks (See Methods section: Edge-centric analysis) in source and latent space. It has been reported that the aforementioned peaks contain a large amount of the signal information (Pope et al., 2021; Zamani Esfahlani et al., 2020). A way to assess this is by observing the correlation between the FC component, created by the timepoints containing peaks, and the original FC. Therefore, we calculated the association between the standard FC and the FC computed only using the timepoints that revealed to contain peaks, resulting in a maximum Pearson correlation value of R=.93 **(Figure 6.2d)**. Furthermore, the same correlation was displayed for all subjects showing an average association of R=.84 **(Figure 6.2e)**.

We compared the distribution of FCD between controls and stroke patients, revealing a significant difference in the source space ($t(1790)= -7.89$, $p < .01$). Nevertheless, the difference gets enhanced when comparing in the latent representation ($t(1790)= -36.20$, $p < .01$)) (**Figure 6.2f**)

While there is no significant difference in the source space while comparing the level of edge metastability between controls and stroke patients ($t(52)=$

.12, p = .9), the difference is significant when comparing in the latent representation *(*t(46)= 3.5, p < .01) (**Figure 6.2g).**

While there is a significant difference in the source space when comparing the level of Modularity between controls and stroke patients (t(121)= 4.48, p < 01), the difference is enhanced when comparing Modularity in the latent representation *(*t(46)= 8.77, p < .01)) (**Figure 6.2h**)

Finally, while there is a significant difference in the source space when comparing the level of Functional Complexity between controls and stroke patients (t(52)= 3.23, p < .01), the difference is comparable when calculating Functional Complexity in the latent representation *(*t(46)= 4.1, p < .01)) (**Figure 6.2i**)

In summary, the latent representation highlights crucial dynamical differences between patients and controls.

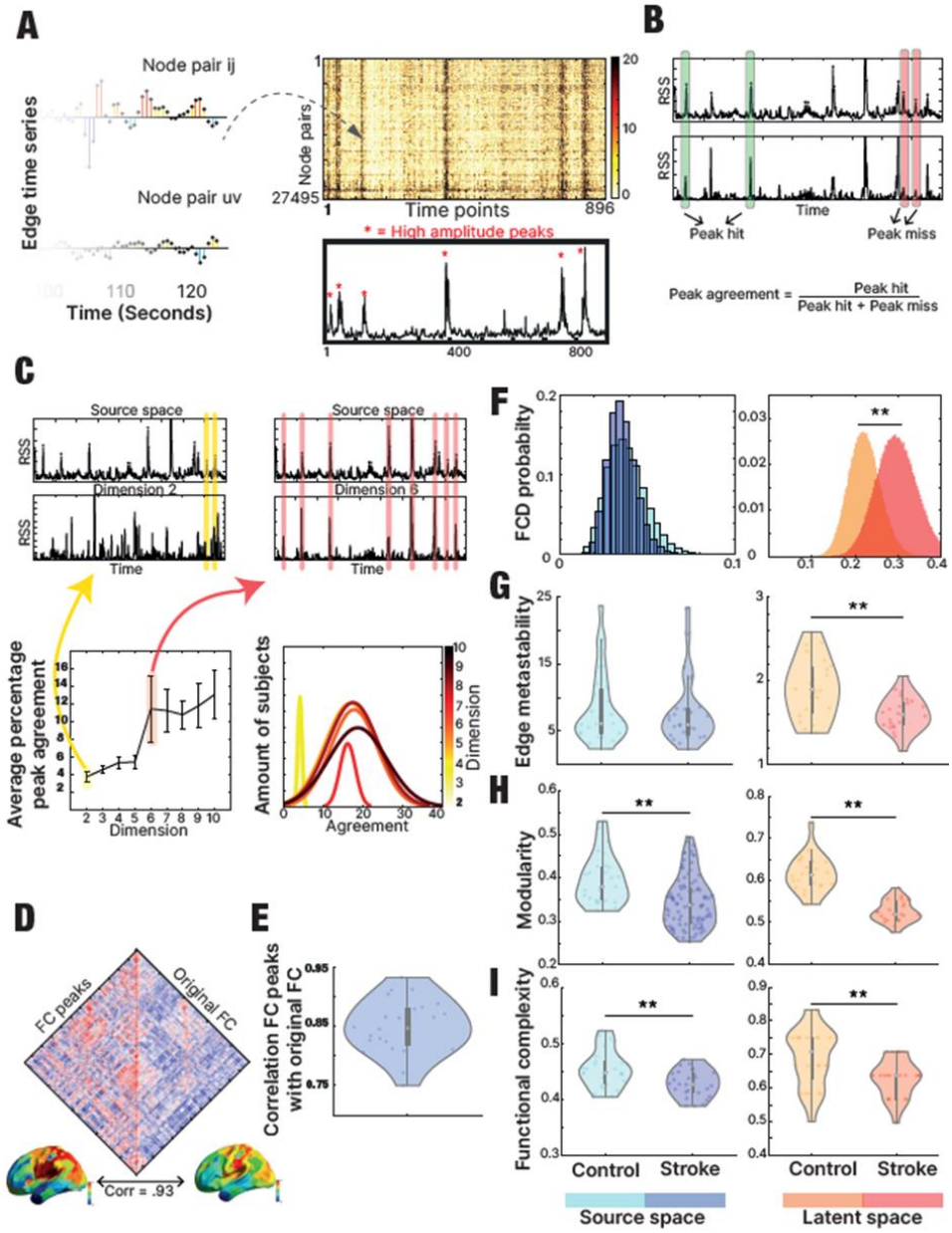

Figure 6.2: Preserved features in latent space

Figure 6.2: Preserved features in latent space: **(A)** Calculation of edge time series by means of dot product at each time point. The highest top amplitude frames (top %10 of co-fluctuation root-sum-squared) were selected. **(B)** The peaks that occur at the same time point in the source and latent space were labeled as "agreement frames" and this amount was used as an indicator of preserved dynamics. **(C)** The amount of agreement frames was calculated for each dimension revealing the dimension 2 as the lowest. There was a significant difference between dimension 2 and 3 (p<.01) and between dimension 5 and 6 (p<.01). Following dimension 6, the number of frames in agreement stabilizes. **(D)** We compared the distribution of the FCD of healthy controls and stroke patients. The difference observed in source space (p<.01) increased when observing the latent representation (p<.01). **(E)** Edge metastability was compared between controls and stroke patients showing no significant difference in the source space (p=.9) in contrast to the latent space (p<.01). **(F)** Level of modularity was significantly different in controls and stroke patients both in source (p<.01) and latent space (p<.01). **(G)** Level of functional complexity was significantly different in controls and stroke patients both in source (p<.01) and latent space (p<.01).

6.3.2 Classification in acute stage and relation with behavior

We assessed patients' diagnostics and severity classification through machine learning algorithms. We performed the same analysis in both source, and latent space, in order to compare if the embedded information in the latent representation was informative. To achieve that goal, we relied on two different metrics, the widely used FC mean, and the brain signal reversibility (see Methods) as a novel metric inferring signal dynamics and complexity. The results revealed how the dimensionality reduction benefits both the metrics, but specially the reversibility one, which obtained the maximum classification accuracy. Furthermore, the content of the latent representation was projected into 2-dimensions (see methods) in order to visualize how the group separation is better described in a non-linear way (**Figure 6.3d**).

We used a random forest classifier to discriminate healthy controls from stroke patients at the acute stage. As an input to the classifier, we considered

two summary metrics, the reversibility (assessing the degree of reversibility of BOLD time series, see Methods), and the mean FC, comparing the results in the source and latent space. The latent information used for this analysis was explained in detail in the methods section. As an alternative, we performed the same analysis but replacing the mean FC by the standard deviation, showing similar results (**Figure D11**). The mean FC and the reversibility matrix were selected as metrics as they integrate spatial and temporal dynamics, together with the complexity of the system. Furthermore, this study aimed to use a traditional metric (mean FC) next to a novel one (reversibility), which has already been used with promising results in previous publications (Deco et al., 2021; Deco et al., 2022).

Reversibility in the latent space showed the highest accuracy performance (mean = .84, SD = .11), followed by Reversibility in the source space (mean = .70, SD = .10), mean FC in the latent space (mean = .67, SD = .13) and mean FC in the source space (mean = .61, SD = .11). (**Figure 6.3b**)

While classifying between stroke patients with high and low lesion volume of damage, reversibility in the latent space showed the highest accuracy performance (mean = .73, SD = .09), followed by mean FC in the latent space (mean = .72, SD = .09), Reversibility in the source space (mean = .65, SD = .10) and mean FC in the source space (mean = .59, SD = .09) (**Figure 6.3c**).

We searched for the association between the previously reported metrics and all the behavioral scores differences normalized ($\frac{1\text{ year score}-2\text{ weeks score}}{2\text{ weeks score}}$) assessing the degree of behavioral recovery (**Figure 6.3f**). Furthermore, we performed the same analysis but using the behavioral scores at the acute stage (2 weeks) in order to see the relations at the initial state (**Figure D8**). Each radar plot shows the relation of each metric with each of the 9 behavioral domains. The further the point is from the center, the higher the Pearson

correlation value is. Furthermore, significant relations are indicated with asterisks (**Figure 6.3f**).

When using the FC at the source space, there was a significant relation with Motor L (r = .25, p < .05) and Attention VF (visuospatial field bias, referred as "AttVF") (r = .24, p < .05) . When using the Reversibility at the source space, the following domains showed a significant relation: Language (r = -.21, p < .05), and AttentionVF (r = .23, p < .05). When using the FC at the latent space, the following domains showed a significant relation: AttValDis (the ability to re-orient attention to unattended stimuli) (r= -.26, p < .05) and memory S (spatial memory) (r = -.22, p < .05). When using the reversibility at the latent space, the following domains showed a significant relation: MotorL (r= .48, p < .05), Att ValDis (r = .40, p < .05), MemoryS (r = .34, p < .05) and Motor IC (r = .36, p < .05) (**Figure 6.3f**). Behavioral tasks abbreviations are explained in detail in the methods section.

In summary, the reversibility matrix got the highest number of significant relations with behavioral domains (4), followed by the reversibility matrix in source space, the FC matrix in latent space and the FC matrix in source space with 2 significant relations. We performed the same analysis but replacing the average FC for the standard deviation showing a higher value in the relationships' strength (**Figure D9**). Mean FC and standard deviation are global metrics that allow the comparison of the source space and the latent representation, converting them in ideal approaches to assess the comparison between the two spaces.

Lastly, each domain's highest association is visualized in **Figure 6.3e**, displaying the highest Pearson correlation value for each behavioral variable. As a control, we inspected the same analysis while replacing the chosen dimension. The result of the association between dimension 10 and the 9 behavioral scores is presented in **Figure D3.**

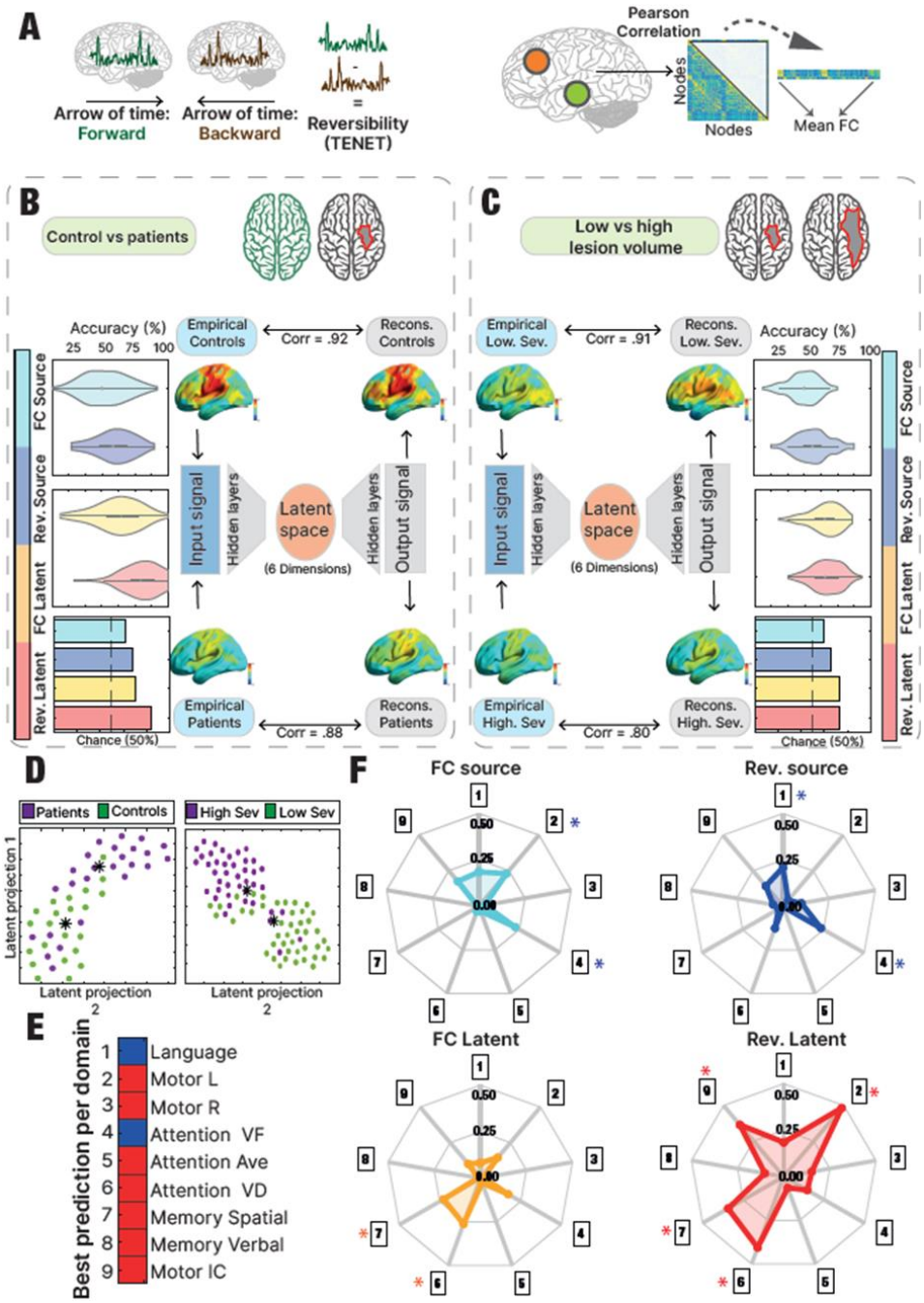

Figure 6.3: Classifications using the acute stage after the incident and its relation with behavior impairment

Figure 6.3: Classification in acute stage and relation with behavior: **(A)** Reversibility was computed by calculating the average of the difference between the time-shifted correlation matrices for the forward and reversed time series. Mean FC was calculated from the mean of the upper triangle of the FC. **(B)** The classification between controls and patients at the acute stage showed the reversibility in the source space as the highest accuracy (mean = 79%). The right part of the panel shows the comparison between the input and the output signal of the autoencoder. **(C)** The distinction between stroke patients with low and high lesion volume indicated that the highest accuracy was given by the reversibility in the latent space (mean = 73%). Same description of the autoencoder as in Panel B was presented in Panel C. **(D)** 2-dimension projection of the latent representation obtained in the controls' vs patients' latent space (left) and the patients with low vs high lesion volume latent space (right). Asterisks represent the mean of each group. **(E)** All the metrics used for the classification approach were related with each of the 9 behavioral domains recovery values (score after 1 year minus score after 2 weeks, divided the 2 weeks score). Asterisks represent which of the relations were significant **(F)** For each behavioral domain, the corresponding metric with the highest association was represented indicating the respective color. Red represents the latent space metric while blue represents the source space.

6.3.3 Prediction of recovery

We intended to assess recovery of stroke patients across one year in 3 different ways.

We aimed to study the patients' behavior, next to their functional dynamics and their functional-structural coupling. As in the previous analysis, we used FC mean and reversibility of the signal as distinctive metrics, and we performed the calculations in both source and latent space in order to demonstrate how latent information predicts better the recovery of the patients, especially when using the reversibility as metric. As an alternative, we performed the same analysis but replacing the mean FC by the standard deviation, showing similar results (**Figure D12**).

To assess the recovery using functional information, for each patient we calculated the FC distance between its FC matrix at each measurement stage (2 weeks, 3 months and 1 year after the stroke incident) and the average FC matrix of the healthy controls (**Figure 6.4a**). There is no significant difference

between acute stage (2 weeks) and intermediate stage (3 months) ($t(47)= 0.48$, $p = .63$), while there is a significant difference between intermediate stage (3 months) and remote stage (1 year) ($t(47)= 38.23$, $p < .01$). Therefore, the FC distance with respect to healthy controls is a functional metric that indicates a progression of recovery across time. As an alternative approach, we calculated the Frobenius distance between the co-classification matrices (See methods), resulting in a similar pattern as presented before. The only significant difference observed was between the second time point (3 months) and the third time point (1 year) when comparing their corresponding distances with the healthy controls (**Figure D4).**

In addition to the previous metric, we analyzed the relation between functional and structural connectivity, which exploits the anatomical data (**Figure 6.4b**). There is a significant difference between healthy controls and patients in acute stage (2 weeks) ($t(76)= 61.11$, $p < .01$). There is no significant difference between acute and intermediate stage ($t(44)= -0.16$, $p = .86$), while there is a significant difference between intermediate and chronic stage ($t(48)= -42.62$, $p < .01$) revealing a more similar level between controls and stroke patients, after 1 year of the incident. It is important to clarify that the structural information is belonging to the healthy control template, and not to each individual patient.

6.3.3.1 Behavior

We inspected the recovery of the patients by using 3 behavioral recovery metrics (**Figure 6.4c**). We classified the recovery level of stroke patients between the ones with a higher (better) recovery against the ones with a lower (worse) recovery, by means of behavior as a division criterion (see Methods section). Reversibility in the latent space showed the highest accuracy performance (mean = 76%, SD = 09%), followed by mean FC in the latent space (mean = 65%, SD = 10%), reversibility in the source space (mean = 54%, SD = 12%) and mean FC in the source space (mean = 52%, SD = 13%).

As an alternative approach, we used the first principal component of the recovery scores (See methods) revealing a similar result. The highest accuracy performance was in the reversibility in the latent space (mean = 79%), followed by mean FC in latent space (mean = 77%), reversibility in the source space (mean = 58%) and last, FC mean in the source space (mean = 52%). These results are displayed in **Figure D6.**

6.3.3.2 FC Distance

The FC distance was used to divide the stroke patients with higher against lower recovery level. Reversibility in the latent space showed the highest accuracy performance (mean = 71%, SD = 11%), followed by mean FC in the latent space (mean = 64%, SD = 14%), reversibility in the source space (mean = 56%, SD = 12%) and mean FC in the source space (mean = 55%, SD = 12%).

6.3.3.3 Correlation FC SC

When classifying between higher and lower recovery level of stroke patients using the correlation between SC and FC as a division criteria, reversibility in the latent space showed the highest accuracy performance (mean = 70%, SD = 12%), followed by mean FC in the latent space (mean = 65%, SD = 12%), reversibility in the source space (mean = 58%, SD = 13%) and mean FC in the source space (mean = 55%, SD = 15%).

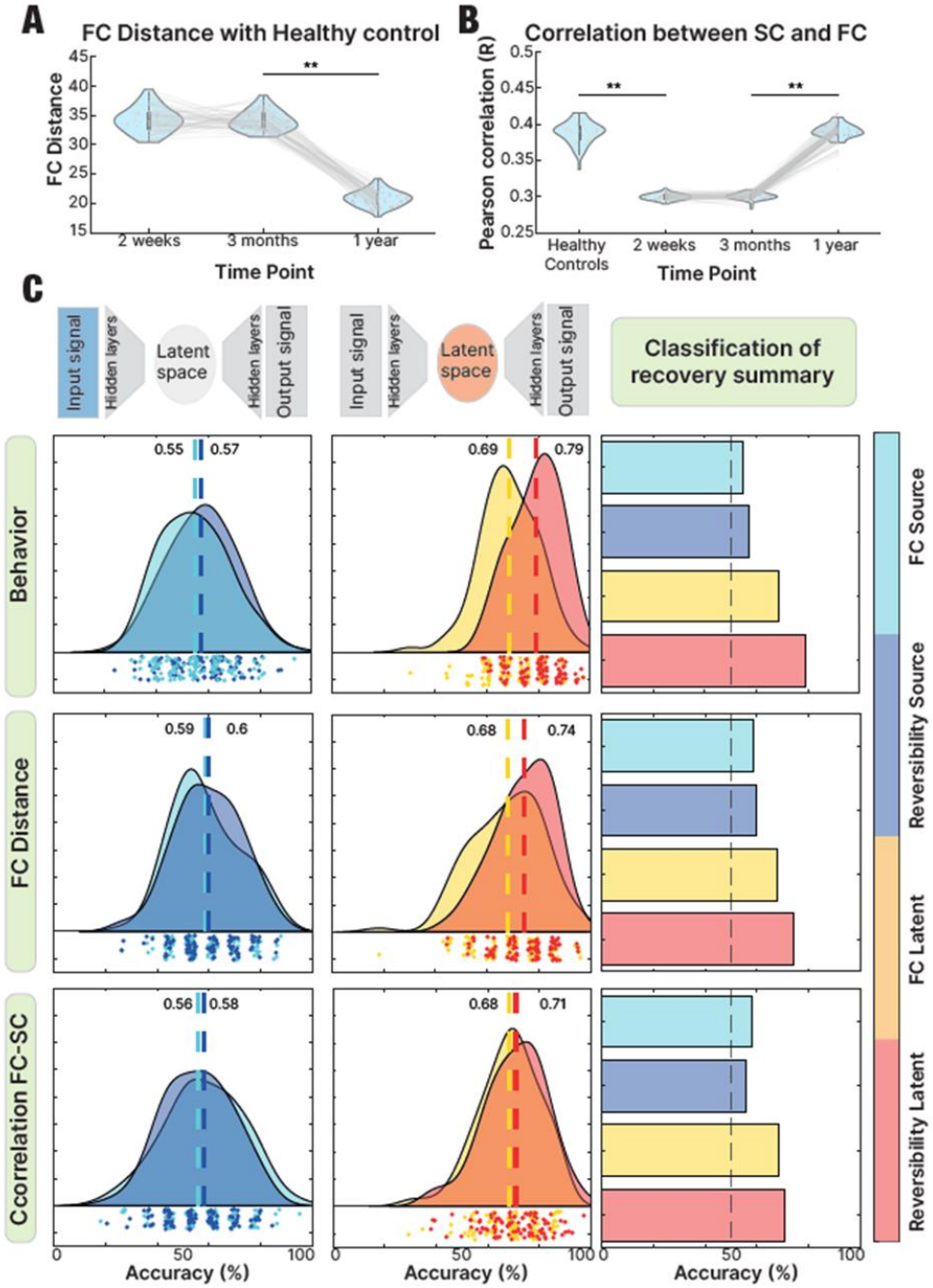

Figure 6.4: Prediction of recovery

Figure 6.4: Prediction of recovery: **(A)** FC distance (Frobenius norm of the difference between the two matrices) between stroke patients at each time point and the healthy controls indicating the decrease of distance after 1 year (p<.01). **(B)** Correlation between SC and FC of healthy controls and stroke patients (at each measurement stage) revealing the increase at the remote stage, showing a similar value to controls after 1 year of the incident (p<.01)., while it is not the case after 2 weeks and 3 months (p=.86). **(C)** Prediction of recovery using as input of the classifier the FC and reversibility matrix of the source space and the FC and reversibility matrix of the latent space. As division criteria to split the subjects in high vs low recovered, 3 different criteria were used: Amount of behavioral domains recovered, the FC distance at remote stage and the correlation between SC-FC at remote stage. In all the scenarios, reversibility in the latent space showed the highest accuracy.

6.4 Discussion

Deep learning models are being increasingly used in precision medicine thanks to their ability to provide accurate predictions of clinical outcome from large-scale datasets of patients' records. However, in the case of brain disorders, the deep learning approach is still limited, since clinical neuroimaging datasets typically have a small sample size. Thus, data scarcity has forced the adoption of simpler feature extraction methods, which are less prone to overfitting. In the current study we tested whether, by reducing the dimensionality of fMRI timeseries of stroke patients, we retain clinically important features of the data. The analysis revealed that the functional features, such as modularity, characterize the alterations caused by stroke, are preserved in the latent representation. Furthermore, the latent information proved to be efficient for clinical classification, discriminating between patients and controls, and between patients with low and high lesion volume at the acute stage. Moreover, the information of the latent space enhanced prediction of behavioral deficit at the acute stage and recovery after one year. These results demonstrate the clinical relevance of dimensionality reduction for brain disease and strengthen the case of its wider adoption to improve non only diagnosis, but also prognosis, hence allowing for a more effective treatment planning.

Our study contributes to the literature on dimensionality reduction approaches in neuroscience (Bolt et al., 2022). Reducing the dimensionality of the neural data is possible because different areas of the brain do not activate independently, but tend to fluctuate in coordinated patterns that can be described in terms of a smaller number of features (Pang et al., 2016). However, a wide variety of dimensionality reduction methods are possible, and it is important to understand the relative strengths and weaknesses of the different approaches.

The most widely used approach is certainly PCA. However, PCA assumes linearity (Manning-Dahan, 2018). A way to tackle the limitations of the PCA (mainly the linearity assumptions), is employing deep learning techniques. These approaches have been increasingly used as a generic family of machine learning tools to learn features from fMRI data. (see (Khosla et al., 2019) for a review). However, deep learning approaches are most effective in a supervised learning setting. In an unsupervised setting, autoencoders are more appropriate. At a theoretical level, our autoencoder has benefits over classical lineal procedures such as PCA. Autoencoders are non-linear and can learn more complicated relations between visible and hidden units (IRIARTE, 2022). A recent study used autoencoders to show that different brain states can be captures in terms of trajectories within a low-dimensional latent space (Sanz Perl et al., 2021). In this study, the authors used a variational autoencoder, rather than a normal autoencoder, due to the necessity to represent new data not used in the training stage. In contrast, the current study does not need to include the variational feature to the autoencoder, as we encoded real data and analyzed what is obtained in the lower dimensions. By doing so, not only does the computational cost gets reduced, but also the reconstruction becomes less complicated.

In our study, we find that the latent space time series retain several important properties of the original fMRI data, such as having common frames with high-

amplitude co-fluctuations, as suggested in previous literature given the modular nature of the original FC (Novelli & Razi, 2021). And critically, the latent space data can be used to successfully classify stroke patients and stroke severity. These points underscore the idea that dimension reduction using the autoencoder framework is helpful, as it reduces the amount of data under investigation while simultaneously retaining relevant characteristics of the original data. Thus, the latent representation can be derived from the source space and by sharing the same embedded characteristics while discarding irrelevant information, improve the achieved classification accuracy.

One future direction is to explore how autoencoder-based dimension reduction can be employed in conjunction with whole-brain models and enhanced by using larger datasets (or simulated data). The mechanisms underlying the emergence of different brain states can be probed using whole-brain models based on conceptually simple local dynamical rules coupled according to empirical measurements of anatomical connectivity, for instance, by coupling nonlinear oscillators with the long-range white matter tracts inferred from diffusion tensor imaging (DTI) (Sanz Perl et al., 2021). Previous studies have already demonstrated the utility of whole-brain models in stroke research (Adhikari, Griffis, et al., 2021; Adhikari et al., 2017; Idesis, Faskowitz, et al., 2022). The output of these models could similarly be embedded in a low-dimensional space, which could be analyzed using similar procedures to the ones described in this project.

Several previous studies have used dimensionality reduction to address stroke. A few studies used Artificial Intelligence to predict stroke incidents (Shanthi et al., 2009; Singh & Choudhary, 2017; Sudha et al., 2012) relying on linear procedures such as PCA for dimensionality reduction. Another study used dimensionality reduction approaches to associate motor and cognitive functions with mood disorders subsequent post-stroke (Hama et al., 2020). In

the study, the authors proposed a non-linear model that effectively predicted post-stroke neuropsychiatric symptoms, outperforming traditional linear classifications. Another study proved that distinction between patients with post-stroke vascular dementia and control subjects was enhanced by using a dimensionality reduction technique (Al-Qazzaz et al., 2018). Furthermore, a recent article showed how four well-known dimensionality reduction techniques can be used to extract relevant features from resting state functional connectivity matrices of stroke patients (Calesella et al., 2021). Nevertheless, their proposed approach relies on linear assumptions in contrast to the ones selected for our study.

To date, machine learning has not been applied to explore in depth the low dimensionality of stroke effects in the brain. One study implemented an unsupervised features learning approach based on an autoencoder for automatically segmenting brain MR images from stroke lesions (Praveen et al., 2018). Nevertheless, the study focused only on anatomical information without considering functional data. Our study is thus novel in that it tries to achieve a low-dimensional representation of the functional data (Bowren et al., 2022; J. C. Griffis et al., 2019; Salvalaggio et al., 2020; Weiss Cohen & Regazzoni, 2020). While autoencoders are routinely used for dimensionality reduction across a wide range of fields, their usage in functional neuroimaging is still scant. Our findings demonstrate the large, and still underexploited potential of machine learning methods in the study of large-scale brain dynamics. Our novel approach may be fruitfully applied to a wide array of brain disorders, subserving both the theoretical goal of a clearer understanding of these diseases, and at the same time, the clinical goal of maximizing patients' classification, diagnosis, and prognosis.

In the present study, we reached high classification accuracies by only relying on functional data. In addition to the classification of low dimensional description of functional data, not only fMRI, but also EEG, could be quite

helpful to select target for non-invasive brain stimulation. Currently, there have been proposals to use patterns of functional connectivity (Fox & Alterman, 2015) to guide invasive and non-invasive brain stimulation. However, high dimensional data set like resting-state fMRI connectivity patterns are difficult to collapse in a small set of coordinates. The low dimensional embedding coupled with classification methods to highlight the most predictive components could be a strategy to select sensitive targets.

It is important to note that nonlinear dimensionality reduction methods are often fragile in the presence of noise (Humphries, 2020) or in the presence of low data quality, which limits their use when statistics are limited. However, datasets with sufficient length, such as the one presented in this article, can avoid this problem. Therefore, before proceeding to nonlinear methods, it is worthwhile to ensure a dense enough sampling of the high-dimensional space such that local neighborhoods include data points from different trajectories.

In our current study, we used an autoencoder model because of its ease-of-use and flexibility. However, there are other interpretable variants that have been proposed to enable the inspection of embedded information (Ahrens et al., 2013; Kerr & Denk, 2008). These methods incorporate additional priors to encourage separability across latent dimensions. As our approach is relatively general, exploring deep representations could provide a way to visualize the representations formed in generative models for other applications in medical imaging. With new strategies for interpreting how deep networks represent data, we may be able to develop new regularization strategies to disentangle and interpret population-level variability. Moreover, future studies could design visualization techniques in order to interpret the features extracted by non-linear dimensionality reduction, which could provide valuable insights to the clinicians for the design of more effective rehabilitation protocols.

We selected a whole-brain metric, the average of the FC, in order to perform the classification and prediction analyses. Even though this metric is outperformed in literature by other stroke-related metrics (Siegel et al., 2016), we used it in order to be comparable to the performance in the latent representation, as when data gets reduced, the anatomical properties such as space localization, get lost.

Lastly, whole-brain models introducing anatomical information (Idesis, Favaretto, et al., 2022) could be applied directly to the latent representation in order to add anatomical restrictions and enrich the information available for the proposed analysis.

In conclusion, this study adds new evidence for the relevance of low-dimensional embeddings for fMRI signals and proposes a non-linear dimensionality reduction approach as a promising tool to explore altered brain dynamics after stroke. In addition, it reveals how complexity metrics such as brain signal reversibility provide indicators that relate to lesion severity and predict lesion recovery, making it the first study of this type with applications to longitudinal stroke studies. Our findings demonstrate the power of a measure of brain signal reversibility as a general marker of pathology. While many complexity measures have been used as biomarkers in functional MRI, our measure has the twofold advantage of its simplicity and interpretability. In fact, the degree of signal reversibility is a general measure of how distant a physical system is from thermodynamic equilibrium. Healthy cognition is associated with complex information processing demanding a far-from-equilibrium state (Lynn et al., 2021; Perl et al., 2021). Therefore, a higher reversibility holds as a strong marker of neurophysiological impairment. We expect similar results in a wide array of neurological and psychiatric conditions.

7.General discussion

We summarize in this chapter the main contributions of this dissertation and describe open questions as well as possible future directions of investigation.

7.1 Main contributions

The presented thesis shed light on the effects of stroke incidents, tackling the problem of interpreting the resulting dynamics in several ways. By introducing whole-brain models, it is possible to estimate and manipulate the possible parameters in order to simulate the outcomes of different treatments and evolutions across time. Furthermore, the possibility of analysis of simulated data contributes to the goal of obstructing the patients in a lower level.

All the presented works contribute clear evidence of the emergence of typical dynamics consequently of stroke incidents, reaffirming the global impact of this damage instead of the previously believed, local effect.

While chapter 2 serves as an exploratory introduction to the dataset that is extensively utilized throughout the thesis, the main contribution of Chapter 3 has been to conceptualize the human brain dynamics following a stroke incident as observed through fMRI recordings. In contrast to the majority of the studies in the field of stroke, which mostly observe anatomical features, this chapter examines the functional properties of brain dynamics following a stroke incident.
We benefited from the longitudinal dataset to see the evolution of the metrics over time and establish connections with the levels of recovery. We proposed an alternative in order to deviate from the typical focus on nodes in fMRI signals by using an approach centered around edges. Through edge-centric methodology, we explored novelty metrics such as normalized entropy, and

high-amplitude co-fluctuations to evaluate the severity of the lesion and the progression of recovery.

In summary, the insights gained from this exploration prove valuable in enhancing our comprehension of whole-brain models, discussed in the subsequent chapters (Chapters 4 and 5) and the analysis of lower-dimensionality representations (Chapter 6). By focusing on the functional aspects, we expand our understanding of the complex mechanisms at play in post-stroke brain dynamics.

Chapter 4 makes a significant contribution by conducting rigorous testing of influential computational models that aim to capture the entirety of the brain. The successful development of these models enables the exploration of fundamental questions that are challenging to investigate empirically. By employing accurate computational whole-brain models, we can systematically examine how variations in resting state organization impact the brain's information processing capacity. This includes both natural variation among healthy individuals and variations caused by brain damage. The presented models integrate both structural and functional information, allowing us to assess the significance of structural disconnection information. Moreover, these models offer the opportunity to manipulate them and simulate potential treatment therapies along with their expected outcomes. In essence, we provide a mechanistic understanding of the effects of stroke on patients. Through the analysis of graph metrics calculated in the model's asymmetric interactions, we are able to replicate the disconnections between brain regions, thereby revealing the underlying interactions among embedded brain regions.
In summary Chapter 4 revealed the accuracy of whole-brain models in a stroke population by integration anatomical and functional information while at the same time, exposing the key role of the structural disconnection information.

The main contribution of chapter 5 lies in the introduction of a fully predictive model that enables the prediction of functional features based solely on structural information. The results demonstrate that functional connectivity in patients can be predicted by a comprehensive computational model using only the structural disconnections caused by the patient's lesion. This suggests that the model captures, to some extent, the mechanistic relationship between anatomical structure and functional activity. While previous research has focused on fitting computational models using functional and structural data from healthy individuals or stroke patients, this study goes a step further by assessing whether these models can accurately predict the effects of a stroke based solely on the associated structural information.

In summary, the study demonstrates that the perturbations in structural connectivity induced by a stroke can be effectively captured by the fully predictive whole-brain computational model. By doing so, this model provides valuable insights into how strokes disrupt the resting brain organization and its functional dynamics.

Finally, Chapter 6 makes a significant contribution by providing evidence of the existence of non-linear and low-dimensional representations within high-dimensional data, which enhance the prediction of recovery. By employing an autoencoder and reducing the data's dimensionality, we gained insights into the dynamics of the brain following stroke incidents. Importantly, we demonstrated a notable improvement in predicting patient recovery when incorporating dynamic metrics such as signal reversibility, particularly when assessed within the latent representations. In summary, we explored how the existing cohort of patients, utilized in previous studies, can be leveraged by uncovering the embedded information within the data. This approach allows for the removal of unnecessary data while enhancing diagnostic capabilities and improving the prediction of recovery for patients. Furthermore, the

presented method performed with a high accuracy in a dataset of 100 patients. Further studies could benefit by applying the same procedures to larger and more complete datasets.

7.2 Challenges and future directions

7.2.1 Limitations

It is important to account for the fact that BOLD signal is an indirect measure, reliant on diverse assumptions, and subject to many different sources of noise (Veldsman et al., 2015). Nevertheless, it is proposed that in order to study stroke populations, resting-state fMRI is better suited than event-related fMRI (Veldsman et al., 2015). This is due to its capacity to expose network-based pathology beyond the lesion site.

One of the most used techniques to relate neurological symptoms to specific brain areas involves identifying overlap in lesion location across patients with similar disorders. This approach, also known as lesion mapping, has been used profitably for decades, making it a reliable source of information for stroke patients diagnostics, treatment, and recovery prediction (Boes, 2015). The primary advantage of this method is that it is sensitive to even small and hyperacute infarction, and can be used to assess if a certain brain region is necessary for a given cognitive function (Karnath et al., 2018; Sperber & Karnath, 2018). Nevertheless, the method could also be limited when the symptoms are not dependent on damage to a single brain region (Boes, 2015). Functional network metrics complement the anatomical features used in the clinic for decades, by adding dynamical and connectional components to study the global effect of the lesions, instead of just a local one. Relations

between areas that before were believed to not be connected, could reveal influence on each other by being connected indirectly.

The current thesis investigates stroke population using resting-state fMRI data. It is worth noting that stroke patients tend to be older than the usual populations where the assumptions of neurovascular coupling and the typical analysis pipelines are based (Veldsman et al., 2015). Lastly, the dataset consisted of mostly ischemic patients and should be replicated in hemorrhagic stroke before being generalized to all the patients who suffered from a stroke.

7.2.2 Novelty approaches for existing datasets

In this thesis, we present a diverse range of approaches that can be applied to the vast amount of existing datasets. These methods encompass, among others, the estimation of connectivity matrix asymmetry, the integration of different acquisition modalities, and dimensionality reduction techniques to explore embedded dynamics. By employing these approaches, we aim to contribute to the existing body of literature by introducing new tools that enable the exploration of available data. Additionally, we have made freely available all the codes used in our studies to facilitate their replication. Future studies can employ these methods to investigate the variability across different brain disorders by applying them to diverse populations.

7.2.3 Exploring bigger and more diverse datasets

The dataset presented in this study predominantly comprises ischemic stroke patients, and it is crucial to replicate these findings in patients with hemorrhagic stroke before generalizing the results to the broader population of individuals who have suffered from a stroke. Additionally, the localization of the lesion has demonstrated its relevance in relation to the observed effects

in the patients. In this thesis, we have described the typical lesion observed in the dataset under investigation (see **Figure A6**). To ensure the robustness and consistency of the presented results, it is necessary to include different cohorts with diverse lesion patterns and examine if the findings hold across these various cases.

By incorporating a broader range of lesion patterns, we can enhance our understanding of the effects and implications of stroke on brain dynamics and recovery. Furthermore, the analysis performed in Chapter 5 exposed the relevance of the lesion location above the lesion amount by calculating the models using the damage of other participants with similar amount but different lesion pattern.

7.2.4 Integrating different neuroimaging techniques

In the presented thesis, we utilized (f)MRI recordings from stroke patients. While (f)MRI offers high spatial resolution at the millimeter level, it has relatively slow dynamics in the order of seconds. On the other hand, EEG provides excellent temporal resolution at the millisecond scale, but its spatial resolution is limited to the centimeter range due to the volume conduction of cortical currents through the head tissues. By combining these two techniques, we could enhance our understanding of brain dynamics by capitalizing on the high spatial resolution of (f)MRI and the superior temporal resolution of EEG. This integration allows us to uncover phenomena that may be hidden or not fully captured by a single technique alone. By leveraging the strengths of each modality, we can explore how the integration of multi-modal data describes the complex phenomenon occurring after stroke incidents. This holistic approach provides a more comprehensive and nuanced understanding of the brain's response and recovery following a stroke. The approach presented in Chapter 6, dimensionality reduction, allows the

exploration of embedded information that allows the integration of several neuroimaging techniques.

7.2.5 Brain stimulation to enhance patients' rehabilitation

The utilization of whole-brain models offers a promising avenue for investigating the potential therapeutic effects of brain stimulation in patients, an area of significant current interest. To achieve the transition from a disease state to a healthy state, a stepwise approach can be followed. Firstly, it is necessary to fit a whole-brain model to a specific patient, optimizing the effective connectivity underlying the brain's functioning. This personalized model serves as a basis for further analysis. Chapter 4 gives evidence of the similarity between the simulations and the empirical data. Secondly, in silico simulations can be performed to exhaustively explore the effects of various parameters, such as the location and intensity of stimulation. The objective is to identify the optimal stimulation strategy that promotes and enforces a specific transition towards a target "healthy" resting brain state, as defined by the average functional connectivity observed in a control group.

Future studies should also investigate the impact of different types of stimulation, such as introducing noise or applying periodic stimulations with varying frequencies and intensities. These investigations will provide insights into how a patient's resting functional connectivity model must be stimulated in order to reproduce a healthy resting functional connectivity model. This knowledge will aid in identifying therapeutic targets for brain stimulation and refining the techniques used in clinical practice. Chapter 5 provides a generalized and predictive model that allows the generalization of the results in order to study the treatment effects in different populations.

7.2.6 Exploring signal propagation after stroke

The models we have presented allow us to investigate the generation of local dynamics and how they spread throughout the brain. This enables us to examine the occurrence of focal sleep-like slow waves and their long-range propagation within the brain. These phenomena are considered important electrophysiological aspects of diaschisis and provide valuable insights into the functional implications of focal and multi-focal injuries. Understanding the underlying signals following stroke incidents holds promise for the development of innovative therapeutic interventions and physical rehabilitation approaches that can enhance functional recovery.

7.3 Closing remarks

The thesis delves into the examination of brain dynamics following a stroke, offering insights and contributions in several key areas. Firstly, by adopting an edge-centric approach, we explore the functional features consequents of damage while introducing novel metrics that provide valuable information about lesion severity and recovery. These metrics enhance our understanding of the impact of stroke on brain dynamics. Additionally, we developed a comprehensive model that offers a mechanistic explanation of this neurological disorder. Notably, the model emphasizes the importance of structural disconnection information, shedding light on the underlying mechanisms at play. Furthermore, we introduce a fully predictive model in which the functional dynamics are predicted only by using anatomical information. Lastly, we present an approach utilizing dimensionality reduction techniques, which significantly improves the accuracy of predicting recovery one year after a stroke incident. This approach holds promise for enhancing diagnostics, treatment strategies, and rehabilitation protocols for stroke patients. In conclusion, this thesis contributes to the expansion of our

knowledge about one of the most significant neurological disorders of our time, stroke. It offers alternative perspectives and methodologies that can advance patients' diagnostics, treatments, and overall rehabilitation. By addressing crucial aspects of stroke-related brain dynamics, this work strives to improve patient outcomes and contribute to the field of stroke research.

A. Appendix A (Supplementary figures of chapter 3)

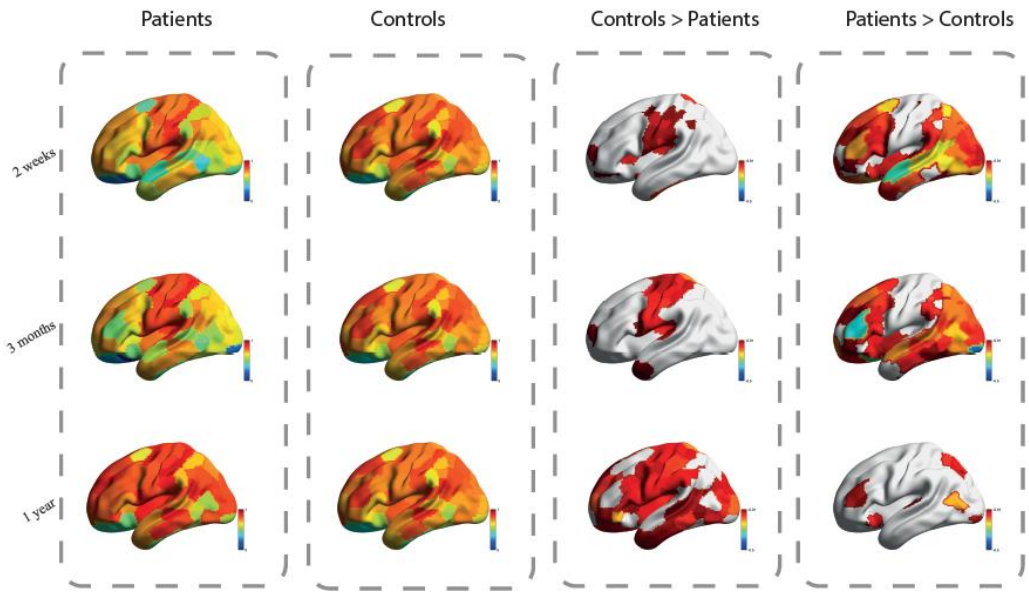

Figure A.1 Entropy localization

Figure A1: Entropy localization: Topological localization of entropy at (top) 2 weeks, (center) 3 months and (down) 1 year for patients and controls. On the right panels the subtraction between the values obtained from controls minus the ones from patients and vice versa are displayed.

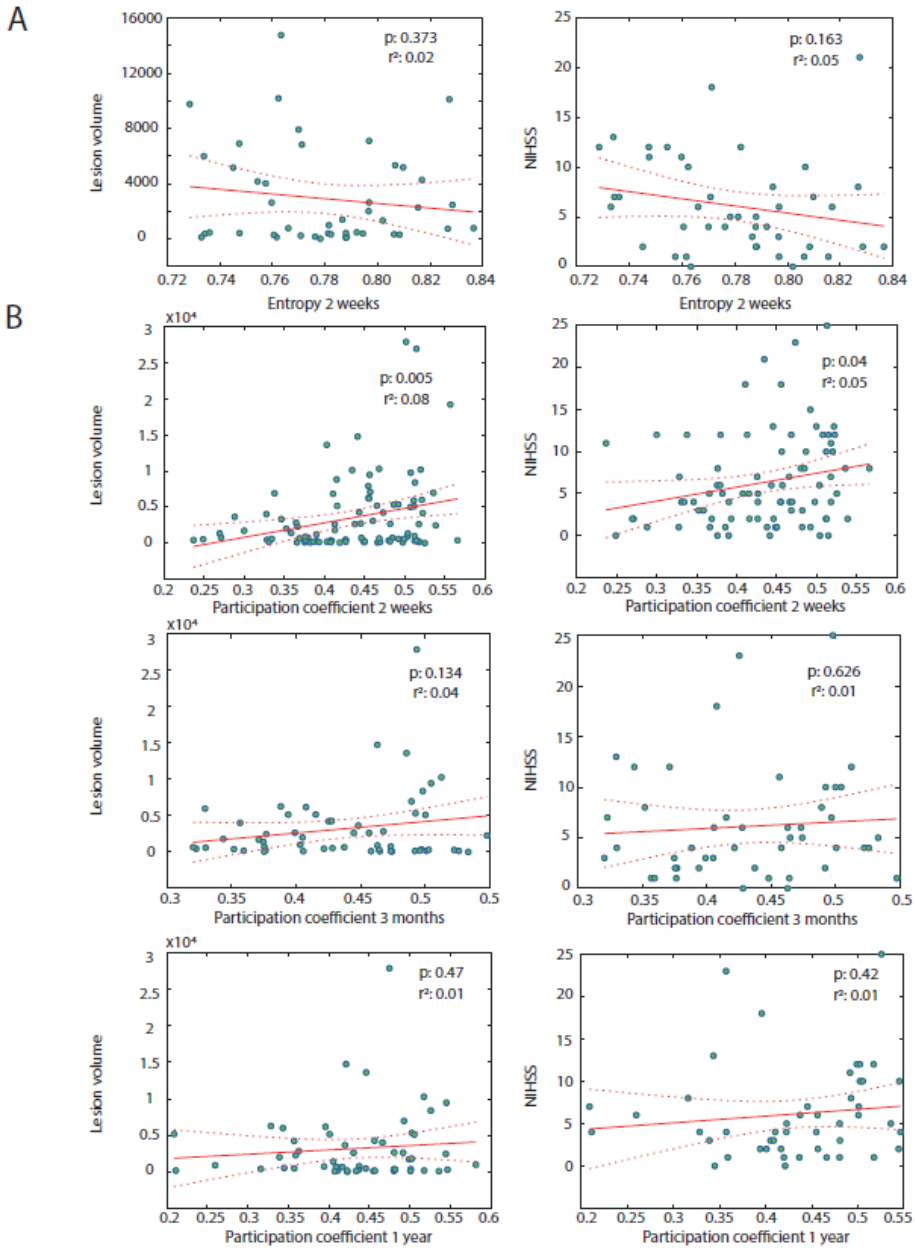

Figure A2 Normalized entropy and participation coefficient relation with stroke metrics across time

Figure A2: Normalized entropy and participation coefficient relation with stroke metrics across time: **(A)** Relation between normalized entropy and stroke metrics at time point 1. **(B)** Relation between participation coefficient with lesion volume and NIHSS score at (top) 2 weeks, (center) 3 months and (bottom) 1 year

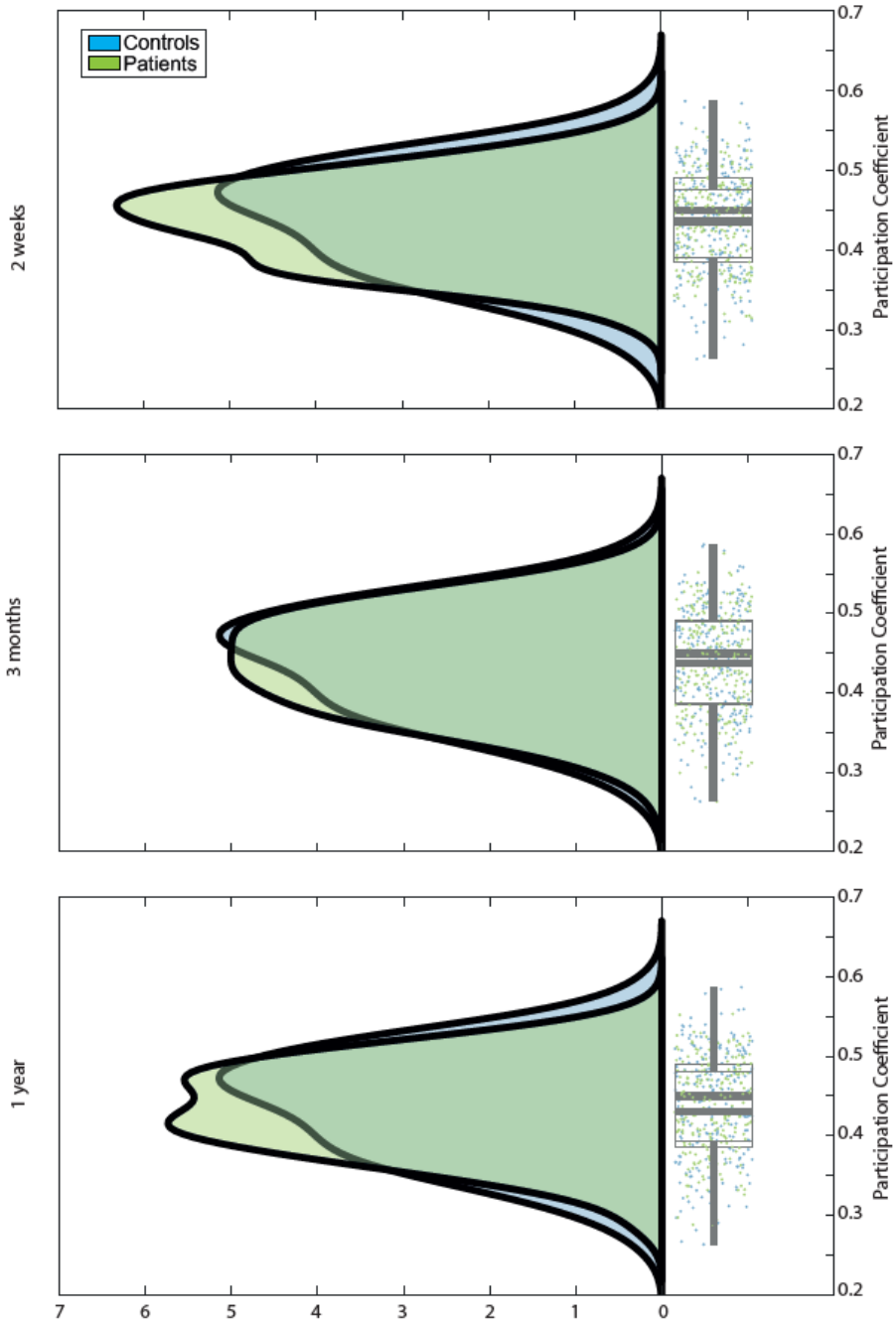

Figure A3 Participation coefficient across time

Figure A3: Participation coefficient across time: Comparison of Participation coefficient between patients and control at each time point revealing no significant difference in any moment.

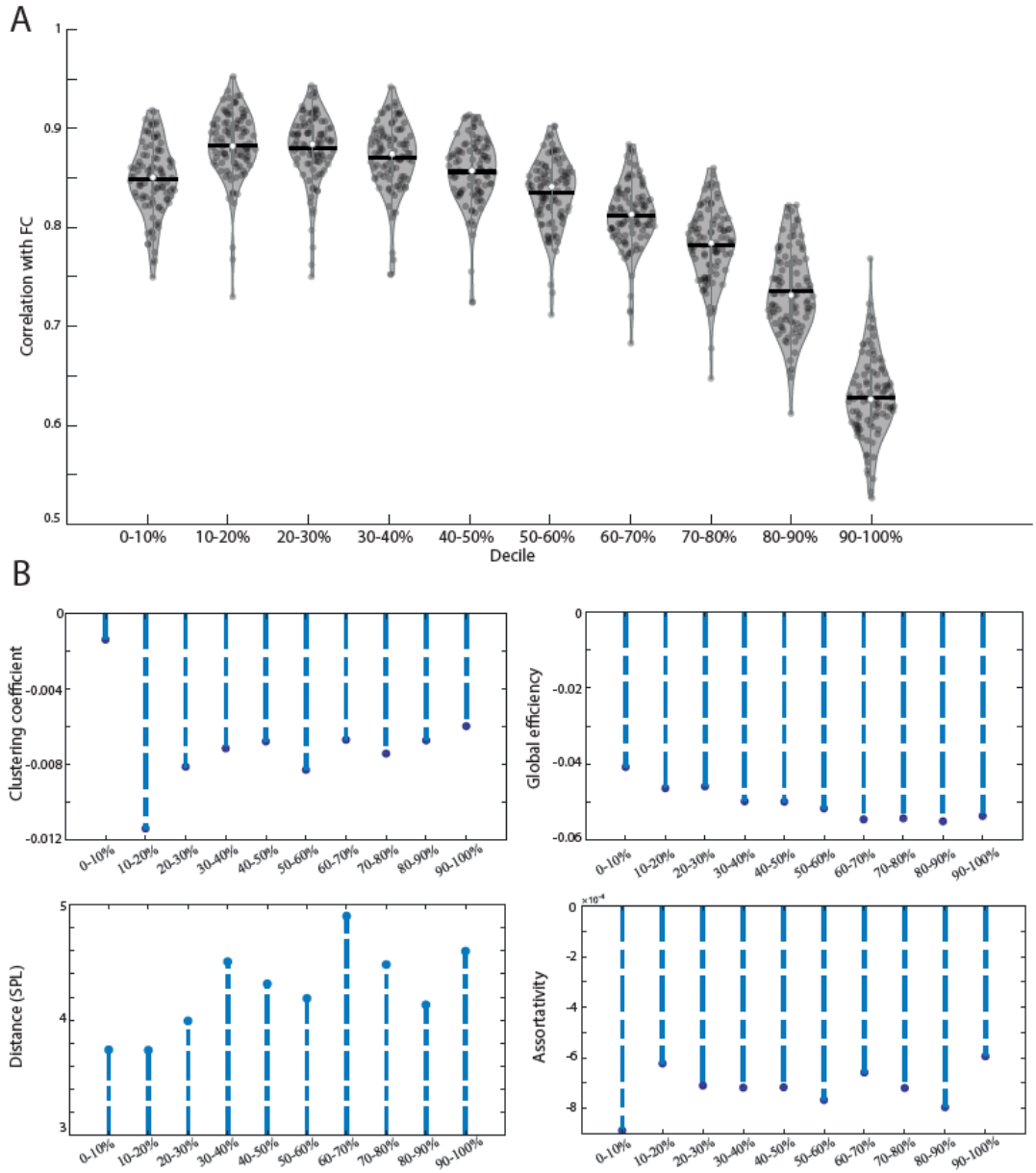

Figure A4: Topographical parameters compared by decile

Figure A4: Topographical parameters compared by decile: **(A)** Correlation between each decile and the total FC. **(B)** Comparison for each decile FC of (top-left) cluster coefficient, (top-right) global efficiency, (bottom-left) distance and (bottom-right) assortativity.

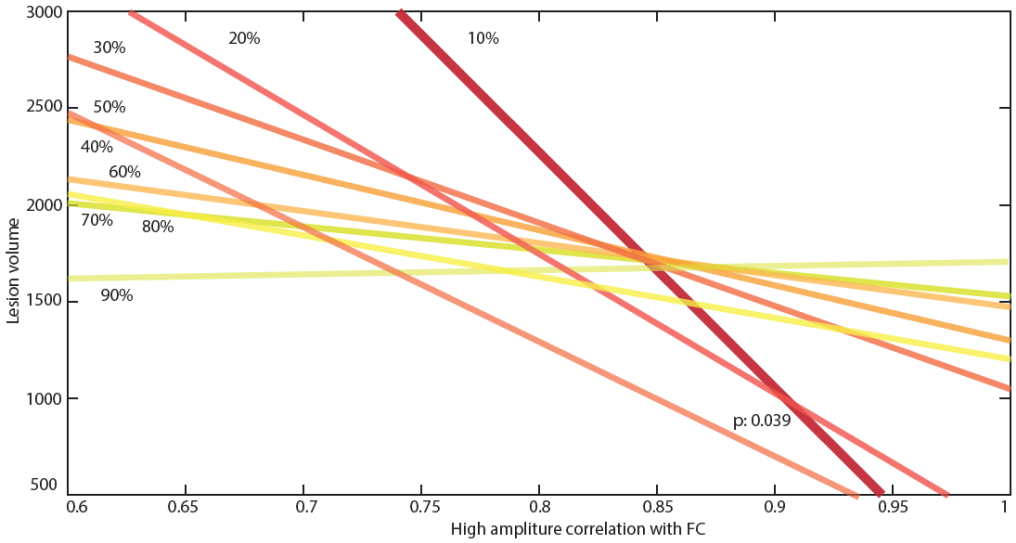

Figure A5: High amplitude per decile relation with lesion volume

Figure A5: High amplitude per decile relation with lesion volume. Lines indicate the relation between each decile matrices correlation with the empirical FC being the top 10 percent the only one revealing significant association (p= 0.039). The remaining deciles are represented with a gradient color going from red to yellow.

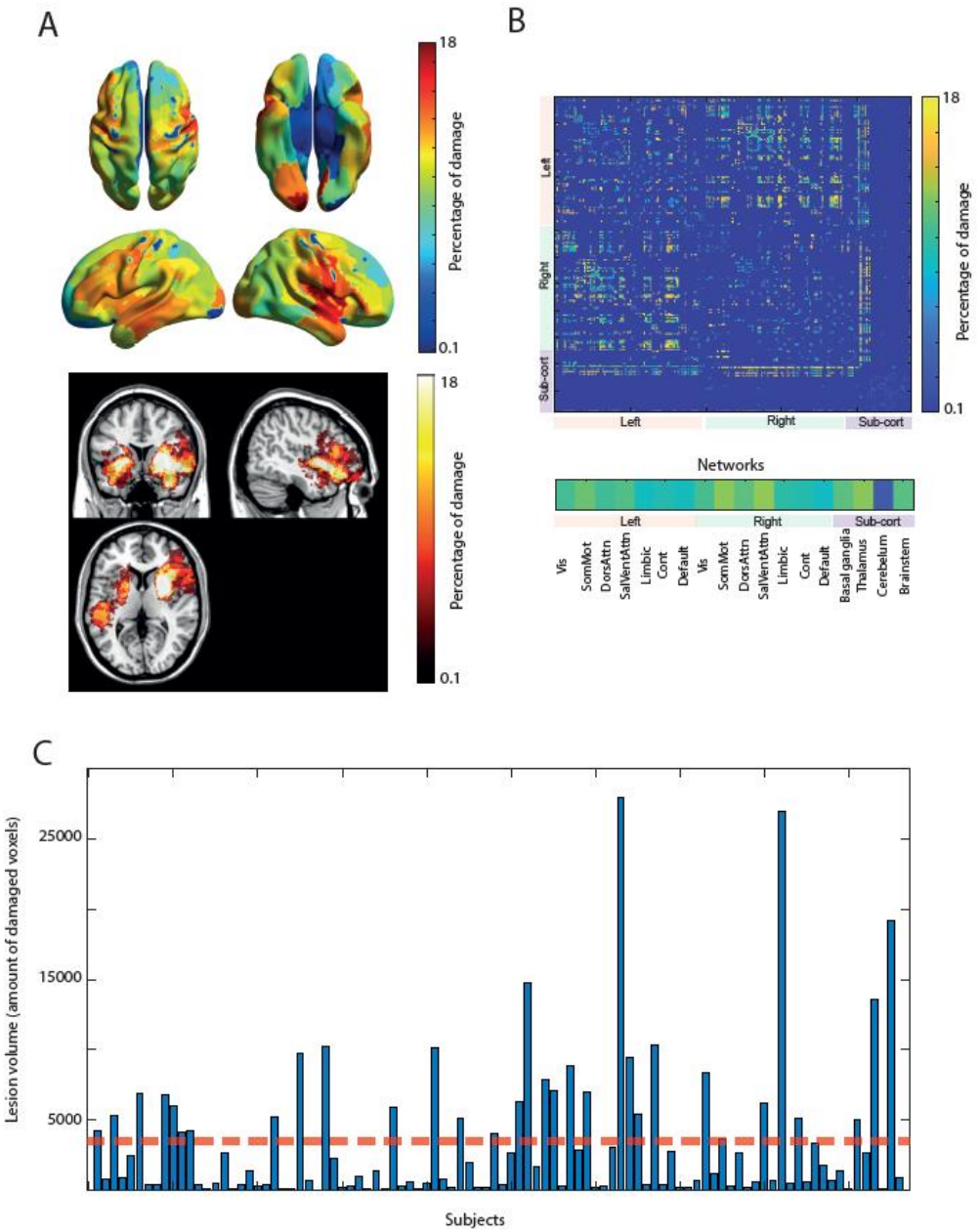

Figure A6: Lesion distribution of the sample

Figure A6: Lesion distribution of the sample: **(A)** Average lesion location indicating the percentage of damage of each region (MNI coordinates: X=115, Y=64,Z=78). **(B)** Average lesion location revealing the impact at the edge level (Top). Same information is visualized grouped by network to provide additional information. **(C)** Lesion volume of each patient. Red dot line indicates the mean of the sample.

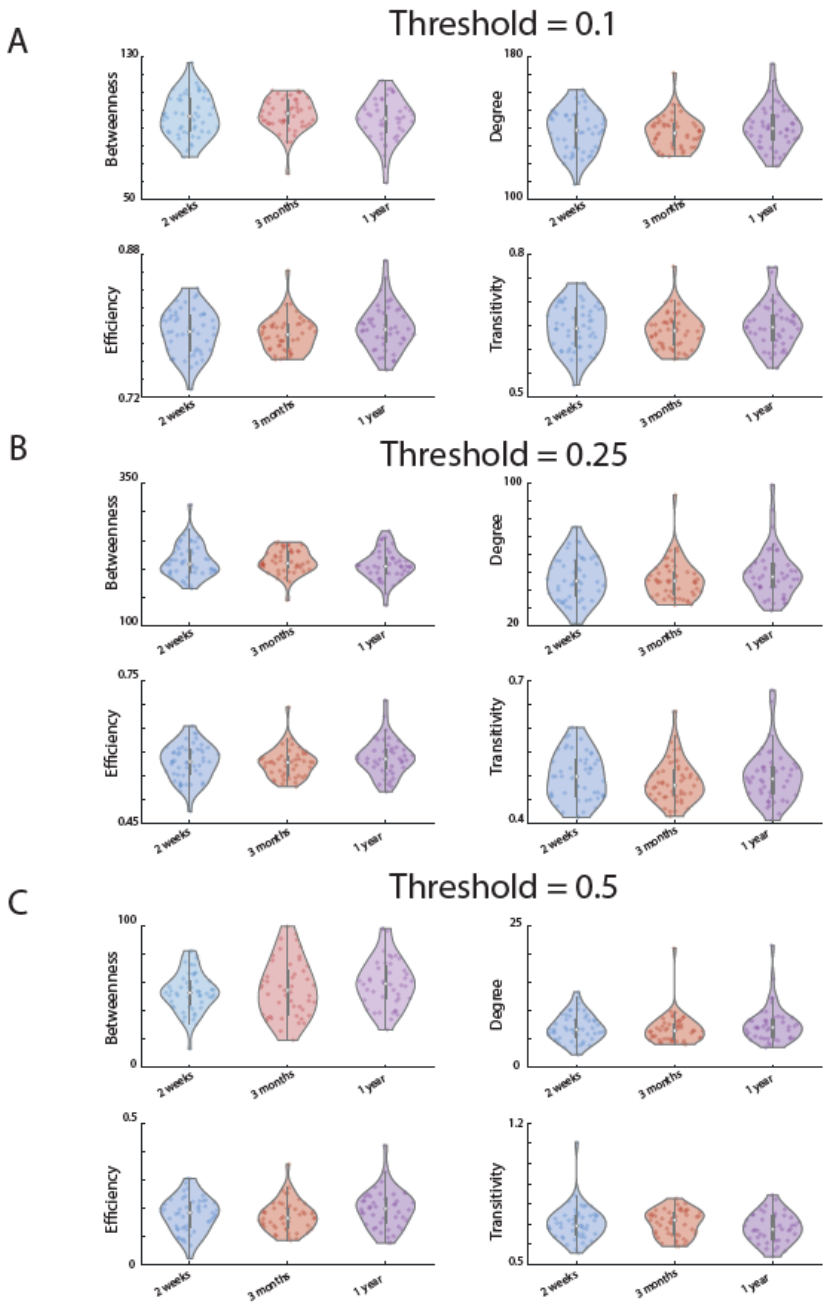

Figure A7: Graph metrics across time

Figure A7: Graph metrics across time: Betweenness (top-left), Degree (top-right), Global efficiency (bottom-left) and Transitivity (bottom-right) were calculated for the sample-average FC matrix after a binarization process using as an absolute threshold of 0.1 **(A)**, 0.25 **(B)** and 0.5 **(C)**.

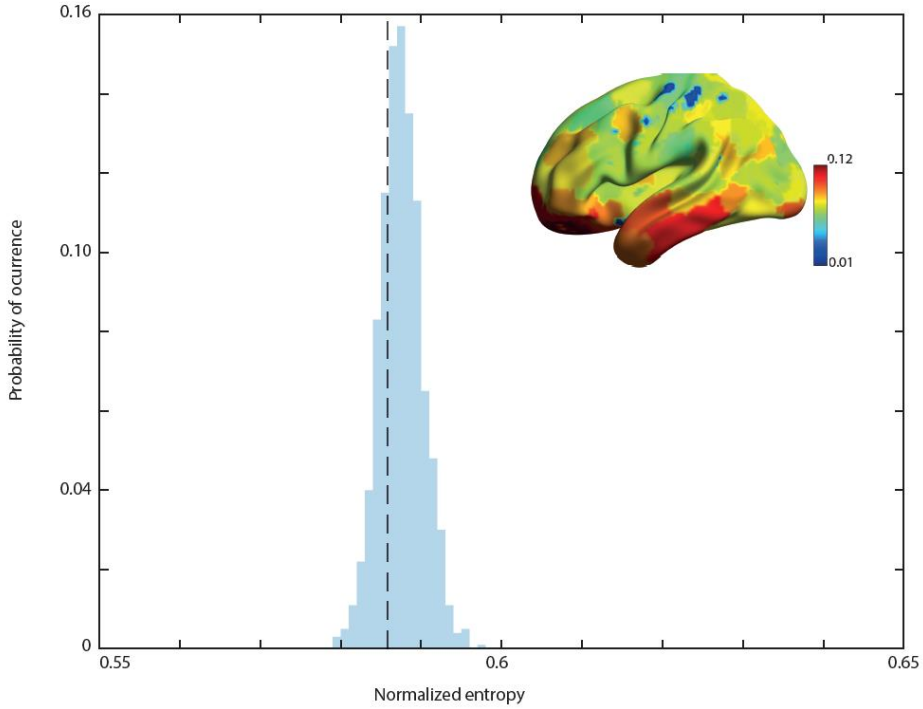

Figure A8: Distribution of normalized entropy across randomly shuffled sub-samples

Figure A8: Distribution of normalized entropy across randomly shuffled sub-samples: Sub-samples of 50 random subjects were generated in order to calculate the average normalized entropy. The process was repeated 1000 times giving one value per iteration. The results are visualized in the presented histogram revealing the low variability of the used cohort. Vertical dashed line represents the average of the complete cohort. Brain surface shows the entropy variability with the corresponding localization

B. Appendix B (Supplementary figures of chapter 4)

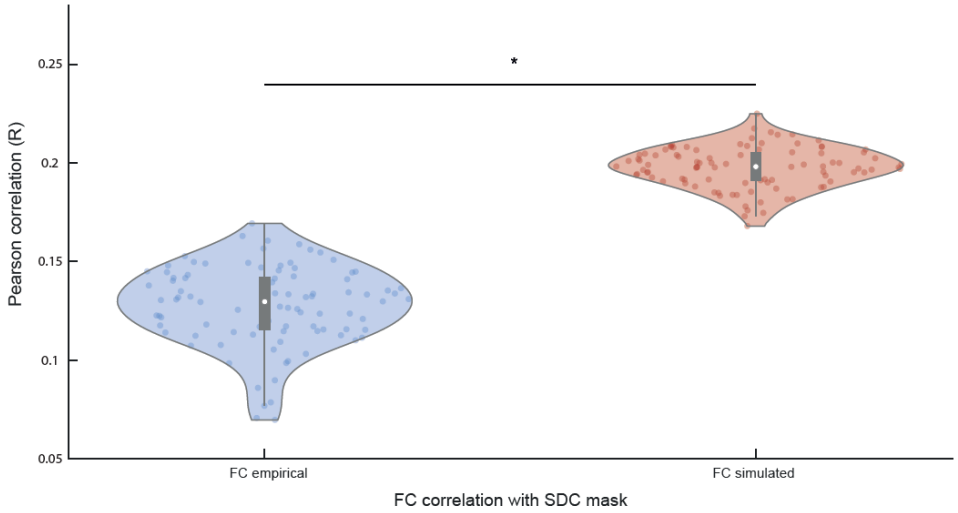

Figure B1: Correlation of SDC mask with the different types of FC

Figure B1: Correlation of SDC mask with the different types of FC: The correlation between the SDC mask of each patient and the FC empirical (left) showed a significant difference from the association between the SDC mask and the FC simulated (right). ($t(190)=-30.32$, $p<.01$)

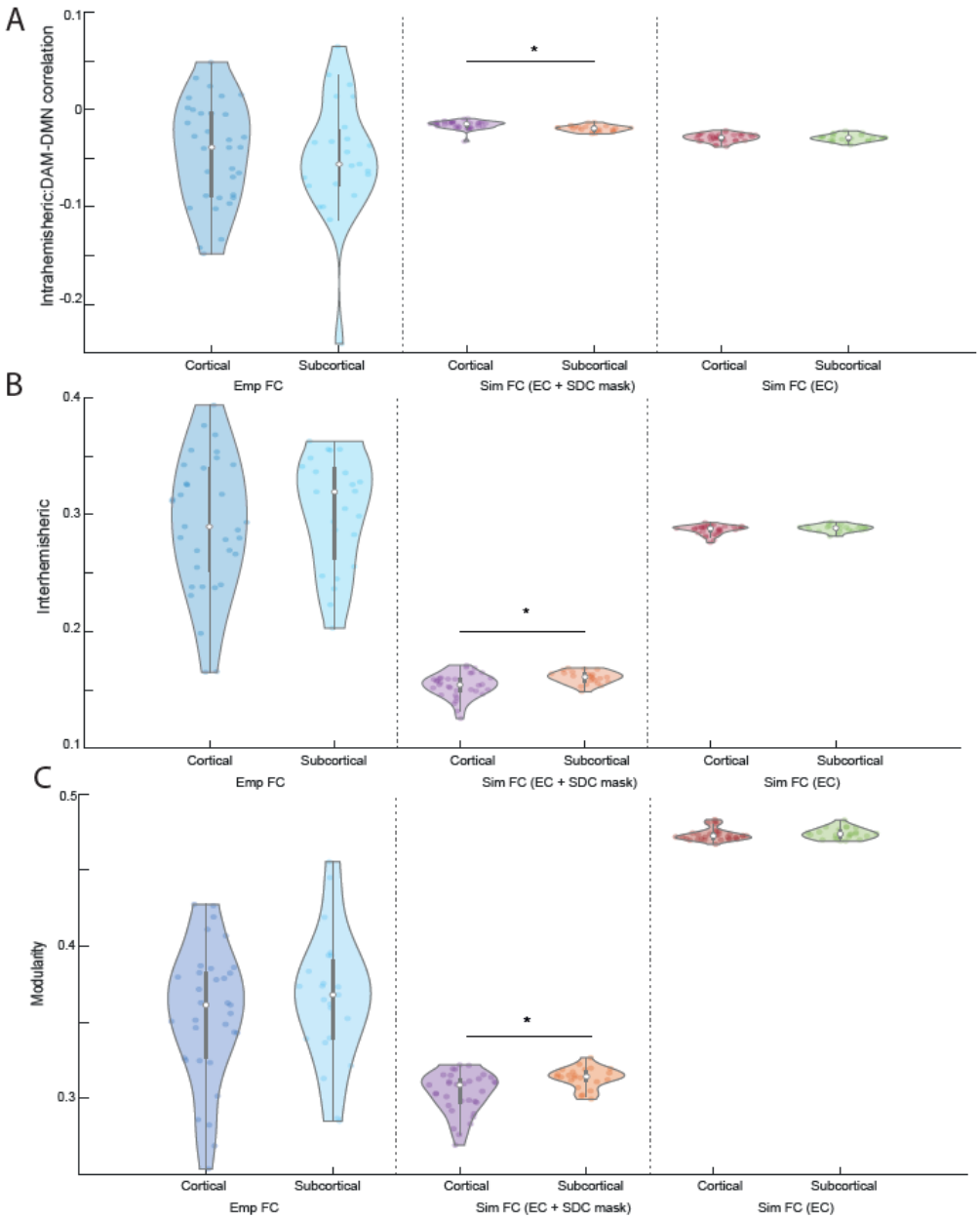

Figure B2: Distinction of FC impairments based in lesion localization

Figure B2: Distinction of FC impairments based in lesion localization: Comparison of patients with cortical vs subcortical lesions in **(A)** interhemispheric level, **(B)** interhemispheric level and **(C)** modularity level, using the (left) empirical FC, (center) GEC model including the SDC mask and (right) GEC model without the SDC mask

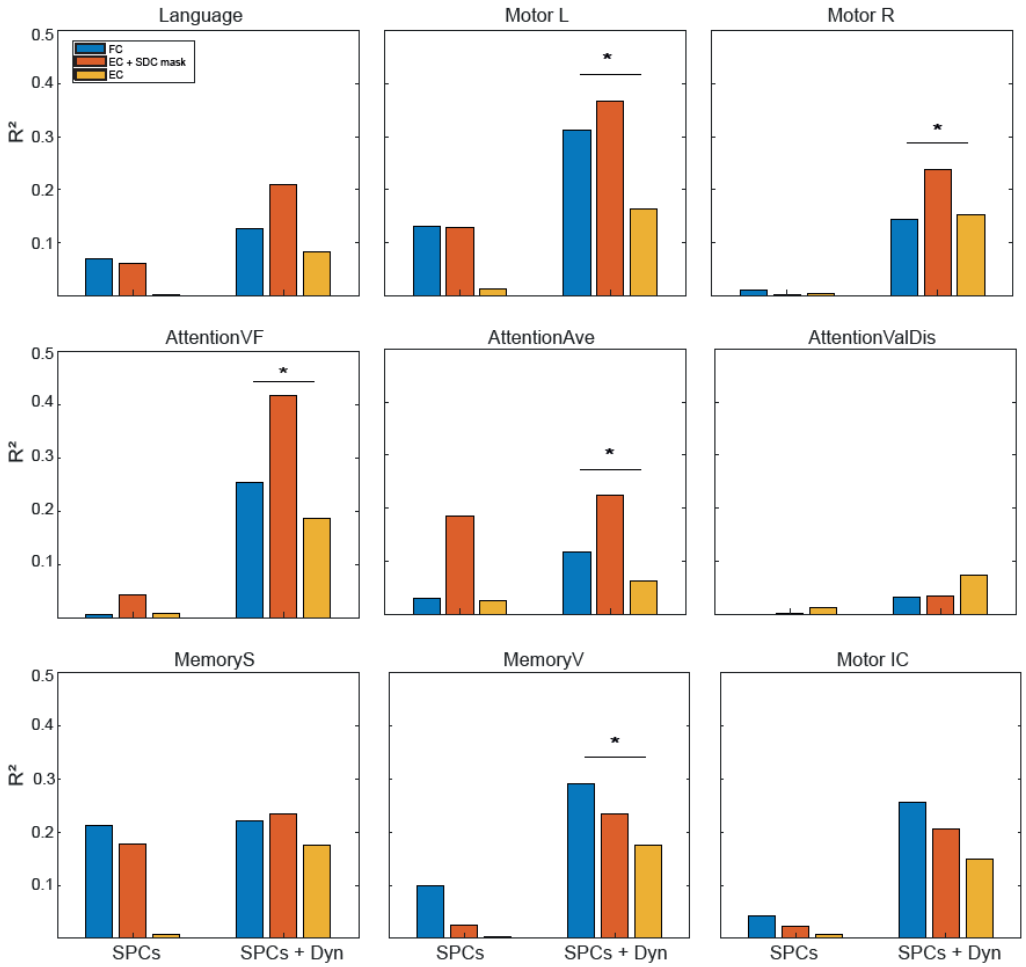

Figure B3: Relationship value of GEC and enhancement by using SDC mask

Figure B3: Relationship value of GEC and enhancement by using SDC mask: Relationship value of nine behavioral domains given by the static PCA (SPCs) of the three approaches (FC, GEC with the SDC mask and GEC without the SDC mask) and with their corresponding interaction with the dynamical components (see Methods for details). Asterisk indicates when only one regressor shows a significant relationship between the three measurements.

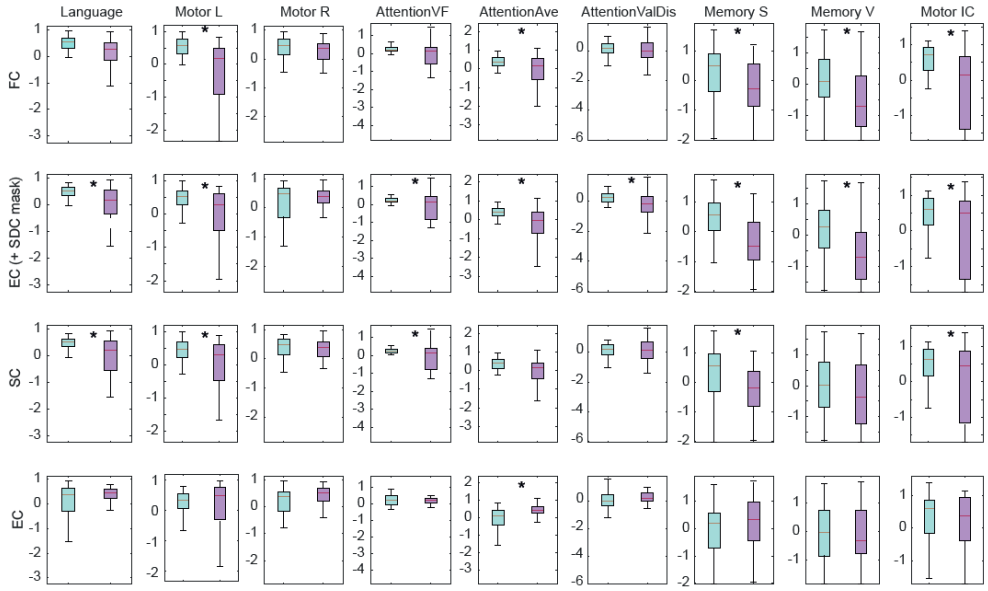

Figure B4: Comparison of behavioral scores of patients divided by severity level

Figure B4: Comparison of behavioral scores of patients divided by severity level: Comparison of behavioral scores of patients divided by severity level. Columns indicate the behavior domain while the rows indicate the criteria used for the severity division (FC, GEC (+ SDC mask), SC, and GEC).

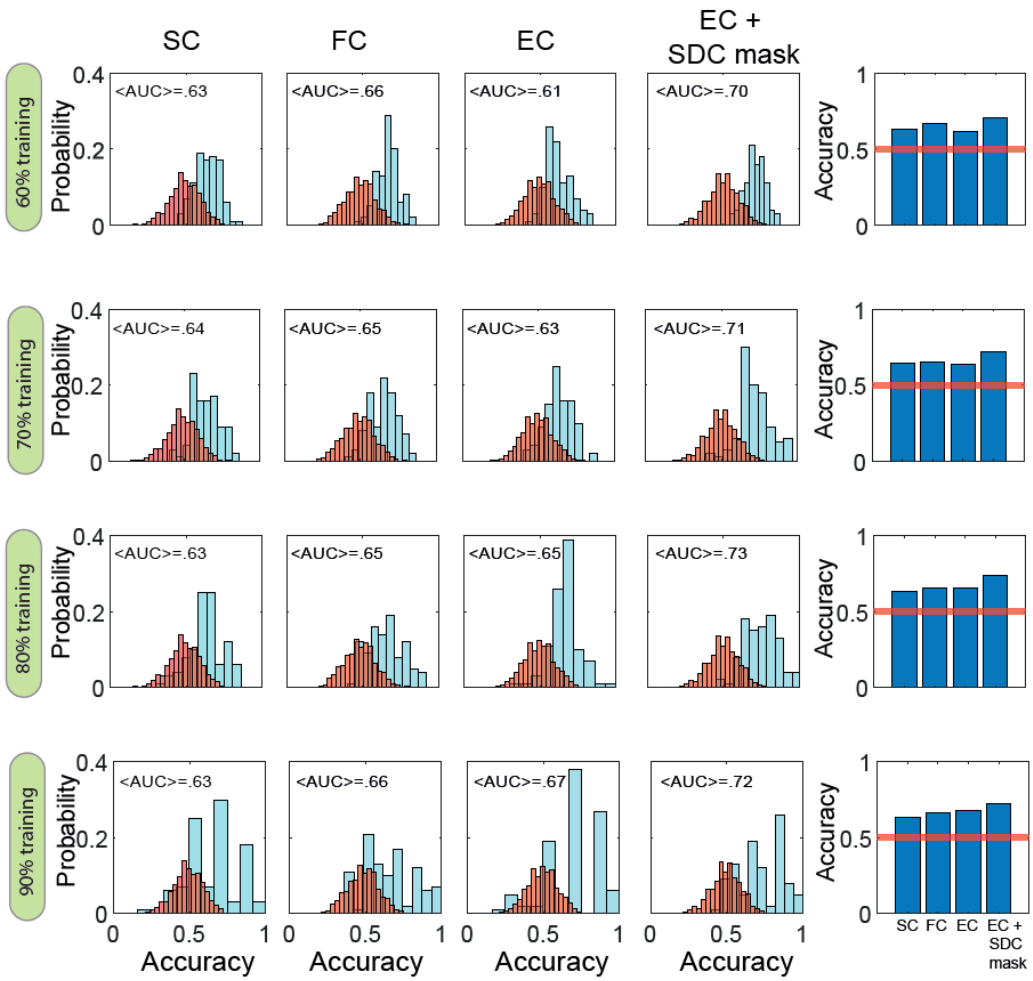

Figure B5: Classification with different training criteria

Figure B5: Classification with different training criteria: Each row represents a different percentage of subjects used to train the cross validation in the classifier. The column on the right compares the accuracy of each division criteria performance in order to show that the GEC + SDC mask model has the highest accuracy disregarding of the percentage used for the training.

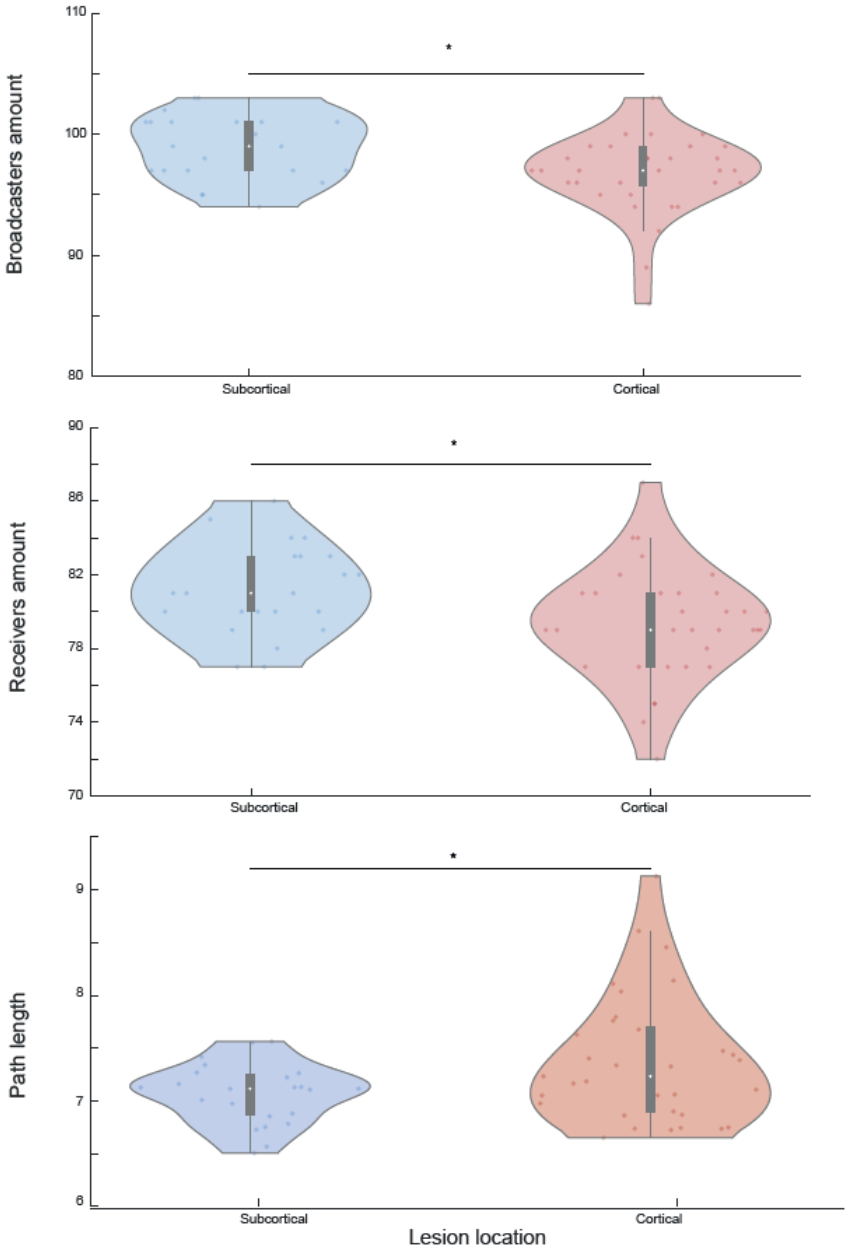

Figure B6: Topological metrics divided by lesion localization

Figure B6: Topological metrics divided by lesion localization: Comparison between patients with a cortical lesion and patients with a cortical lesion in (top) broadcasters' amount, (center) receivers' amount, and (bottom) path length.

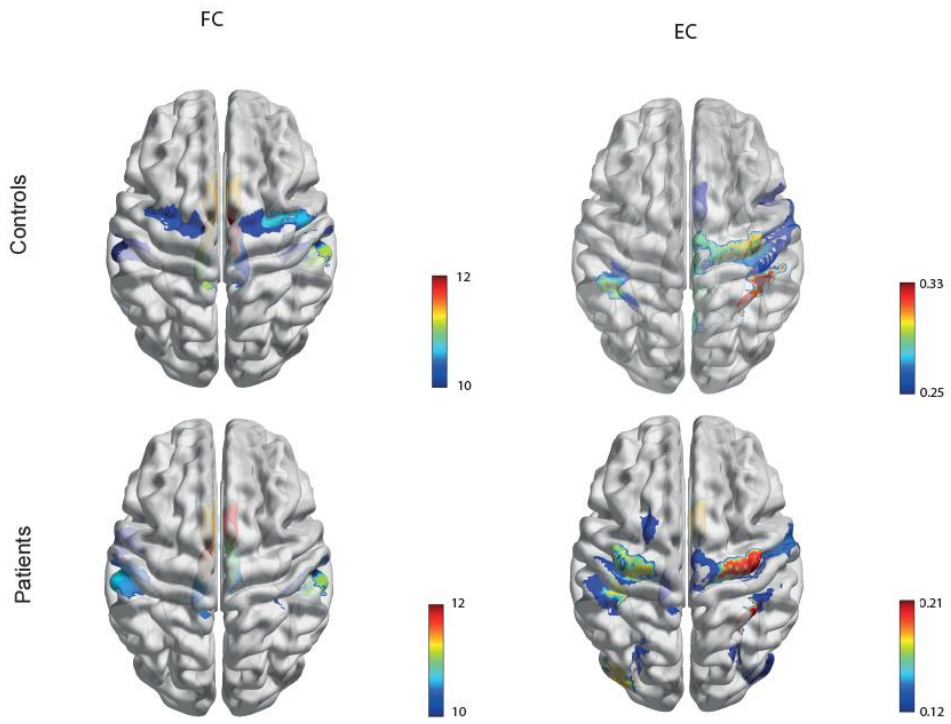

Figure B7: Top-Weighted areas topological localization

Figure B7: Top-Weighted areas topological localization: Area localization of the nodes with the highest 5% weights for (top-left) controls FC, (bottom-left) patients FC, (top-right) controls GEC and (bottom-right) patients GEC.

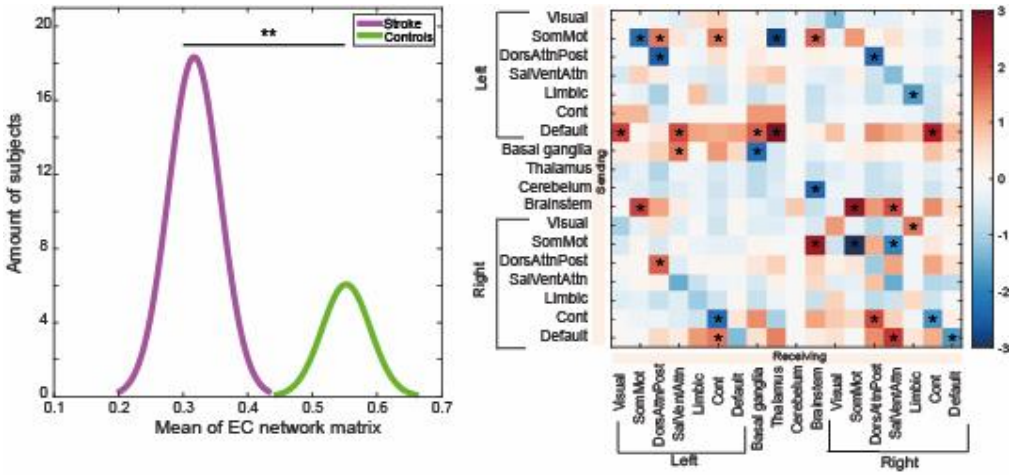

Figure B8: Groups' distribution comparison and significant networks interactions

Figure B8: Groups' distributions, comparison, and significant networks' interactions: Groups' distribution of the corresponding mean of GEC network matrix is shown on the left, revealing a significant difference between the two groups ([F(1, 17460) =174.19,p<.01]. When observing the comparison by networks (right), the network with the largest amount of significant differences between controls and stroke subjects is the DMN. Asterisks represent a p-value inferior to 0.05.

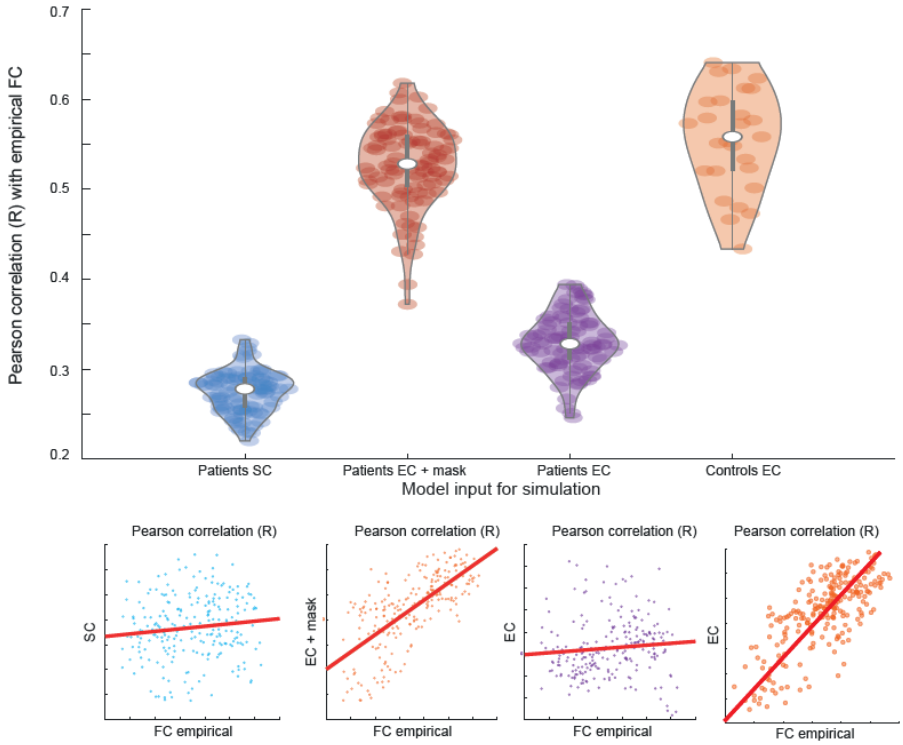

Figure B9: Model similarity compared to controls

Figure B9: Model similarity compared to controls: Model similarity is presented as shown in Figure 3 while adding the control group on the right for reference. The patients GEC + SDC model showed a similar range of similarity to the observed in the control group model.

C. Appendix C (Supplementary figures of chapter 5)

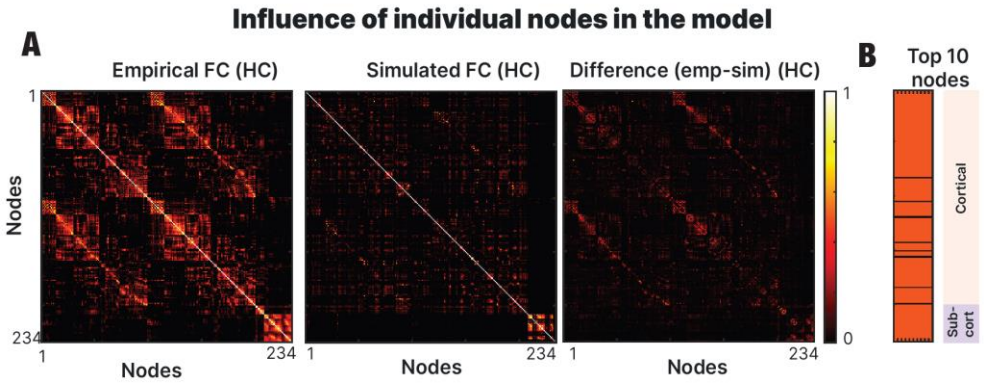

Figure C1: Influence of connectome nodes in the model

Figure C1: Influence of connectome nodes in the model: (**A**) Using the healthy control group, we calculated the empirical FC, simulated FC, and the corresponding difference between the previous two matrices. The output was a difference matrix indicating the accuracy of the fitting in each pair of nodes. (**B**) We displayed the 10 nodes with the highest difference value revealing the locations where the model was less accurate.

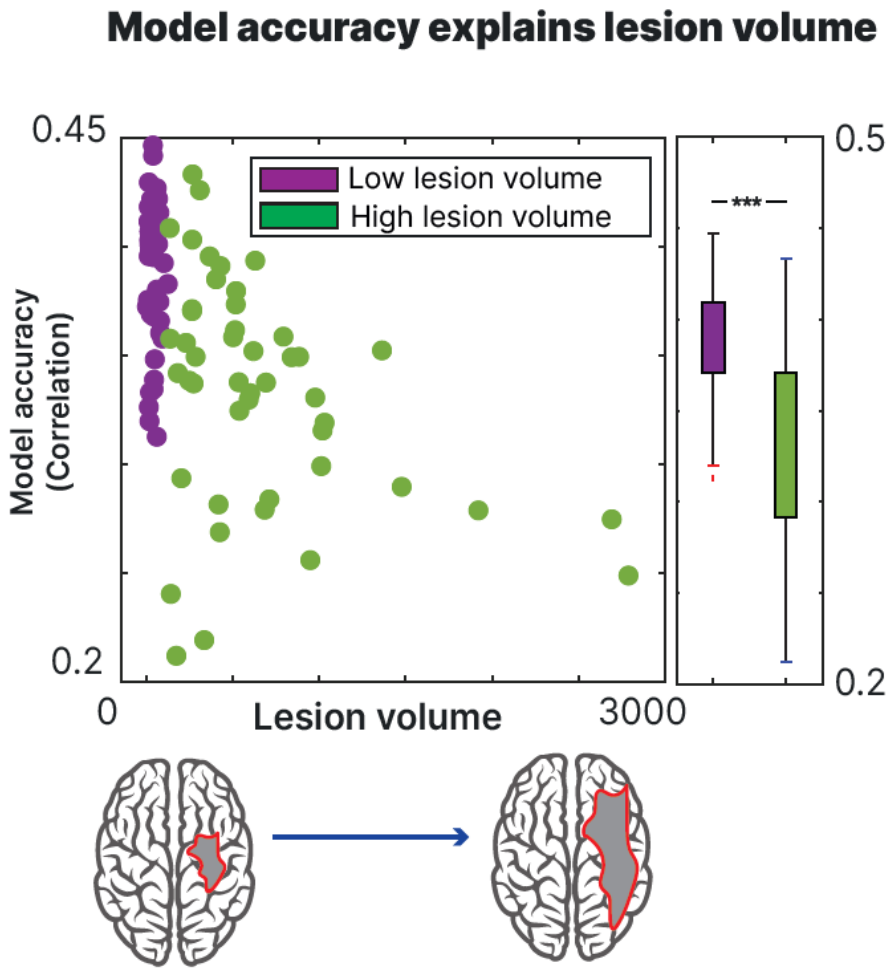

Figure C2: Relation of model accuracy with lesion volume

Figure C2: Relation of model accuracy with lesion volume: The subjects with higher lesion severity exhibited a lower accuracy (correlation between empirical and simulated data) in the model compared to the subjects with lower lesion severity.

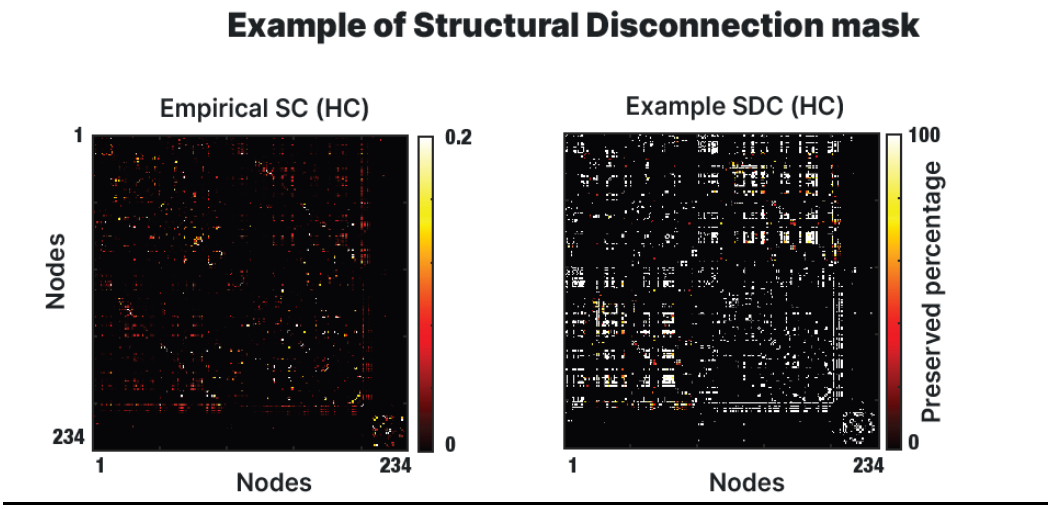

Figure C3: Anatomical information

Figure C3: Anatomical information: Matrix representation of the healthy group structural connectivity (left) and a SDC matrix of one stroke patient for visualization purposes.

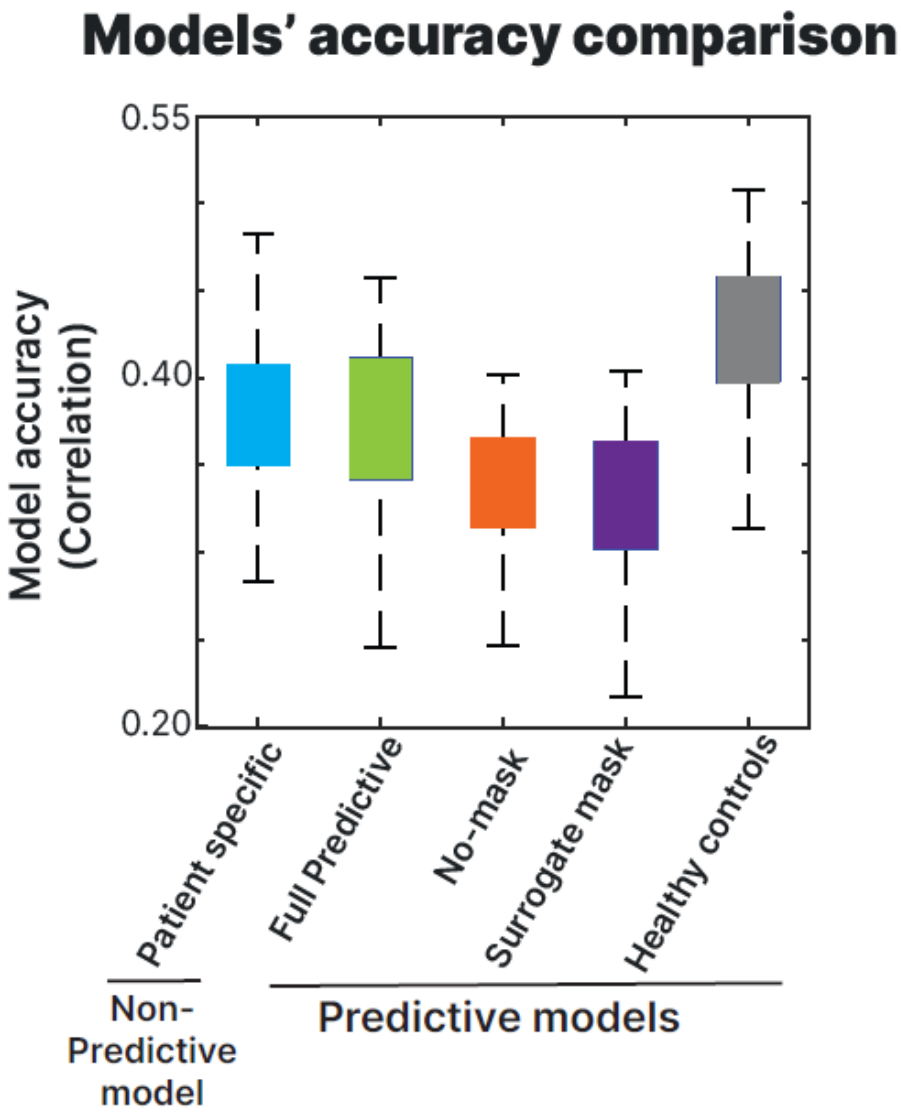

Figure C4: Model accuracy

Figure C4: Model accuracy: The similarity between the empirical and simulated FC was assessed for each model showing a similar performance for the patient specific mask and the full predictive model, while revealing a lower level for the surrogate mask model and the no-mask model. The healthy controls were included to assess the influence of the stroke lesion in the simulations.

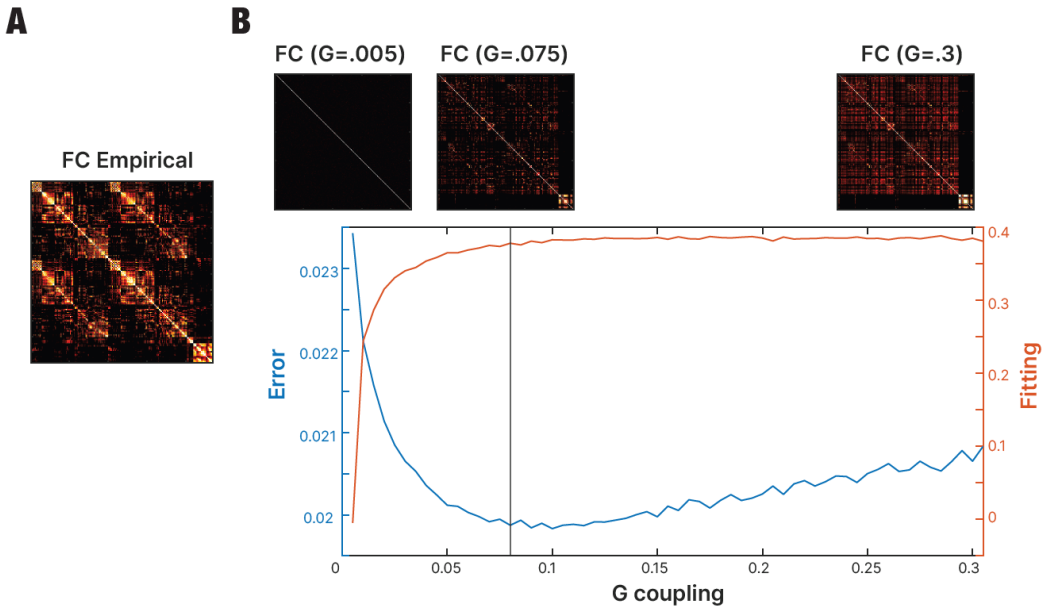

Figure C5: Influence of GC

Figure C5: Influence of GC: The similarity between the **(A)** empirical and **(B)** simulated data was assessed with different values of global coupling revealing the optimal point for the simulations.

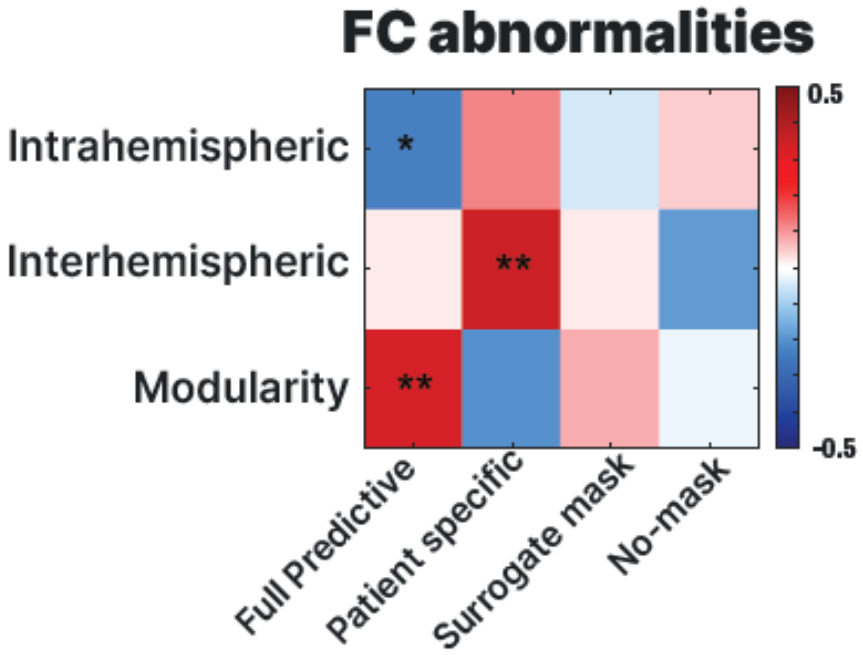

Figure C6: Relation of model accuracy to the magnitude of FC abnormalities

Figure C6: Relation of model accuracy to the magnitude of FC abnormalities: The accuracy of the patient specific model was significantly correlated with inter-hemispheric FC (R=.41, p<.01), but not with intra-hemispheric FC or modularity. All the other models (including all the possibilities of the surrogate mask model and the No-mask model), showed no significant relationship with FC abnormalities.

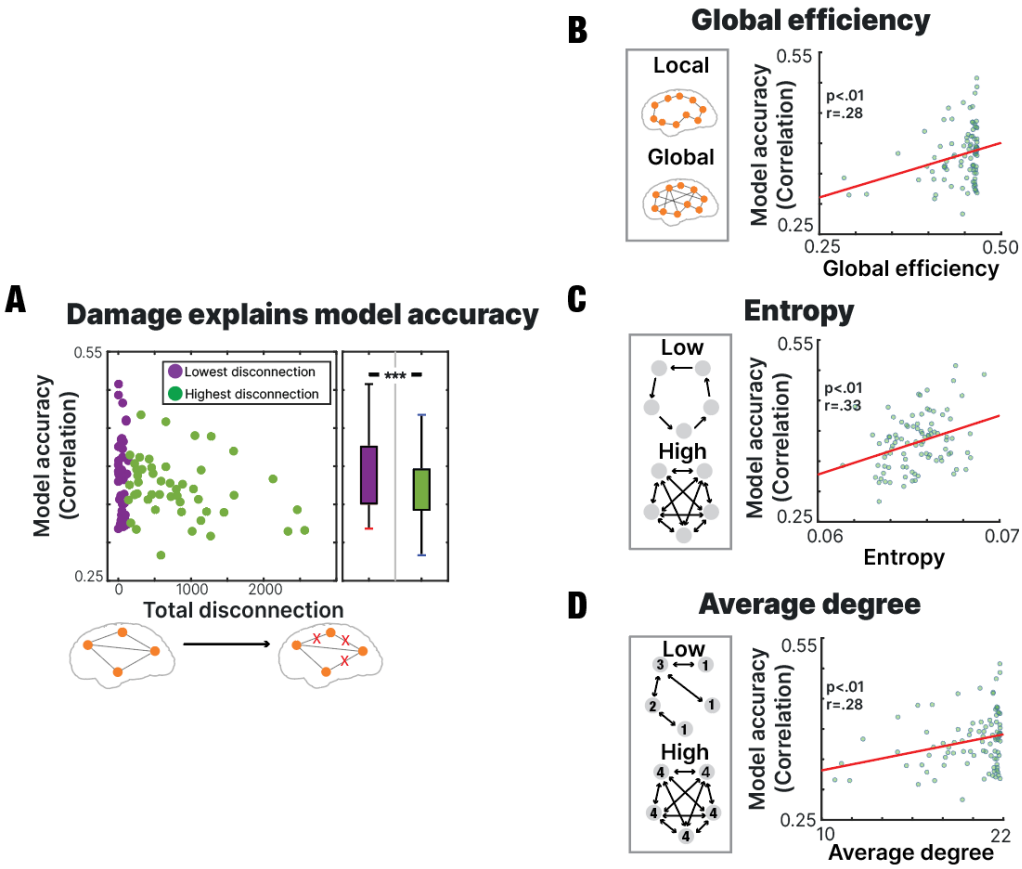

Figure C7: Relation of the accuracy of the non-predictive patient specific model to stroke metrics

Figure C7: Relation of the accuracy of the non-predictive patient specific model to stroke metrics **(A)** Subjects with lower levels of disconnection exhibited a higher correlation between the empirical and simulated FC matrices, indicating better model performance for patients with less severe lesions. **(B-C-D)** Higher global efficiency **(B)**, higher entropy **(C)** and higher average degree **(D)** were associated with higher model accuracy.

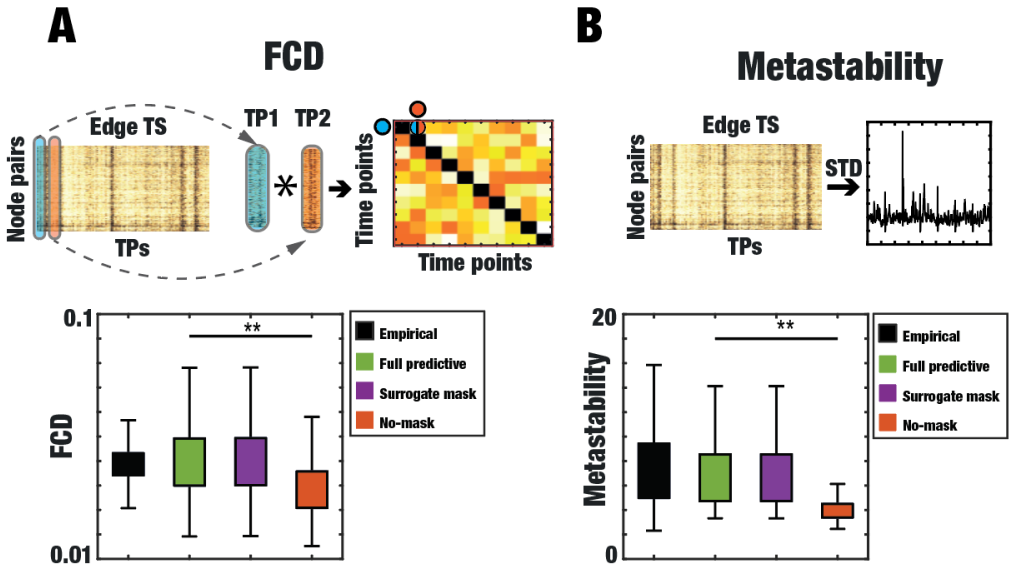

Figure C8: Dynamical metrics calculation for the different models

Figure C8: Dynamical metrics calculation for the different models **(A)** Time versus-time matrix representing the functional connectivity dynamics (FCD), where each entry FCD(t1, t2) is defined by a measure of resemblance between FC(t1) and FC(t2). Therefore, the FCD captures the spatiotemporal organization of FC by representing the coincidences between FC(t) matrices. It results in a symmetric matrix where an entry (ts1, ts2) is defined by the Pearson correlation between FC(ts1) and FC(ts2). FCD was estimated for the empirical data and the three predictive models showing a significant difference between the predictive models and the model without mask. Specially, there was a significant difference between the full-predictive model and the "No-mask" model ($t(95)= 31.87$, $p<.01$) **(B)** We calculated the standard deviation of the edge time series which represents the temporal metastability. This metric gives information about temporal variability in the level of synchronization. Edge metastability was estimated for the empirical data and the three predictive models showing a significant difference between the predictive models and the model without mask. In particular, the difference was significant between the full-predictive model and the "No-mask" model ($t(95)= 19.05$, $p<.01$).

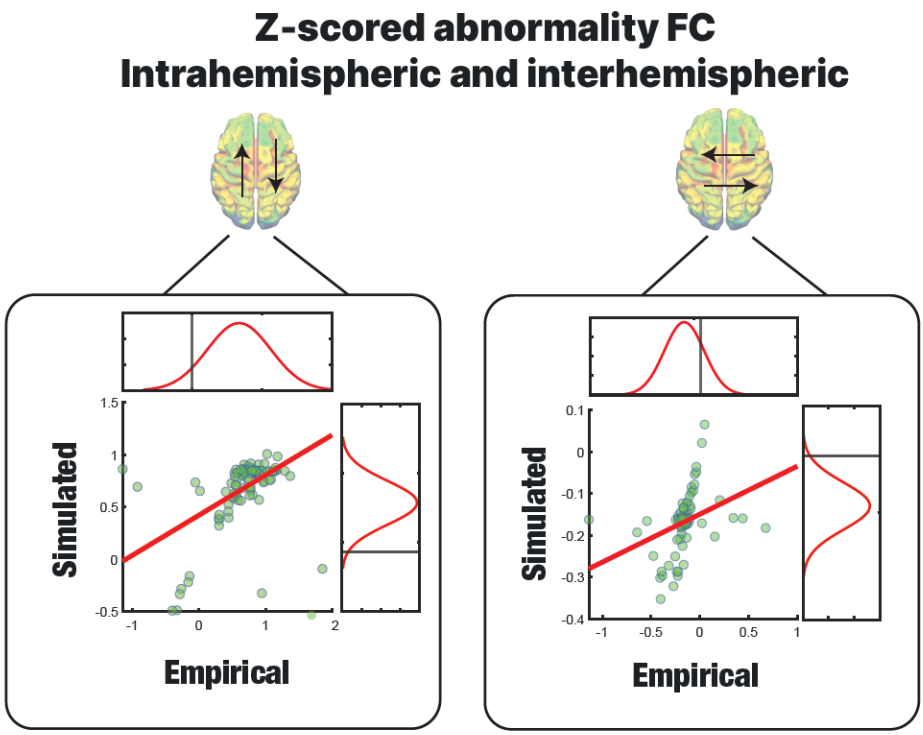

Figure C9: Model accuracy for predicting patient z-scored abnormalities.

Figure C9: Model accuracy for predicting patient z-scored abnormalities in DAN-DMN FC (left panel) and homotopic interhemispheric FC (right panel). For each patient, the entries in the z-scored FC abnormality matrix corresponding to DAN-DMN FC and interhemispheric homotopic FC were separately averaged for both the empirical and simulated abnormality matrices. Then the simulated and empirical averaged quantities were plotted against one another across patients. Because DAN-DMN FC for patients tends to be more positive than controls, the corresponding patient z-scores also tends to be positive. Conversely, because interhemispheric homotopic FC for patients tends to be less positive than controls, the corresponding patient z-scores tends to be negative.

D. Appendix D (Supplementary figures of chapter 6)

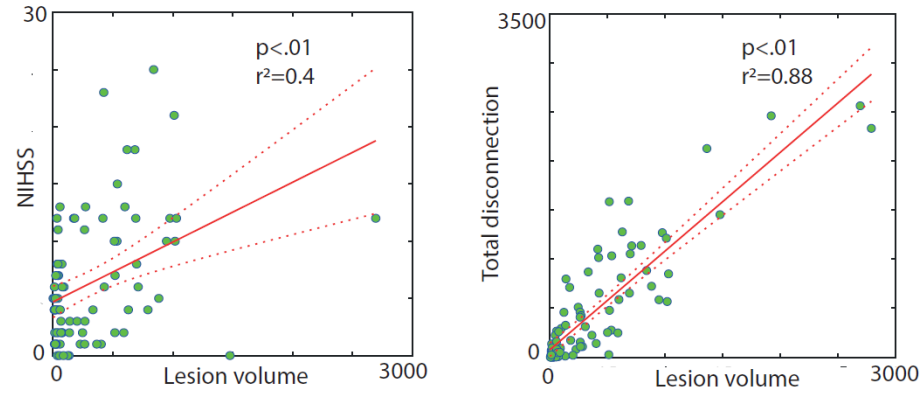

Figure D1: Correlation between lesion volume, NIHSS and total disconnection

Figure D1: Correlation between Lesion volume and NIHSS (Left) and Total number of disconnected tracts (Right). Both relations showed a significant relation probing the robustness of the elected metric.

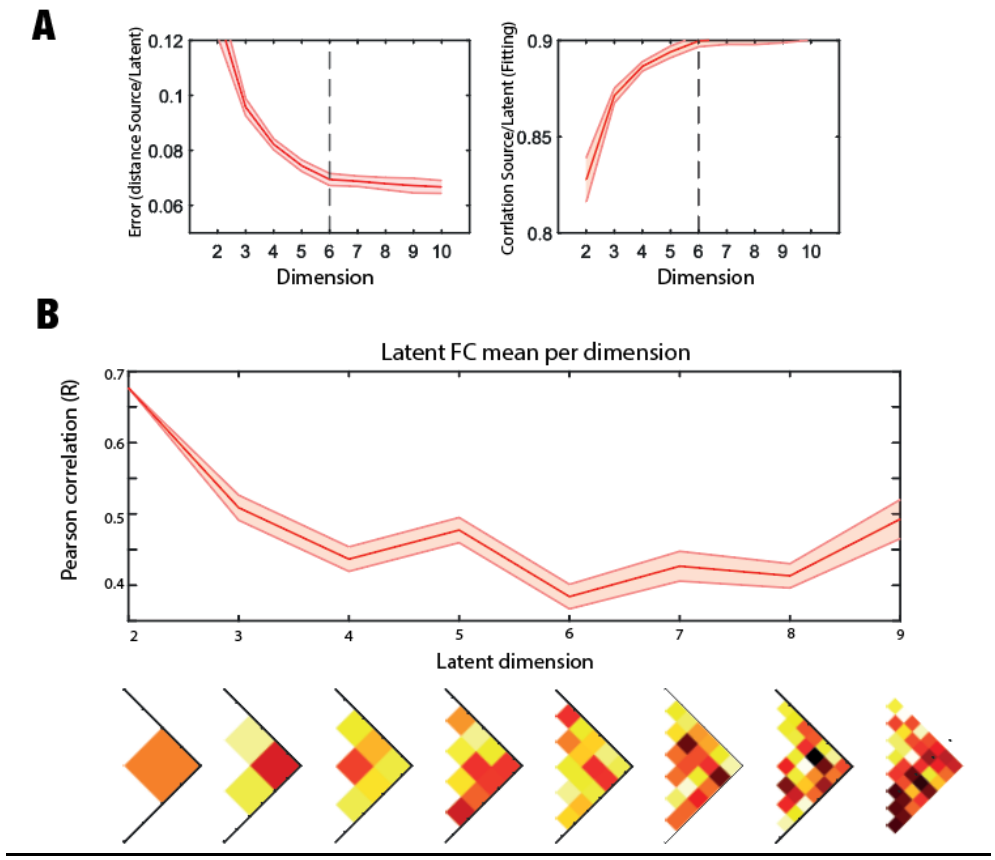

Figure D2: Reconstruction error and latent FC per dimension

Figure D2: Reconstruction error and Latent FC per dimension: **(A)** Reconstruction error reached a level of 0.06 at dimension 6 showing no rate of change higher than 0.005 after it. Fitting level reached a level of 0.89 showing no rate of change higher than 0.005 after it. **(B)** The highest correlation between the latent FC and the source FC is shown at dimension 2 (r= .67) while the lowest correlation value is shown at dimension 6 (r=.38)

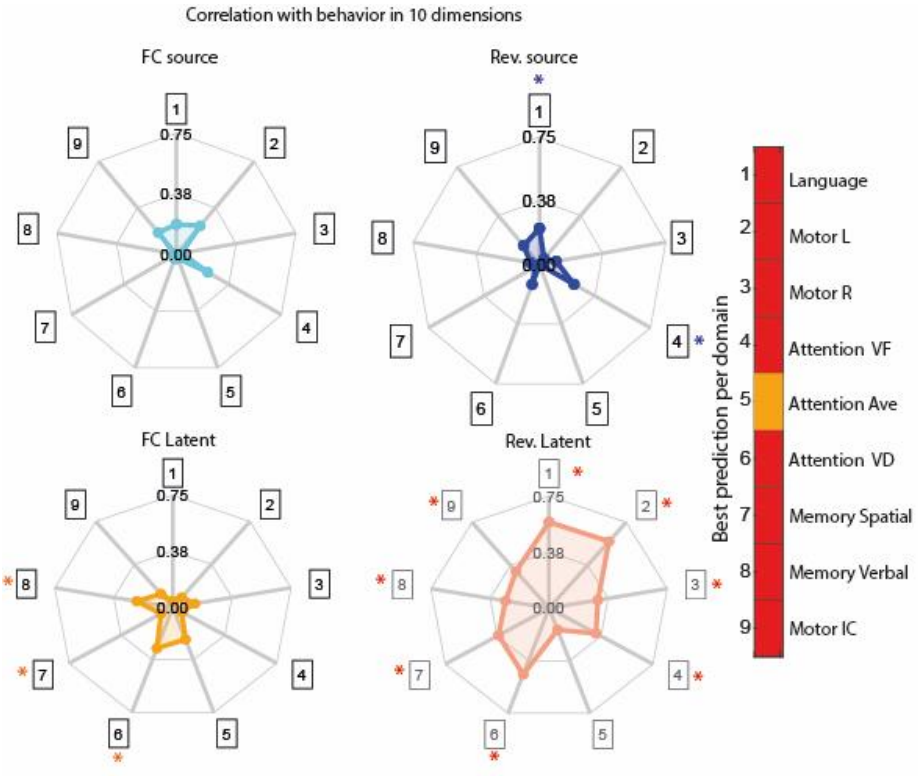

Figure D3: Association between dimension 10 and behavioral scores

Figure D3: Association between dimension 10 and behavioral scores. For each behavioral domain, the corresponding metric with the highest association was represented indicating the respective color. Red represents the latent space metric while blue represents the source space.

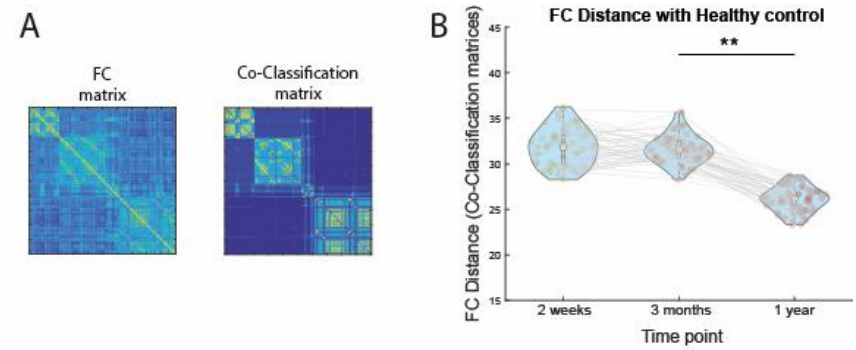

Figure D4: Co-Classification matrix

Figure D4: Co-classification matrix reveals same pattern as empirical FC when compared with healthy controls across time. This analysis was performed in comparison to the one presented in **Figure 6.4a.**

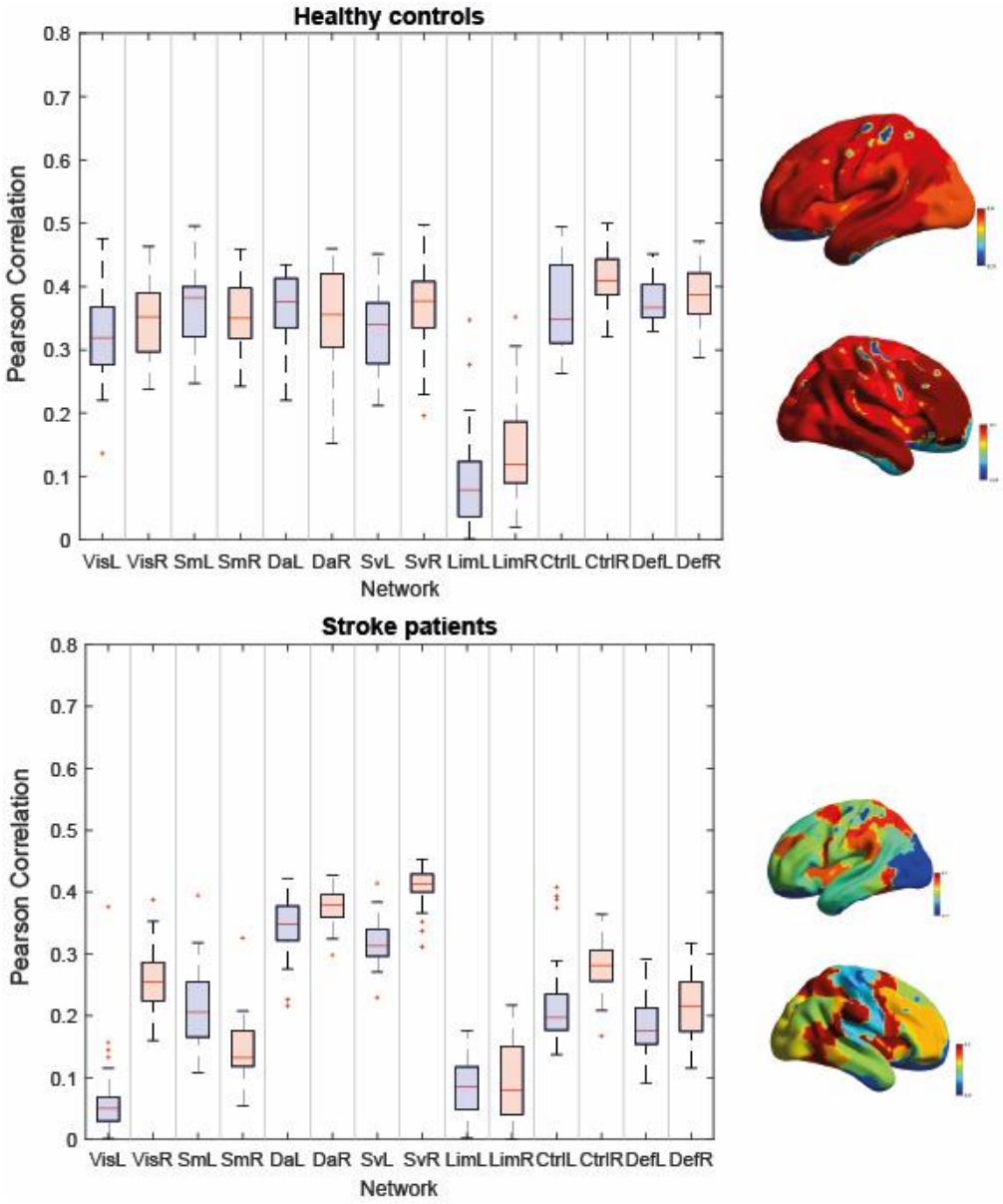

Figure D5: SC-FC correlation per network

Figure D5: SC-FC correlation per network: The relation between structural and functional information of networks reveals a symmetry between homotopic regions in the healthy control and asymmetry in the stroke patients' group

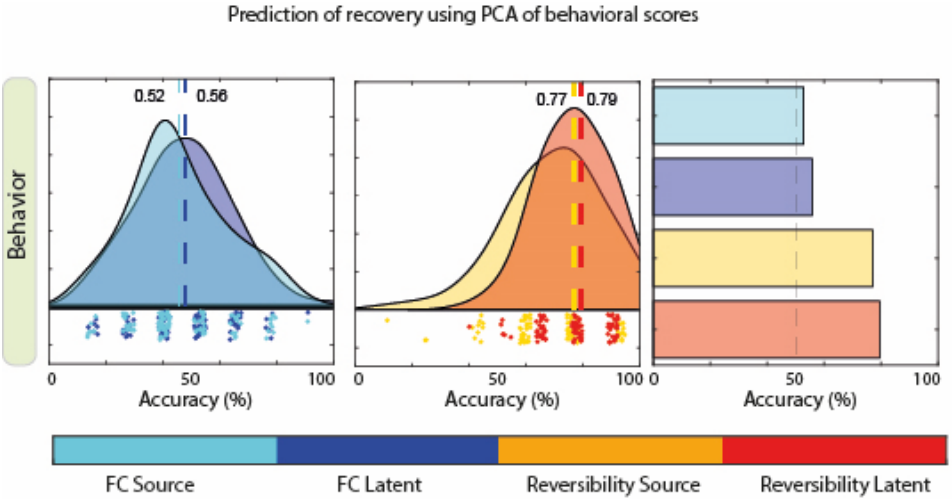

Figure D6 Prediction of recovery using PCA

Figure D6: Prediction of recovery using the first principal component as separation criteria.

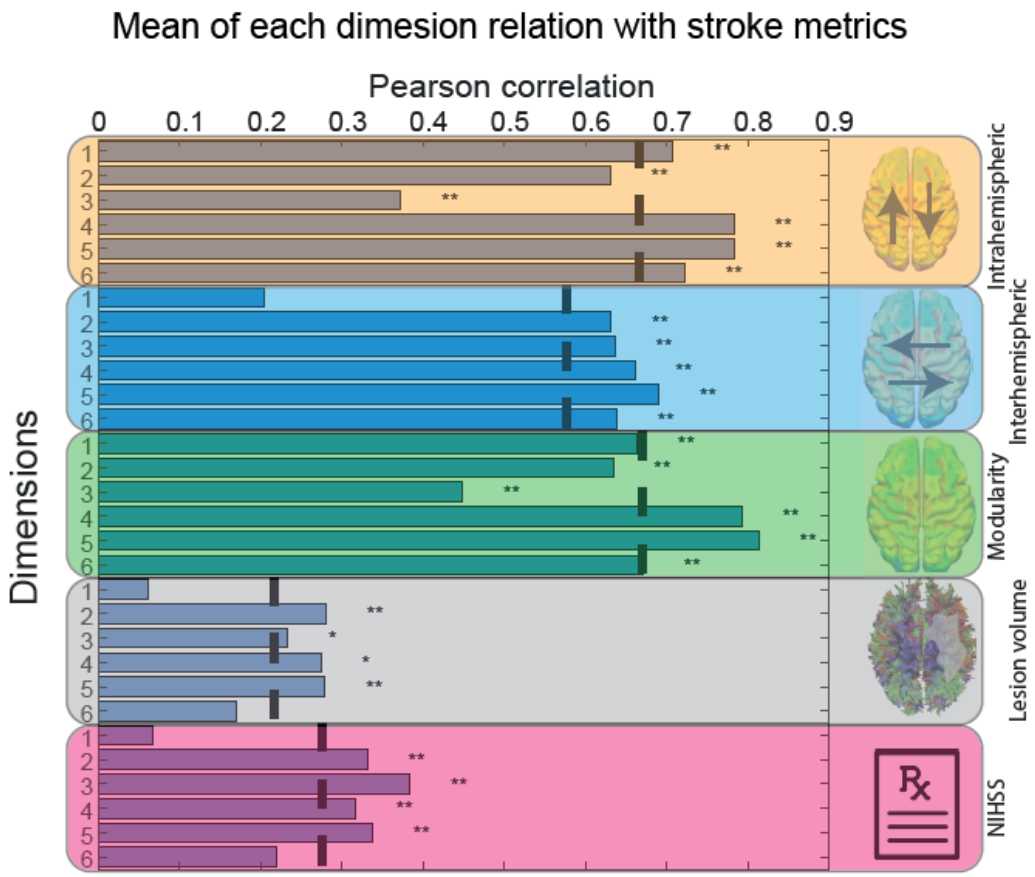

Figure D7 Association of latent representation with structural and functional features

Figure D7: Association between latent representation pattern and structural/functional features: We calculated the Pearson correlation R value for each dimension mean and standard deviation, with the corresponding metric of interest. By studying the mean of each of the 6 of the latent dimensions, intrahemispheric value showed a significant relation with all of them, interhemispheric with 5 of them, modularity with all of them, lesion volume with 4 of them and NIHSS with 4 of them.

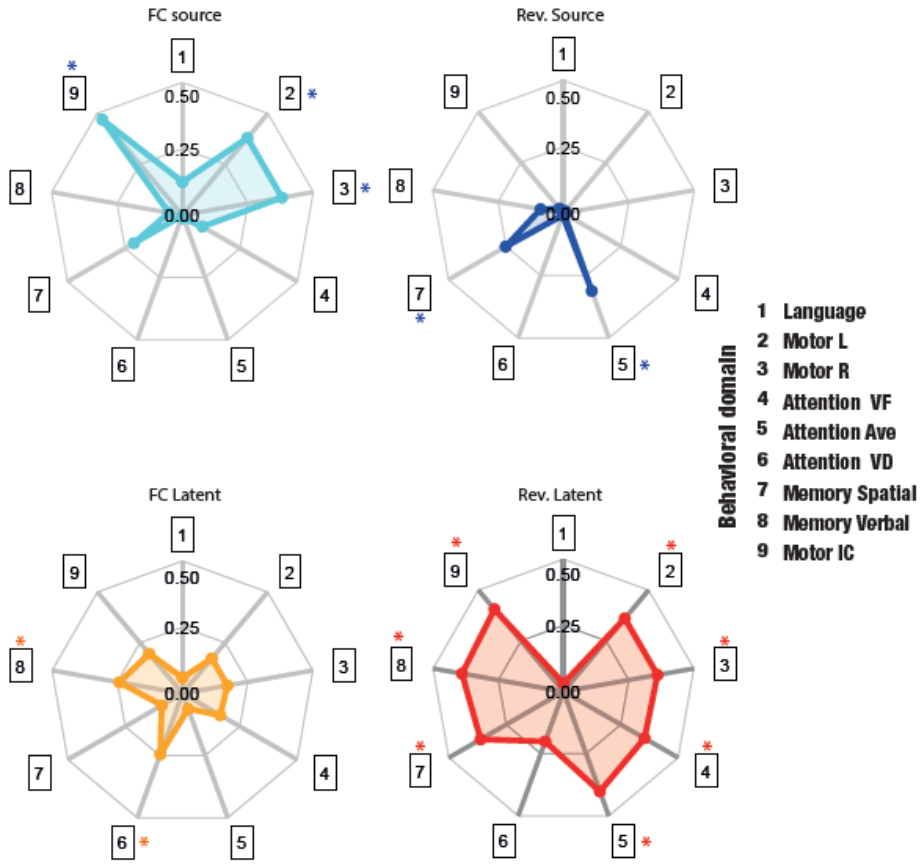

Figure D8: Correlation of mean FC with behavior impairment

Figure D8: Correlation of mean FC with behavior impairment at acute stage (2 months after stroke incident): Each behavioral domain at the acute stage was related with the mean FC and reversibility in both source and latent space. Asterisks indicate significant relations. The reported values are as follows: FC Source: .12, .38, .38, .08, . 01, .001, .21, .05,.46; Rev Source: .003, .01, .01, .002, .31, .008, .25, .08, .02; FC Latent: .05, .17, .17, .16, .06, .24, .09, .24, .19; Rev Latent: .03, .36, .36, .35, .40, .20, .36, .28, .40.

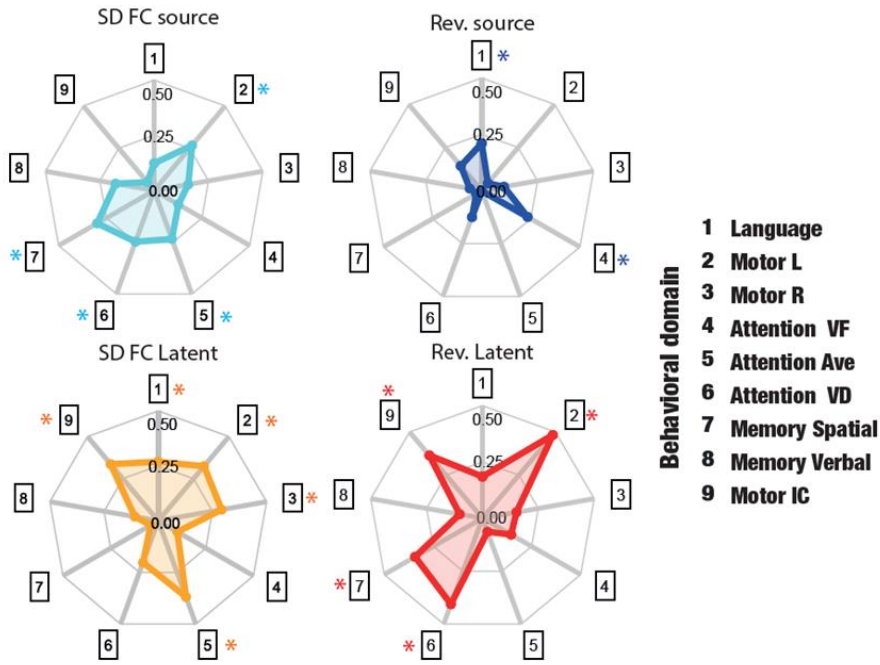

Figure D9: Correlation of FC STD with behavior impairment recovery

Figure D9: Correlation of FCs' standard deviation with behavior impairment recovery: All the metrics used for the classification approach were related with each of the 9 behavioral domains recovery values (score after 1 year minus score after 2 weeks, divided the 2 weeks score). Asterisks represent which of the relations were significant. The reported values are as follows: FC Source: .24, .27, .16, .29, . 07, .33, .24, .15,.22; Rev Source: .04, .001, .01, .05, .00, .01, .00, .00, .02; FC Latent: .02, .32, .29, .10, .36, .20, .03, .10, .33; Rev Latent: .18, .06, .28, .21, .07, .14, .23, .07, .26.

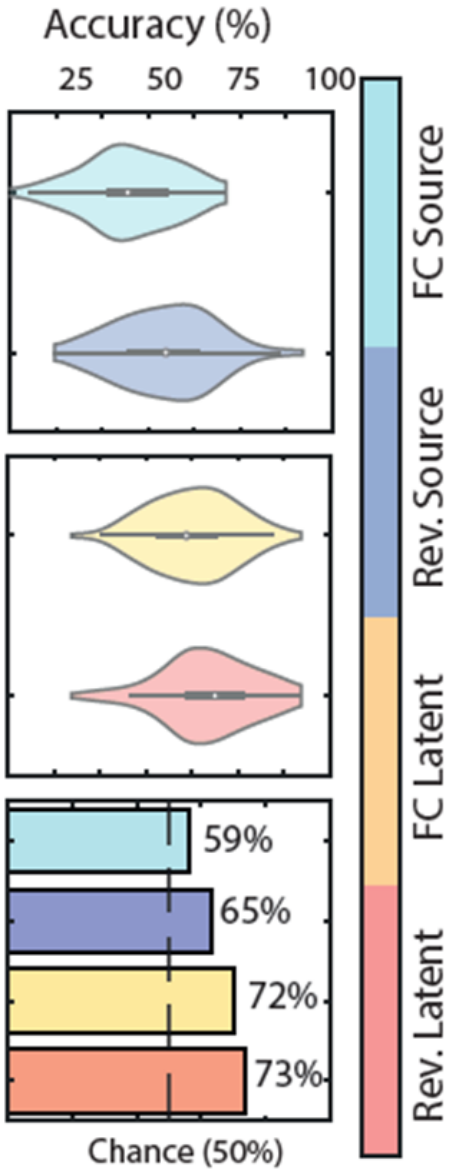

Figure D10: Classification of severity using NIHSS as division criteria

Figure D10: Classification of severity using NIHSS as division criteria: The distinction between stroke patients with low and high lesion volume indicated that the highest accuracy was given by the reversibility in the latent space (mean = 74%).

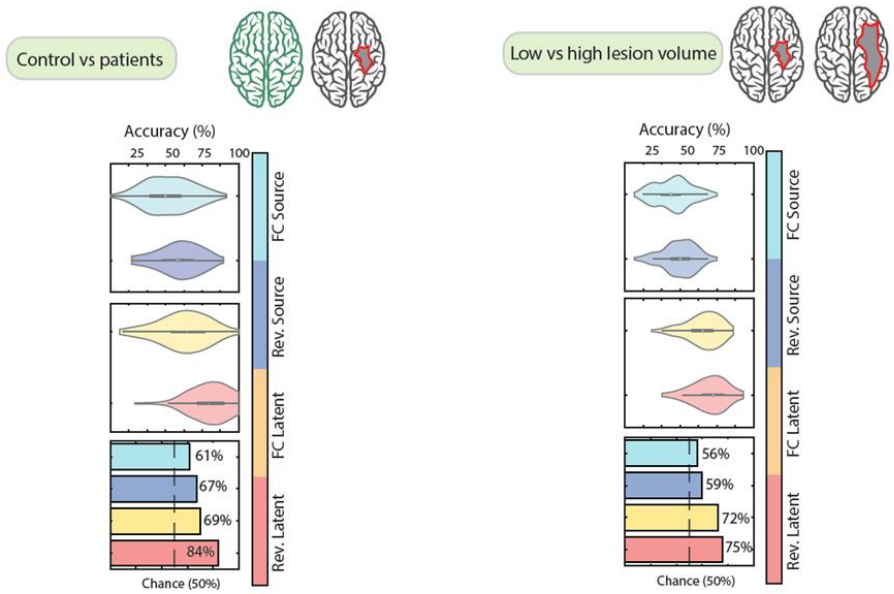

Figure D11: Classification using the STD instead of FC mean

Figure D11: Classification using the standard deviation instead of the FC average: The distinction between stroke patients with low and high lesion volume and between healthy controls and patients showed the highest accuracy in both cases in the reversibility of the latent space.

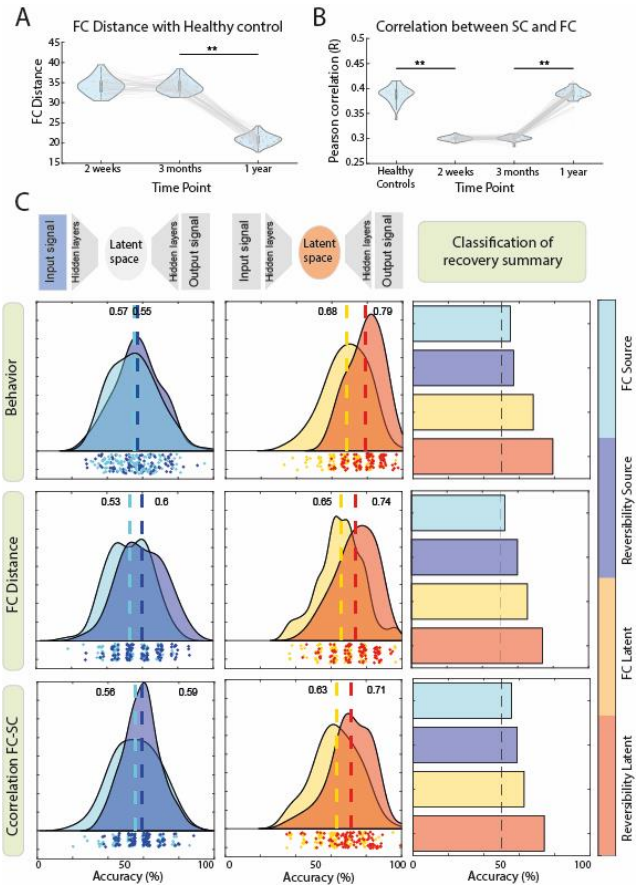

Figure D12: Prediction of recovery using STD instead of FC mean

Figure D12: Prediction of recovery using the standard deviation instead of the FC average: **(A)** FC distance (Frobenius norm of the difference between the two matrices) between stroke patients at each time point and the healthy controls indicating the decrease of distance after 1 year ($p<.01$). **(B)** Correlation between SC and FC of healthy controls and stroke patients (at each measurement stage) revealing the increase at the remote stage, showing a similar value to controls after 1 year of the incident ($p<.01$)., while it is not the case after 2 weeks and 3 months ($p=.86$). **(C)** Prediction of recovery using as input of the classifier the FC's standard deviation and reversibility matrix of the source space and the FC and reversibility matrix of the latent space. To split the subjects in high vs low recovered, 3 different criteria were used: Amount of behavioral domains recovered, the FC distance at remote stage and the correlation between SC-FC at remote stage. In all the scenarios, reversibility in the latent space showed the highest accuracy.

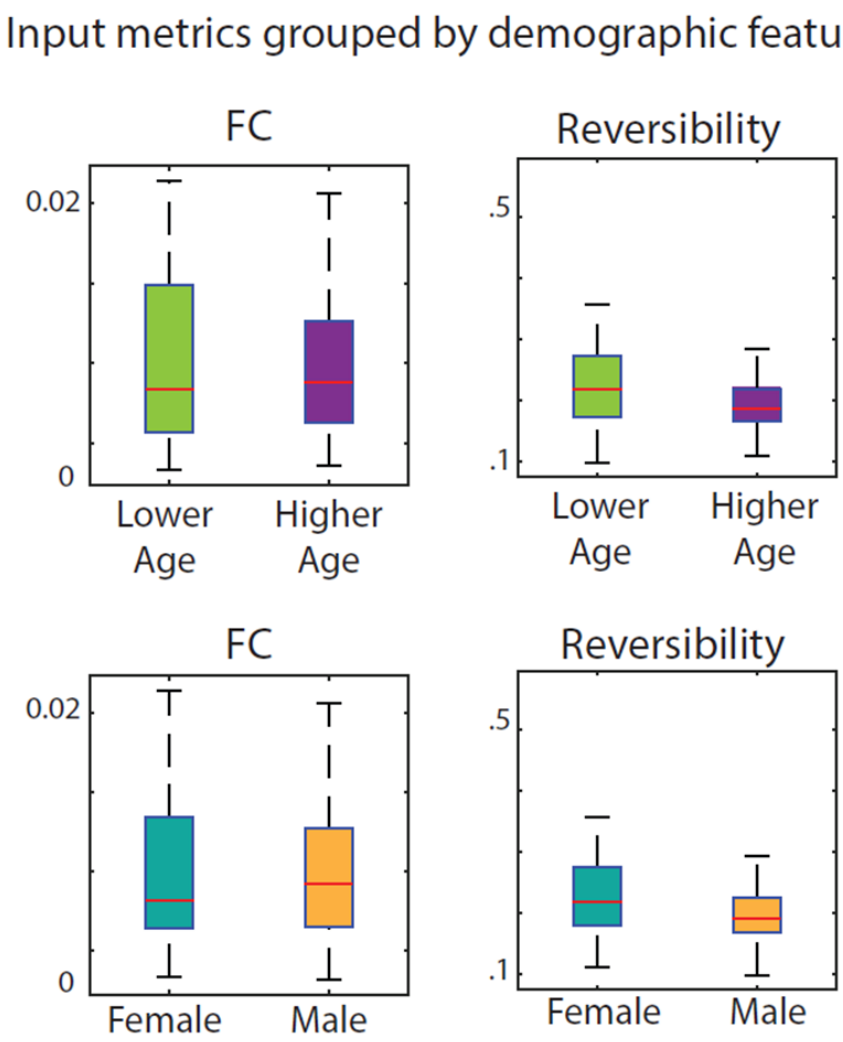

Figure D13: Input metrics grouped by demographic features

Figure D13: Input metrics grouped by demographic features: In order to assess the influence of demographical factors, we calculated the classifier input metrics (FC and reversibility) for subgroups divided by the median age (top subpanels) and by gender (low subpanels) showing no significant differences (p>.2) between the groups.

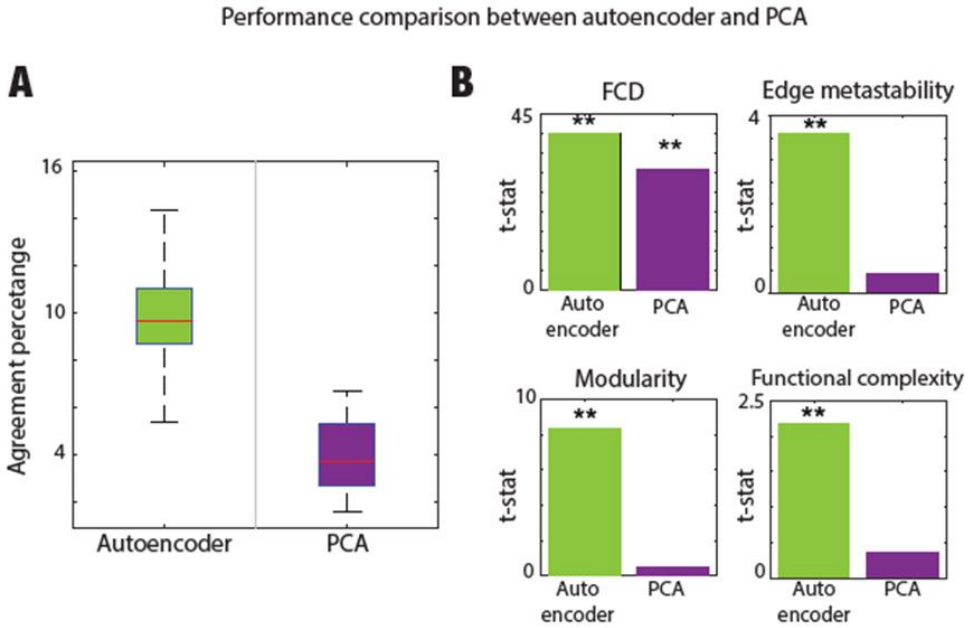

Figure D14: Preserved features in latent space compared to PCA performance

Figure D14: Preserved features in latent space compared to PCA performance: **(A)** Agreement percentage was compared for the 6 latent dimensions and the 6 first principal components, showing a higher performance of the autoencoder. **(B)** Difference between the healthy control and the stroke patients was assessed in the latent space and in the 6 first principal components for all the studied metrics. The difference in metrics was significant for each application of the autoencoder while the only significant difference in metrics for the application of PCA was for FCD.

Supp. Table D1

	Healthy Control	Stroke patients
Age	56.6	52.3
Gender	M=59% F=41%	M= 57% F=43%
Education	13.9	13.4
Handedness	R=91% L=9%	R=94% L=6%

Supp. Table D1: Demographic information of the involved subjects

Supp. Table D1: Demographic information of the involved subjects. For more information and detailed scores in behavioral tasks, see (Corbetta et al., 2015)

Bibliography

Abbas, A., Bassil, Y., & Keilholz, S. (2019). Quasi-periodic patterns of brain activity in individuals with attention-deficit/hyperactivity disorder. *Neuroimage Clin*, *21*, 101653. https://doi.org/10.1016/j.nicl.2019.101653

Achard, S., & Bullmore, E. (2007). Efficiency and cost of economical brain functional networks. *PLoS computational biology*, *3*(2), e17.

Acharya, U. R., Meiburger, K. M., Faust, O., Koh, J. E. W., Oh, S. L., Ciaccio, E. J., Subudhi, A., Jahmunah, V., & Sabut, S. (2019). Automatic detection of ischemic stroke using higher order spectra features in brain MRI images. *Cognitive systems research*, *58*, 134-142.

Adhikari, M. H., Belloy, M. E., Van der Linden, A., Keliris, G. A., & Verhoye, M. (2020). Resting-State Co-activation Patterns as Promising Candidates for Prediction of Alzheimer's Disease in Aged Mice. *Front Neural Circuits*, *14*, 612529. https://doi.org/10.3389/fncir.2020.612529

Adhikari, M. H., Belloy, M. E., Van der Linden, A., Keliris, G. A., & Verhoye, M. (2021). Resting-State Co-activation Patterns as Promising Candidates for Prediction of Alzheimer's Disease in Aged Mice. *Frontiers in Neural Circuits*, 91.

Adhikari, M. H., Griffis, J., Siegel, J. S., Thiebaut de Schotten, M., Deco, G., Instabato, A., Gilson, M., & Corbetta, M. (2021). Effective connectivity extracts clinically relevant prognostic information from resting state activity in stroke. *Brain communications*, *3*(4), fcab233.

Adhikari, M. H., Hacker, C. D., Siegel, J. S., Griffa, A., Hagmann, P., Deco, G., & Corbetta, M. (2017). Decreased integration and information capacity in stroke measured by whole brain models of resting state activity. *Brain*, *140*(4), 1068-1085.

Ahn, Y.-Y., Bagrow, J. P., & Lehmann, S. (2010). Link communities reveal multiscale complexity in networks. *nature*, *466*(7307), 761-764.

Aho, K., Harmsen, P., Hatano, S., Marquardsen, J., Smirnov, V. E., & Strasser, T. (1980). Cerebrovascular disease in the community: results of a WHO collaborative study. *Bulletin of the World Health Organization*, *58*(1), 113.

Ahrens, M. B., Orger, M. B., Robson, D. N., Li, J. M., & Keller, P. J. (2013). Whole-brain functional imaging at cellular resolution using light-sheet microscopy. *Nature methods*, *10*(5), 413-420.

Al-Qazzaz, N. K., Ali, S. H. B. M., Ahmad, S. A., Islam, M. S., & Escudero, J. (2018). Discrimination of stroke-related mild cognitive impairment and vascular dementia using EEG signal analysis. *Medical & biological engineering & computing*, *56*(1), 137-157.

Allan, T. W., Francis, S. T., Caballero-Gaudes, C., Morris, P. G., Liddle, E. B., Liddle, P. F., Brookes, M. J., & Gowland, P. A. (2015). Functional connectivity in MRI is driven by spontaneous BOLD events. *PloS one*, *10*(4), e0124577.

Allegra, M., Favaretto, C., Metcalf, N., Corbetta, M., & Brovelli, A. (2021). Stroke-related alterations in inter-areal communication. *NeuroImage: Clinical*, *32*, 102812.

Alstott, J., Breakspear, M., Hagmann, P., Cammoun, L., & Sporns, O. (2009). Modeling the impact of lesions in the human brain. *PLoS computational biology*, *5*(6), e1000408.

Arnemann, K. L., Chen, A. J.-W., Novakovic-Agopian, T., Gratton, C., Nomura, E. M., & D'Esposito, M. (2015). Functional brain network modularity predicts response to cognitive training after brain injury. *Neurology*, *84*(15), 1568-1574.

Baldassarre, A., Ramsey, L., Rengachary, J., Zinn, K., Siegel, J. S., Metcalf, N. V., Strube, M. J., Snyder, A. Z., Corbetta, M., & Shulman, G. L. (2016). Dissociated functional connectivity profiles for motor and attention deficits in acute right-hemisphere stroke. *Brain*, *139*(7), 2024-2038.

Bassett, D. S., & Sporns, O. (2017). Network neuroscience. *Nat Neurosci*, *20*(3), 353-364. https://doi.org/10.1038/nn.4502

Bassett, D. S., Wymbs, N. F., Porter, M. A., Mucha, P. J., Carlson, J. M., & Grafton, S. T. (2011). Dynamic reconfiguration of human brain networks during learning. *Proc Natl Acad Sci U S A*, *108*(18), 7641-7646. https://doi.org/10.1073/pnas.1018985108

Bates, E., Reilly, J., Wulfeck, B., Dronkers, N., Opie, M., Fenson, J., Kriz, S., Jeffries, R., Miller, L., & Herbst, K. (2001). Differential effects of unilateral lesions on language production in children and adults. *Brain and language*, *79*(2), 223-265.

Bayrak, Ş., Khalil, A. A., Villringer, K., Fiebach, J. B., Villringer, A., Margulies, D. S., & Ovadia-Caro, S. (2019). The impact of ischemic stroke on connectivity gradients. *NeuroImage: Clinical*, *24*, 101947.

Betzel, R., Cutts, S., Greenwell, S., & Sporns, O. (2021). Individualized event structure drives individual differences in whole-brain functional connectivity. *bioRxiv*.

Betzel, R. F., Byrge, L., Esfahlani, F. Z., & Kennedy, D. P. (2020). Temporal fluctuations in the brain's modular architecture during movie-watching. *Neuroimage*, *213*, 116687.

Blicher, J. U., Stagg, C. J., O'shea, J., Østergaard, L., MacIntosh, B. J., Johansen-Berg, H., Jezzard, P., & Donahue, M. J. (2012). Visualization of altered neurovascular coupling in chronic stroke patients using multimodal functional MRI. *Journal of Cerebral Blood Flow & Metabolism*, *32*(11), 2044-2054.

Boes, C. J. (2015). History of neurologic examination books. Baylor University Medical Center Proceedings,

Bolt, T., Nomi, J. S., Bzdok, D., Salas, J. A., Chang, C., Thomas Yeo, B., Uddin, L. Q., & Keilholz, S. D. (2022). A parsimonious description of global functional brain organization in three spatiotemporal patterns. *Nature neuroscience*, *25*(8), 1093-1103.

Bowren, M., Bruss, J., Manzel, K., Edwards, D., Liu, C., Corbetta, M., Tranel, D., & Boes, A. D. (2022). Post-stroke outcomes predicted from multivariate lesion-behaviour and lesion network mapping. *Brain*.

Breiman, L. (2001). Random forests. *Machine learning*, *45*(1), 5-32.

Broca, P. (1861). Remarques sur le siège de la faculté du langage articulé, suivies d'une observation d'aphémie (perte de la parole). *Bulletin et Memoires de la Societe anatomique de Paris*, *6*, 330-357.

Brott, T., Adams, H. P., Jr., Olinger, C. P., Marler, J. R., Barsan, W. G., Biller, J., Spilker, J., Holleran, R., Eberle, R., Hertzberg, V., & et al. (1989). Measurements of acute cerebral infarction: a clinical examination scale. *Stroke*, *20*(7), 864-870. https://doi.org/10.1161/01.str.20.7.864

Bullmore, E., & Sporns, O. (2009). Complex brain networks: graph theoretical analysis of structural and functional systems. *Nature reviews neuroscience*, *10*(3), 186-198.

Cabral, J., Hugues, E., Kringelbach, M. L., & Deco, G. (2012). Modeling the outcome of structural disconnection on resting-state functional connectivity. *Neuroimage*, *62*(3), 1342-1353.

Cabral, J., Kringelbach, M. L., & Deco, G. (2017). Functional connectivity dynamically evolves on multiple time-scales over a static structural connectome: Models and mechanisms. *Neuroimage*, *160*, 84-96.

Cabral, J., Vidaurre, D., Marques, P., Magalhães, R., Silva Moreira, P., Miguel Soares, J., Deco, G., Sousa, N., & Kringelbach, M. L. (2017). Cognitive performance in healthy older adults relates to spontaneous switching between states of functional connectivity during rest. *Scientific reports*, *7*(1), 1-13.

Calesella, F., Testolin, A., De Filippo De Grazia, M., & Zorzi, M. (2021). A comparison of feature extraction methods for prediction of neuropsychological scores from functional connectivity data of stroke patients. *Brain informatics*, *8*(1), 1-13.

Capouskova, K., Kringelbach, M. L., & Deco, G. (2022). Modes of cognition: Evidence from metastable brain dynamics. *Neuroimage*, *260*, 119489.

Carrera, E., & Tononi, G. (2014). Diaschisis: past, present, future. *Brain*, *137*(9), 2408-2422.

Chen, C., Yuan, K., Chu, W. C.-w., & Tong, R. K.-y. (2021). The effects of 10 Hz and 20 Hz tACS in network integration and segregation in chronic stroke: a graph theoretical fMRI study. *Brain Sciences*, *11*(3), 377.

Chumin, E. J., Faskowitz, J., Esfahlani, F. Z., Jo, Y., Merritt, H. L., Tanner, J. C., Cutts, S. A., Pope, M. E., Sporns, O., & Betzel, R. (2021).

Cortico-Subcortical Interactions in Overlapping Communities of Edge Functional Connectivity. *bioRxiv*.

Cifre, I., Zarepour, M., Horovitz, S., Cannas, S. A., & Chialvo, D. R. (2020). Further results on why a point process is effective for estimating correlation between brain regions. *Papers in physics*, *12*, 120003-120003.

Cofré, R., Herzog, R., Mediano, P. A., Piccinini, J., Rosas, F. E., Sanz Perl, Y., & Tagliazucchi, E. (2020). Whole-brain models to explore altered states of consciousness from the bottom up. *Brain Sciences*, *10*(9), 626.

Coletta, L., Pagani, M., Whitesell, J. D., Harris, J. A., Bernhardt, B., & Gozzi, A. (2020). Network structure of the mouse brain connectome with voxel resolution. *Science Advances*, *6*(51), eabb7187.

Corbetta, M., Ramsey, L., Callejas, A., Baldassarre, A., Hacker, C. D., Siegel, J. S., Astafiev, S. V., Rengachary, J., Zinn, K., & Lang, C. E. (2015). Common behavioral clusters and subcortical anatomy in stroke. *Neuron*, *85*(5), 927-941.

Corbetta, M., Siegel, J. S., & Shulman, G. L. (2018). On the low dimensionality of behavioral deficits and alterations of brain network connectivity after focal injury. *Cortex*, *107*, 229-237. https://doi.org/10.1016/j.cortex.2017.12.017

Crofts, J. J., Higham, D. J., Bosnell, R., Jbabdi, S., Matthews, P. M., Behrens, T., & Johansen-Berg, H. (2011). Network analysis detects changes in the contralesional hemisphere following stroke. *Neuroimage*, *54*(1), 161-169.

Cunningham, J. P., & Yu, B. M. (2014). Dimensionality reduction for large-scale neural recordings. *Nature neuroscience*, *17*(11), 1500-1509.

Davison, E. N., Schlesinger, K. J., Bassett, D. S., Lynall, M.-E., Miller, M. B., Grafton, S. T., & Carlson, J. M. (2015). Brain network adaptability across task states. *PLoS computational biology*, *11*(1), e1004029.

De Filippi, E., Wolter, M., Melo, B. R., Tierra-Criollo, C. J., Bortolini, T., Deco, G., & Moll, J. (2021). Classification of complex emotions using EEG and virtual environment: proof of concept and therapeutic implication. *Frontiers in human neuroscience*, *15*.

Deco, G., Cruzat, J., Cabral, J., Tagliazucchi, E., Laufs, H., Logothetis, N. K., & Kringelbach, M. L. (2019). Awakening: Predicting external stimulation to force transitions between different brain states. *Proceedings of the National Academy of Sciences*, *116*(36), 18088-18097. https://www.ncbi.nlm.nih.gov/pmc/articles/PMC6731634/pdf/pnas.201905534.pdf

Deco, G., Hagmann, P., Hudetz, A. G., & Tononi, G. (2014). Modeling resting-state functional networks when the cortex falls asleep: local and global changes. *Cerebral Cortex*, *24*(12), 3180-3194.

Deco, G., & Jirsa, V. K. (2012). Ongoing cortical activity at rest: criticality, multistability, and ghost attractors. *Journal of Neuroscience*, *32*(10), 3366-3375.
Deco, G., Jirsa, V. K., & McIntosh, A. R. (2011). Emerging concepts for the dynamical organization of resting-state activity in the brain. *Nature reviews neuroscience*, *12*(1), 43-56.
Deco, G., & Kringelbach, M. L. (2016). Metastability and coherence: extending the communication through coherence hypothesis using a whole-brain computational perspective. *Trends in neurosciences*, *39*(3), 125-135.
Deco, G., Kringelbach, M. L., Jirsa, V. K., & Ritter, P. (2017). The dynamics of resting fluctuations in the brain: metastability and its dynamical cortical core. *Scientific reports*, *7*(1), 1-14.
Deco, G., Lynn, C., Perl, Y. S., & Kringelbach, M. L. (2023). Violations of the fluctuation-dissipation theorem reveal distinct non-equilibrium dynamics of brain states. *arXiv preprint arXiv:2304.07027*.
Deco, G., Perl, Y. S., Sitt, J. D., Tagliazucchi, E., & Kringelbach, M. L. (2021). Deep learning the arrow of time in brain activity: characterising brain-environment behavioural interactions in health and disease. *bioRxiv*.
Deco, G., Ponce-Alvarez, A., Hagmann, P., Romani, G. L., Mantini, D., & Corbetta, M. (2014). How local excitation–inhibition ratio impacts the whole brain dynamics. *Journal of Neuroscience*, *34*(23), 7886-7898.
Deco, G., Sanz Perl, Y., Bocaccio, H., Tagliazucchi, E., & Kringelbach, M. L. (2022). The INSIDEOUT framework provides precise signatures of the balance of intrinsic and extrinsic dynamics in brain states. *Communications Biology*, *5*(1), 1-13.
Deco, G., Tononi, G., Boly, M., & Kringelbach, M. L. (2015). Rethinking segregation and integration: contributions of whole-brain modelling. *Nature reviews neuroscience*, *16*(7), 430-439.
Dubreuil, A., Valente, A., Beiran, M., Mastrogiuseppe, F., & Ostojic, S. (2020). Complementary roles of dimensionality and population structure in neural computations. *bioRxiv*.
Faskowitz, J., Esfahlani, F. Z., Jo, Y., Sporns, O., & Betzel, R. F. (2020). Edge-centric functional network representations of human cerebral cortex reveal overlapping system-level architecture. *Nat Neurosci*, *23*(12), 1644-1654. https://doi.org/10.1038/s41593-020-00719-y
Faskowitz, J., Yan, X., Zuo, X. N., & Sporns, O. (2018). Weighted Stochastic Block Models of the Human Connectome across the Life Span. *Sci Rep*, *8*(1), 12997. https://doi.org/10.1038/s41598-018-31202-1
Favaretto, C. A., Michele; Deco, Gustavo; Metcalf, Nicholas; Griffis, Joseph; Shulman, Gordon; Brovelli, Andrea; Corbetta, Maurizio. (2022). Subcortical-cortical dynamical states of the human brain and their breakdown in stroke. *Nature communications*, *13*.

Firat, O., Aksan, E., Oztekin, I., & Yarman Vural, F. T. (2015). Learning deep temporal representations for fMRI brain decoding. Medical Learning Meets Medical Imaging,
Foulon, C., Cerliani, L., Kinkingnehun, S., Levy, R., Rosso, C., Urbanski, M., Volle, E., & Thiebaut de Schotten, M. (2018). Advanced lesion symptom mapping analyses and implementation as BCBtoolkit. *Gigascience*, *7*(3), giy004.
Fox, M. D., & Alterman, R. L. (2015). Brain stimulation for torsion dystonia. *JAMA neurology*, *72*(6), 713-719.
Friston, K. J. (2011). Functional and effective connectivity: a review. *Brain connectivity*, *1*(1), 13-36.
Friston, K. J., Harrison, L., & Penny, W. (2003). Dynamic causal modelling. *Neuroimage*, *19*(4), 1273-1302.
Fukushima, M., Betzel, R. F., He, Y., van den Heuvel, M. P., Zuo, X.-N., & Sporns, O. (2018). Structure–function relationships during segregated and integrated network states of human brain functional connectivity. *Brain Structure and Function*, *223*(3), 1091-1106.
Gilson, M., Moreno-Bote, R., Ponce-Alvarez, A., Ritter, P., & Deco, G. (2016). Estimation of directed effective connectivity from fMRI functional connectivity hints at asymmetries of cortical connectome. *PLoS computational biology*, *12*(3), e1004762.
Govindarajan, P., Soundarapandian, R. K., Gandomi, A. H., Patan, R., Jayaraman, P., & Manikandan, R. (2020). Classification of stroke disease using machine learning algorithms. *Neural Computing and Applications*, *32*(3), 817-828.
Gratton, C., Nomura, E. M., Pérez, F., & D'Esposito, M. (2012). Focal brain lesions to critical locations cause widespread disruption of the modular organization of the brain. *Journal of cognitive neuroscience*, *24*(6), 1275-1285.
Greenwell, S., Faskowitz, J., Pritschet, L., Santander, T., Jacobs, E. G., & Betzel, R. F. (2021). High-amplitude network co-fluctuations linked to variation in hormone concentrations over menstrual cycle. *bioRxiv*.
Griffis, J. C., Metcalf, N. V., Corbetta, M., & Shulman, G. L. (2019). Structural disconnections contribute to lesion-induced brain functional connectivity disruptions via direct and indirect mechanisms. *bioRxiv*, 785576.
Griffis, J. C., Metcalf, N. V., Corbetta, M., & Shulman, G. L. (2019). Structural Disconnections Explain Brain Network Dysfunction after Stroke. *Cell Rep*, *28*(10), 2527-2540 e2529. https://doi.org/10.1016/j.celrep.2019.07.100
Griffis, J. C., Metcalf, N. V., Corbetta, M., & Shulman, G. L. (2020). Damage to the shortest structural paths between brain regions is associated with disruptions of resting-state functional connectivity after stroke. *Neuroimage*, *210*, 116589.
Griffis, J. C., Metcalf, N. V., Corbetta, M., & Shulman, G. L. (2021). Lesion Quantification Toolkit: A MATLAB software tool for estimating grey

matter damage and white matter disconnections in patients with focal brain lesions. *Neuroimage Clin*, *30*, 102639. https://doi.org/10.1016/j.nicl.2021.102639

Hama, S., Yoshimura, K., Yanagawa, A., Shimonaga, K., Furui, A., Soh, Z., Nishino, S., Hirano, H., Yamawaki, S., & Tsuji, T. (2020). Relationships between motor and cognitive functions and subsequent post-stroke mood disorders revealed by machine learning analysis. *Scientific reports*, *10*(1), 1-10.

Han, X., Jin, H., Li, K., Ning, Y., Jiang, L., Chen, P., Liu, H., Zhang, Y., Zhang, H., & Tan, Z. (2020). Acupuncture Modulates Disrupted Whole-Brain Network after Ischemic Stroke: Evidence Based on Graph Theory Analysis. *Neural Plasticity*, *2020*.

Han, X., Zhong, Y., He, L., Yu, P. S., & Zhang, L. (2015). The unsupervised hierarchical convolutional sparse auto-encoder for neuroimaging data classification. International Conference on Brain Informatics and Health,

He, B. J., Snyder, A. Z., Vincent, J. L., Epstein, A., Shulman, G. L., & Corbetta, M. (2007). Breakdown of functional connectivity in frontoparietal networks underlies behavioral deficits in spatial neglect. *Neuron*, *53*(6), 905-918.

Hejazi, M., & Nasrabadi, A. M. (2019). Prediction of epilepsy seizure from multi-channel electroencephalogram by effective connectivity analysis using Granger causality and directed transfer function methods. *Cognitive neurodynamics*, *13*(5), 461-473.

Honey, C. J., Kötter, R., Breakspear, M., & Sporns, O. (2007). Network structure of cerebral cortex shapes functional connectivity on multiple time scales. *Proceedings of the National Academy of Sciences*, *104*(24), 10240-10245.

Honey, C. J., Sporns, O., Cammoun, L., Gigandet, X., Thiran, J. P., Meuli, R., & Hagmann, P. (2009). Predicting human resting-state functional connectivity from structural connectivity. *Proc Natl Acad Sci U S A*, *106*(6), 2035-2040. https://doi.org/10.1073/pnas.0811168106

Hotelling, H. (1957). The relations of the newer multivariate statistical methods to factor analysis. *British Journal of Statistical Psychology*, *10*(2), 69-79.

Huang, D., Abdel-Khalik, H., Rabiti, C., & Gleicher, F. (2017). Dimensionality reducibility for multi-physics reduced order modeling. *Annals of Nuclear Energy*, *110*, 526-540.

Humphries, M. D. (2020). Strong and weak principles of neural dimension reduction. *arXiv preprint arXiv:2011.08088*.

Idesis, S., Faskowitz, J., Betzel, R. F., Corbetta, M., Sporns, O., & Deco, G. (2022). Edge-centric analysis of stroke patients: An alternative approach for biomarkers of lesion recovery. *NeuroImage: Clinical*, 103055.

Idesis, S., Favaretto, C., Metcalf, N. V., Griffis, J. C., Shulman, G. L., Corbetta, M., & Deco, G. (2022). Inferring the dynamical effects of

stroke lesions through whole-brain modeling. *NeuroImage: Clinical*, 103233.
IRIARTE, D. (2022). A deep learning approach for feature extraction from resting state functional connectivity of stroke patients and prediction of neuropsychological scores.
Jeub, L. G., Sporns, O., & Fortunato, S. (2018). Multiresolution consensus clustering in networks. *Scientific reports*, *8*(1), 1-16.
Jo, Y., Esfahlani, F. Z., Faskowitz, J., Chumin, E. J., Sporns, O., & Betzel, R. F. (2021). The diversity and multiplexity of edge communities within and between brain systems. *Cell reports*, *37*(7), 110032.
Jo, Y., Faskowitz, J., Esfahlani, F. Z., Sporns, O., & Betzel, R. F. (2021). Subject identification using edge-centric functional connectivity. *Neuroimage*, 118204.
Jobst, B. M., Hindriks, R., Laufs, H., Tagliazucchi, E., Hahn, G., Ponce-Alvarez, A., Stevner, A. B. A., Kringelbach, M. L., & Deco, G. (2017). Increased Stability and Breakdown of Brain Effective Connectivity During Slow-Wave Sleep: Mechanistic Insights from Whole-Brain Computational Modelling. *Scientific reports*, *7*(1), 4634. https://doi.org/10.1038/s41598-017-04522-x
Karahanoglu, F. I., & Van De Ville, D. (2015). Transient brain activity disentangles fMRI resting-state dynamics in terms of spatially and temporally overlapping networks. *Nat Commun*, *6*, 7751. https://doi.org/10.1038/ncomms8751
Karnath, H.-O., Sperber, C., & Rorden, C. (2018). Mapping human brain lesions and their functional consequences. *Neuroimage*, *165*, 180-189.
Kerr, J. N., & Denk, W. (2008). Imaging in vivo: watching the brain in action. *Nature reviews neuroscience*, *9*(3), 195-205.
Khosla, M., Jamison, K., Ngo, G. H., Kuceyeski, A., & Sabuncu, M. R. (2019). Machine learning in resting-state fMRI analysis. *Magnetic resonance imaging*, *64*, 101-121.
Kringelbach, M. L., Cruzat, J., Cabral, J., Knudsen, G. M., Carhart-Harris, R., Whybrow, P. C., Logothetis, N. K., & Deco, G. (2020). Dynamic coupling of whole-brain neuronal and neurotransmitter systems. *Proceedings of the National Academy of Sciences*, *117*(17), 9566-9576.
Kringelbach, M. L., McIntosh, A. R., Ritter, P., Jirsa, V. K., & Deco, G. (2015). The rediscovery of slowness: exploring the timing of cognition. *Trends in cognitive sciences*, *19*(10), 616-628.
Krishnan, A., Williams, L. J., McIntosh, A. R., & Abdi, H. (2011). Partial Least Squares (PLS) methods for neuroimaging: a tutorial and review. *Neuroimage*, *56*(2), 455-475.
Kuznetsov, Y. A. (1998). Elements of applied bifurcation theory. *Applied mathematical sciences*, *112*, 591.
Latora, V., & Marchiori, M. (2001). Efficient behavior of small-world networks. *Physical review letters*, *87*(19), 198701.

Liégeois, R., Santos, A., Matta, V., Van De Ville, D., & Sayed, A. H. (2020). Revisiting correlation-based functional connectivity and its relationship with structural connectivity. *Network Neuroscience*, *4*(4), 1235-1251.
Lin, W., Hao, Q., Rosengarten, B., Leung, W., & Wong, K. (2011). Impaired neurovascular coupling in ischaemic stroke patients with large or small vessel disease. *European Journal of Neurology*, *18*(5), 731-736.
Lin, Y.-K., Lee, C.-Y., & Chen, C.-Y. (2022). Robustness of autoencoders for establishing psychometric properties based on small sample sizes: results from a Monte Carlo simulation study and a sports fan curiosity study. *PeerJ Computer Science*, *8*, e782.
Liu, X., & Duyn, J. H. (2013). Time-varying functional network information extracted from brief instances of spontaneous brain activity. *Proc Natl Acad Sci U S A*, *110*(11), 4392-4397. https://doi.org/10.1073/pnas.1216856110
Liu, Z.-Q., Vázquez-Rodríguez, B., Spreng, R. N., Bernhardt, B. C., Betzel, R. F., & Misic, B. (2021). Time-resolved structure-function coupling in brain networks. *bioRxiv*.
Lynn, C. W., Cornblath, E. J., Papadopoulos, L., Bertolero, M. A., & Bassett, D. S. (2021). Broken detailed balance and entropy production in the human brain. *Proceedings of the National Academy of Sciences*, *118*(47), e2109889118.
Manning-Dahan, T. (2018). PCA and Autoencoders. *Montreal: Concordia University, INSE*, *6220*.
Margulies, D. S., Ghosh, S. S., Goulas, A., Falkiewicz, M., Huntenburg, J. M., Langs, G., Bezgin, G., Eickhoff, S. B., Castellanos, F. X., & Petrides, M. (2016). Situating the default-mode network along a principal gradient of macroscale cortical organization. *Proceedings of the National Academy of Sciences*, *113*(44), 12574-12579.
Mesulam, M. M. (1981). A cortical network for directed attention and unilateral neglect. *Annals of Neurology: Official Journal of the American Neurological Association and the Child Neurology Society*, *10*(4), 309-325.
Meunier, D., Lambiotte, R., & Bullmore, E. T. (2010). Modular and hierarchically modular organization of brain networks. *Frontiers in neuroscience*, *4*, 200.
Mitra, A., & Raichle, M. E. (2016). How networks communicate: propagation patterns in spontaneous brain activity. *Philosophical Transactions of the Royal Society B: Biological Sciences*, *371*(1705), 20150546.
Mitra, A., Snyder, A. Z., Hacker, C. D., Pahwa, M., Tagliazucchi, E., Laufs, H., Leuthardt, E. C., & Raichle, M. E. (2016). Human cortical–hippocampal dialogue in wake and slow-wave sleep. *Proceedings of the National Academy of Sciences*, *113*(44), E6868-E6876.

Newman, M. E., & Girvan, M. (2004). Finding and evaluating community structure in networks. *Phys Rev E Stat Nonlin Soft Matter Phys*, *69*(2 Pt 2), 026113. https://doi.org/10.1103/PhysRevE.69.026113
Novelli, L., & Razi, A. (2021). A mathematical perspective on edge-centric functional connectivity. *arXiv preprint arXiv:2106.10631*.
Olafson, E. R., Jamison, K. W., Sweeney, E. M., Liu, H., Wang, D., Bruss, J. E., Boes, A. D., & Kuceyeski, A. (2021). Functional connectome reorganization relates to post-stroke motor recovery and structural and functional disconnection. *Neuroimage*, *245*, 118642. https://doi.org/10.1016/j.neuroimage.2021.118642
Ovadia-Caro, S., Villringer, K., Fiebach, J., Jungehulsing, G. J., Van Der Meer, E., Margulies, D. S., & Villringer, A. (2013). Longitudinal effects of lesions on functional networks after stroke. *Journal of Cerebral Blood Flow & Metabolism*, *33*(8), 1279-1285.
Pallarés, V., Insabato, A., Sanjuán, A., Kühn, S., Mantini, D., Deco, G., & Gilson, M. (2018). Extracting orthogonal subject-and condition-specific signatures from fMRI data using whole-brain effective connectivity. *Neuroimage*, *178*, 238-254.
Pang, R., Lansdell, B. J., & Fairhall, A. L. (2016). Dimensionality reduction in neuroscience. *Current Biology*, *26*(14), R656-R660.
Park, H.-J., & Friston, K. (2013). Structural and functional brain networks: from connections to cognition. *Science*, *342*(6158).
Park, H. J., & Friston, K. (2013). Structural and functional brain networks: from connections to cognition. *Science*, *342*(6158), 1238411. https://doi.org/10.1126/science.1238411
Perl, Y. S., Bocaccio, H., Pallavicini, C., Pérez-Ipiña, I., Laureys, S., Laufs, H., Kringelbach, M., Deco, G., & Tagliazucchi, E. (2021). Nonequilibrium brain dynamics as a signature of consciousness. *Physical Review E*, *104*(1), 014411.
Petridou, N., Gaudes, C. C., Dryden, I. L., Francis, S. T., & Gowland, P. A. (2013). Periods of rest in fMRI contain individual spontaneous events which are related to slowly fluctuating spontaneous activity. *Human brain mapping*, *34*(6), 1319-1329.
Piccinini, J., Deco, G., Kringelbach, M. L., Laufs, H., Perl, Y. S., & Tagliazucchi, E. (2022). Data-driven discovery of canonical large-scale brain dynamics. *bioRxiv*.
Pini, L., Salvalaggio, A., De Filippo De Grazia, M., Zorzi, M., Thiebaut de Schotten, M., & Corbetta, M. (2021). A novel stroke lesion network mapping approach: improved accuracy yet still low deficit prediction. *Brain communications*, *3*(4), fcab259.
Pope, M., Fukushima, M., Betzel, R., & Sporns, O. (2021). Modular origins of high-amplitude co-fluctuations in fine-scale functional connectivity dynamics. *bioRxiv*.
Power, J. D., Cohen, A. L., Nelson, S. M., Wig, G. S., Barnes, K. A., Church, J. A., Vogel, A. C., Laumann, T. O., Miezin, F. M., & Schlaggar, B. L.

(2011). Functional network organization of the human brain. *Neuron*, *72*(4), 665-678.
Power, J. D., Schlaggar, B. L., Lessov-Schlaggar, C. N., & Petersen, S. E. (2013). Evidence for hubs in human functional brain networks. *Neuron*, *79*(4), 798-813.
Praveen, G., Agrawal, A., Sundaram, P., & Sardesai, S. (2018). Ischemic stroke lesion segmentation using stacked sparse autoencoder. *Computers in biology and medicine*, *99*, 38-52.
Pustina, D., Coslett, H. B., Ungar, L., Faseyitan, O. K., Medaglia, J. D., Avants, B., & Schwartz, M. F. (2017). Enhanced estimations of post-stroke aphasia severity using stacked multimodal predictions. *Human brain mapping*, *38*(11), 5603-5615.
Rabuffo, G., Fousek, J., Bernard, C., & Jirsa, V. (2021). Neuronal cascades shape whole-brain functional dynamics at rest. *bioRxiv*, 2020.2012. 2025.424385.
Ramsey, L., Siegel, J., Lang, C., Strube, M., Shulman, G., & Corbetta, M. (2017). Behavioural clusters and predictors of performance during recovery from stroke. *Nature Human Behaviour*, *1*(3), 0038.
Raut, R. V., Snyder, A. Z., & Raichle, M. E. (2020). Hierarchical dynamics as a macroscopic organizing principle of the human brain. *Proceedings of the National Academy of Sciences*, *117*(34), 20890-20897.
Reber, J., Hwang, K., Bowren, M., Bruss, J., Mukherjee, P., Tranel, D., & Boes, A. D. (2021). Cognitive impairment after focal brain lesions is better predicted by damage to structural than functional network hubs. *Proceedings of the National Academy of Sciences*, *118*(19).
Rocha, R. P., Koçillari, L., Suweis, S., De Filippo De Grazia, M., de Schotten, M. T., Zorzi, M., & Corbetta, M. (2022). Recovery of neural dynamics criticality in personalized whole-brain models of stroke. *Nature communications*, *13*(1), 3683.
Rubinov, M., & Sporns, O. (2010). Complex network measures of brain connectivity: uses and interpretations. *Neuroimage*, *52*(3), 1059-1069. https://doi.org/10.1016/j.neuroimage.2009.10.003
Rubinov, M., & Sporns, O. (2011). Weight-conserving characterization of complex functional brain networks. *Neuroimage*, *56*(4), 2068-2079. https://doi.org/10.1016/j.neuroimage.2011.03.069
Russo, S., Pigorini, A., Mikulan, E., Sarasso, S., Rubino, A., Zauli, F. M., Parmigiani, S., d'Orio, P., Cattani, A., & Francione, S. (2021). Focal lesions induce large-scale percolation of sleep-like intracerebral activity in awake humans. *Neuroimage*, *234*, 117964.
Saenger, V. M., Ponce-Alvarez, A., Adhikari, M., Hagmann, P., Deco, G., & Corbetta, M. (2018). Linking Entropy at Rest with the Underlying Structural Connectivity in the Healthy and Lesioned Brain. *Cerebral Cortex*, *28*(8), 2948-2958. https://doi.org/10.1093/cercor/bhx176
Salvalaggio, A., De Filippo De Grazia, M., Zorzi, M., Thiebaut de Schotten, M., & Corbetta, M. (2020). Post-stroke deficit prediction from lesion

and indirect structural and functional disconnection. *Brain*, *143*(7), 2173-2188.
Sanz Perl, Y., Escrichs, A., Tagliazucchi, E., Kringelbach, M. L., & Deco, G. (2022). Strength-dependent perturbation of whole-brain model working in different regimes reveals the role of fluctuations in brain dynamics. *PLoS computational biology*, *18*(11), e1010662.
Sanz Perl, Y., Pallavicini, C., Pérez Ipiña, I., Demertzi, A., Bonhomme, V., Martial, C., Panda, R., Annen, J., Ibañez, A., & Kringelbach, M. (2021). Perturbations in dynamical models of whole-brain activity dissociate between the level and stability of consciousness. *PLoS computational biology*, *17*(7), e1009139.
Sarasso, S., D'Ambrosio, S., Fecchio, M., Casarotto, S., Viganò, A., Landi, C., Mattavelli, G., Gosseries, O., Quarenghi, M., & Laureys, S. (2020). Local sleep-like cortical reactivity in the awake brain after focal injury. *Brain*, *143*(12), 3672-3684.
Schaefer, A., Kong, R., Gordon, E. M., Laumann, T. O., Zuo, X. N., Holmes, A. J., Eickhoff, S. B., & Yeo, B. T. T. (2018). Local-Global Parcellation of the Human Cerebral Cortex from Intrinsic Functional Connectivity MRI. *Cereb Cortex*, *28*(9), 3095-3114. https://doi.org/10.1093/cercor/bhx179
Schuessler, F., Mastrogiuseppe, F., Dubreuil, A., Ostojic, S., & Barak, O. (2020). The interplay between randomness and structure during learning in RNNs. *Advances in neural information processing systems*, *33*, 13352-13362.
Senden, M., Reuter, N., van den Heuvel, M. P., Goebel, R., & Deco, G. (2017). Cortical rich club regions can organize state-dependent functional network formation by engaging in oscillatory behavior. *Neuroimage*, *146*, 561-574.
Shalev-Shwartz, S., & Ben-David, S. (2014). *Understanding machine learning: From theory to algorithms*. Cambridge university press.
Shanthi, D., Sahoo, G., & Saravanan, N. (2009). Designing an artificial neural network model for the prediction of thrombo-embolic stroke. *International Journals of Biometric and Bioinformatics (IJBB)*, *3*(1), 10-18.
Shinn, M., Romero-Garcia, R., Seidlitz, J., Vasa, F., Vertes, P. E., & Bullmore, E. (2017). Versatility of nodal affiliation to communities. *Sci Rep*, *7*(1), 4273. https://doi.org/10.1038/s41598-017-03394-5
Siegel, J. S., Ramsey, L. E., Snyder, A. Z., Metcalf, N. V., Chacko, R. V., Weinberger, K., Baldassarre, A., Hacker, C. D., Shulman, G. L., & Corbetta, M. (2016). Disruptions of network connectivity predict impairment in multiple behavioral domains after stroke. *Proc Natl Acad Sci U S A*, *113*(30), E4367-4376. https://doi.org/10.1073/pnas.1521083113
Siegel, J. S., Seitzman, B. A., Ramsey, L. E., Ortega, M., Gordon, E. M., Dosenbach, N. U. F., Petersen, S. E., Shulman, G. L., & Corbetta, M. (2018). Re-emergence of modular brain networks in stroke

recovery. *Cortex*, *101*, 44-59. https://doi.org/10.1016/j.cortex.2017.12.019
Silasi, G., & Murphy, T. H. (2014). Stroke and the connectome: how connectivity guides therapeutic intervention. *Neuron*, *83*(6), 1354-1368.
Singh, M. S., & Choudhary, P. (2017). Stroke prediction using artificial intelligence. 2017 8th Annual Industrial Automation and Electromechanical Engineering Conference (IEMECON),
Sperber, C., & Karnath, H.-O. (2018). On the validity of lesion-behaviour mapping methods. *Neuropsychologia*, *115*, 17-24.
Sporns, O. (2013). Network attributes for segregation and integration in the human brain. *Current opinion in neurobiology*, *23*(2), 162-171.
Sporns, O. (2014). Contributions and challenges for network models in cognitive neuroscience. *Nature neuroscience*, *17*(5), 652-660.
Sporns, O., Faskowitz, J., Teixeira, A. S., Cutts, S. A., & Betzel, R. F. (2021). Dynamic expression of brain functional systems disclosed by fine-scale analysis of edge time series. *Network Neuroscience*, *5*(2), 405-433.
Sporns, O., Honey, C. J., & Kotter, R. (2007). Identification and classification of hubs in brain networks. *PLoS One*, *2*(10), e1049. https://doi.org/10.1371/journal.pone.0001049
Sprigg, N., Gray, L. J., Bath, P. M., Lindenstrøm, E., Boysen, G., De Deyn, P. P., Friis, P., Leys, D., Marttila, R., & Olsson, J.-E. (2007). Stroke severity, early recovery and outcome are each related with clinical classification of stroke: data from the 'Tinzaparin in Acute Ischaemic Stroke Trial'(TAIST). *Journal of the neurological sciences*, *254*(1-2), 54-59.
Sudha, A., Gayathri, P., & Jaisankar, N. (2012). Effective analysis and predictive model of stroke disease using classification methods. *International Journal of Computer Applications*, *43*(14), 26-31.
Sun, J., Wang, D., Chen, S., Pang, R., Liu, H., Wang, J., Zhang, Y., Wang, C., & Yang, A. (2021). The behavioral significance of resting state network after stroke: A study via graph theory analysis with near-infrared spectroscopy. *Medicine in Novel Technology and Devices*, *11*, 100083.
Tagliazucchi, E., Balenzuela, P., Fraiman, D., & Chialvo, D. R. (2012). Criticality in large-scale brain FMRI dynamics unveiled by a novel point process analysis. *Front Physiol*, *3*, 15. https://doi.org/10.3389/fphys.2012.00015
Tagliazucchi, E., Von Wegner, F., Morzelewski, A., Brodbeck, V., & Laufs, H. (2012). Dynamic BOLD functional connectivity in humans and its electrophysiological correlates. *Frontiers in human neuroscience*, *6*, 339.
Tononi, G., Sporns, O., & Edelman, G. M. (1994). A measure for brain complexity: relating functional segregation and integration in the

nervous system. *Proceedings of the National Academy of Sciences*, *91*(11), 5033-5037.
Traag, V. A., Van Dooren, P., & Nesterov, Y. (2011). Narrow scope for resolution-limit-free community detection. *Physical review E*, *84*(1), 016114.
Tsang, A., Lebel, C. A., Bray, S. L., Goodyear, B. G., Hafeez, M., Sotero, R. C., McCreary, C. R., & Frayne, R. (2017). White matter structural connectivity is not correlated to cortical resting-state functional connectivity over the healthy adult lifespan. *Frontiers in aging neuroscience*, 144.
Tzourio-Mazoyer, N., Landeau, B., Papathanassiou, D., Crivello, F., Etard, O., Delcroix, N., Mazoyer, B., & Joliot, M. (2002). Automated anatomical labeling of activations in SPM using a macroscopic anatomical parcellation of the MNI MRI single-subject brain. *Neuroimage*, *15*(1), 273-289.
van den Heuvel, M. P., & Sporns, O. (2013). Network hubs in the human brain. *Trends in cognitive sciences*, *17*(12), 683-696.
Van der Maaten, L., & Hinton, G. (2008). Visualizing data using t-SNE. *Journal of machine learning research*, *9*(11).
van Oort, E. S., Mennes, M., Schröder, T. N., Kumar, V. J., Jimenez, N. I. Z., Grodd, W., Doeller, C. F., & Beckmann, C. F. (2018). Functional parcellation using time courses of instantaneous connectivity. *Neuroimage*, *170*, 31-40.
Vattikonda, A., Surampudi, B. R., Banerjee, A., Deco, G., & Roy, D. (2016). Does the regulation of local excitation–inhibition balance aid in recovery of functional connectivity? A computational account. *Neuroimage*, *136*, 57-67.
Vecchio, F., Caliandro, P., Reale, G., Miraglia, F., Piludu, F., Masi, G., Iacovelli, C., Simbolotti, C., Padua, L., & Leone, E. (2019). Acute cerebellar stroke and middle cerebral artery stroke exert distinctive modifications on functional cortical connectivity: A comparative study via EEG graph theory. *Clinical Neurophysiology*, *130*(6), 997-1007.
Vecchio, F., Tomino, C., Miraglia, F., Iodice, F., Erra, C., Di Iorio, R., Judica, E., Alù, F., Fini, M., & Rossini, P. M. (2019). Cortical connectivity from EEG data in acute stroke: A study via graph theory as a potential biomarker for functional recovery. *International Journal of Psychophysiology*, *146*, 133-138.
Veldsman, M., Cumming, T., & Brodtmann, A. (2015). Beyond BOLD: optimizing functional imaging in stroke populations. *Human brain mapping*, *36*(4), 1620-1636.
Wagner, T., Valero-Cabre, A., & Pascual-Leone, A. (2007). Noninvasive human brain stimulation. *Annual review of biomedical engineering*, *9*(1), 527-565.
Wang, S. H., Lobier, M., Siebenhühner, F., Puoliväli, T., Palva, S., & Palva, J. M. (2018). Hyperedge bundling: A practical solution to spurious

interactions in MEG/EEG source connectivity analyses. *Neuroimage*, *173*, 610-622.
Wang, X., Seguin, C., Zalesky, A., Wong, W.-w., Chu, W. C.-w., & Tong, R. K.-y. (2019). Synchronization lag in post stroke: relation to motor function and structural connectivity. *Network Neuroscience*, *3*(4), 1121-1140.
Warren, D. E., Power, J. D., Bruss, J., Denburg, N. L., Waldron, E. J., Sun, H., Petersen, S. E., & Tranel, D. (2014). Network measures predict neuropsychological outcome after brain injury. *Proceedings of the National Academy of Sciences*, *111*(39), 14247-14252.
Wei, L., Wu, G.-R., Bi, M., & Baeken, C. (2021). Effective connectivity predicts cognitive empathy in cocaine addiction: a spectral dynamic causal modeling study. *Brain Imaging and Behavior*, *15*(3), 1553-1561.
Weiss Cohen, M., & Regazzoni, D. (2020). Hand rehabilitation assessment system using leap motion controller. *Ai & Society*, *35*(3), 581-594.
Wodeyar, A., Cassidy, J. M., Cramer, S. C., & Srinivasan, R. (2020). Damage to the structural connectome reflected in resting-state fMRI functional connectivity. *Network Neuroscience*, *4*(4), 1197-1218.
Wold, S., Sjöström, M., & Eriksson, L. (2001). PLS-regression: a basic tool of chemometrics. *Chemometrics and intelligent laboratory systems*, *58*(2), 109-130.
Yeh, F.-C., Panesar, S., Fernandes, D., Meola, A., Yoshino, M., Fernandez-Miranda, J. C., Vettel, J. M., & Verstynen, T. (2018). Population-averaged atlas of the macroscale human structural connectome and its network topology. *Neuroimage*, *178*, 57-68.
Yeh, F.-C., & Tseng, W.-Y. I. (2011). NTU-90: a high angular resolution brain atlas constructed by q-space diffeomorphic reconstruction. *Neuroimage*, *58*(1), 91-99.
Yeo, B. T., Krienen, F. M., Sepulcre, J., Sabuncu, M. R., Lashkari, D., Hollinshead, M., Roffman, J. L., Smoller, J. W., Zöllei, L., & Polimeni, J. R. (2011). The organization of the human cerebral cortex estimated by intrinsic functional connectivity. *Journal of neurophysiology*.
Zamani Esfahlani, F., Jo, Y., Faskowitz, J., Byrge, L., Kennedy, D. P., Sporns, O., & Betzel, R. F. (2020). High-amplitude cofluctuations in cortical activity drive functional connectivity. *Proc Natl Acad Sci U S A*, *117*(45), 28393-28401. https://doi.org/10.1073/pnas.2005531117
Zamora-López, G., Chen, Y., Deco, G., Kringelbach, M. L., & Zhou, C. (2016). Functional complexity emerging from anatomical constraints in the brain: the significance of network modularity and rich-clubs. *Scientific reports*, *6*(1), 1-18.
Zhang, J., Zhang, Y., Wang, L., Sang, L., Yang, J., Yan, R., Li, P., Wang, J., & Qiu, M. (2017). Disrupted structural and functional connectivity networks in ischemic stroke patients. *Neuroscience*, *364*, 212-225.